Variability in Diel Vertical Migration of Zooplankton and Physical Properties in Saanich Inlet, British Columbia

by

Mei Sato
B.Sc., Tokyo University of Fisheries, 2004
M.Sc., University of Maine, 2006

A Dissertation Submitted in Partial Fulfillment of the
Requirements for the Degree of

DOCTOR OF PHILOSOPHY

in the School of Earth and Ocean Sciences

Variability in Diel Vertical Migration of Zooplankton and Physical Properties in Saanich Inlet, British Columbia

by

Mei Sato
B.Sc., Tokyo University of Fisheries, 2004
M.Sc., University of Maine, 2006

Supervisory Committee

Dr. John F. Dower, Co-Supervisor
(School of Earth and Ocean Sciences)

Dr. Eric Kunze, Co-Supervisor
(Applied Physics Laboratory, University of Washington)

Dr. Jody M. Klymak, Departmental Member
(School of Earth and Ocean Sciences)

Dr. Richard Dewey, Departmental Member
(School of Earth and Ocean Sciences)

Dr. David L. Mackas, Departmental Member
(School of Earth and Ocean Sciences)

Dr. Andrew Jirasek, Outside Member
(Department of Physics and Astronomy)

Supervisory Committee

Dr. John F. Dower, Co-Supervisor
(School of Earth and Ocean Sciences)

Dr. Eric Kunze, Co-Supervisor
(Applied Physics Laboratory, University of Washington)

Dr. Jody M. Klymak, Departmental Member
(School of Earth and Ocean Sciences)

Dr. Richard Dewey, Departmental Member
(School of Earth and Ocean Sciences)

Dr. David L. Mackas, Departmental Member
(School of Earth and Ocean Sciences)

Dr. Andrew Jirasek, Outside Member
(Department of Physics and Astronomy)

ABSTRACT

In Saanich Inlet, a fjord located in southern Vancouver Island, British Columbia, dense aggregations of euphausiids exhibit diel vertical migration behavior and their capability of generating turbulence has been suggested. Despite decades of research on diel vertical migration of zooplankton, its variability has not been well studied. In addition, the physical oceanographic environment in Saanich Inlet has not been thoroughly quantified, which raises the possibility of previously observed turbulent

bursts of O(10^{-5} – 10^{-4} W kg^{-1}) having physical (rather than biological) origin. This work characterizes variability of diel vertical migration behavior using a moored 200-kHz echosounder, complemented by plankton sampling. Physical properties such as barotropic, baroclinic and turbulent signals are described, and the relationship between turbulence and internal waves/scattering layer examined.

A two-year high-resolution biacoustic time-series provided by the Victoria Experimental Network Under the Sea (VENUS) cabled observatory allowed quantification of the seasonal variability in migration timing of euphausiids. During spring – fall, early dusk ascent and late dawn descent relative to civil twilight occur. During winter, late dusk ascent and early dawn descent occur. Factors regulating the seasonal changes in migration timing are light availability at the daytime depth of the scattering layers, and size-dependent visual predation risk of euphausiids. Instead of the traditional view of diel vertical migration timing correlated solely with civil twilight, euphausiids also adapt their migration timing to accommodate changes in environmental cues as well as their growth. The pre-spawning period (February – April) is an exception to this seasonal pattern, likely due to the higher energy demands for reproduction.

Turbulence and internal waves in Saanich Inlet are characterized based on a one-month mooring deployment. Average dissipation rates are nearly an order of magnitude larger than previously reported values and higher dissipation rates of O(10^{-7} – 10^{-6} W kg^{-1}) are occasionally observed. A weak correlation is observed between turbulent dissipation rates and baroclinic velocity/shear. To examine the possibility of biological generation of turbulence, an echosounder at the VENUS cabled observatory is used to simultaneously measure the intensity of the euphausiid scattering layer and its vertical position. Turbulent bursts of the sort previously reported are not observed, and no relation between diel vertical migration and turbulent dissipation rates is found. Physical forcing at the main channel remains as a possible cause of the turbulent bursts.

Contents

List of Tables

List of Figures

ACKNOWLEDGEMENTS

I would like to thank my supervisors, John Dower and Eric Kunze, for your kind support, freedom, and continual encouragement for the interdisciplinary project. I also thank my committee members, Jody Klymak and Richard Dewey; Jody, for directing me in the physics component of the thesis and giving me insights on understanding internal waves and turbulence in Saanich Inlet; Richard, for guiding me the field component of the thesis, especially the mooring experiment from its design to the recovery.

A big thank you to the VENUS team for their efforts to collect continuous time-series and maintain the instruments with your technical expertise; Paul Macoun and Denis Hedji, for teaching me how to maintain and service the underwater sensors; Verena Tunnicliffe, for her continuous support and encouragement throughout my Ph.D program. ASL Environmental Sciences Ltd. (particularly Gary Borstad, David Lemon, Murray Clarke) were generous with advice and patient with me as I learned how to calibrate the echosounders. Nortek AS loaned me a 6-MHz Acoustic Doppler Velocimeter (Vector) through the 6th Annual Nortek USA Student Equipment Grant.

Field support was provided by Captain Ken Brown and the crew of MSV *John Strickland*, with the help of Ian Beveridge, Lu Guan, Kevin Sorochan, Jonathan Rose, Dan Bevan, Emma Murowinski, Kevin Bartlett, and Jeannette Bedard. I would like to thank John Horne for his advice on calibration analysis, Jim Gower for providing the chlorophyll *a* data from the MEOS buoy, Ed Wiebe for providing the insolation data from the University of Victoria's school-based weather station network, and Sarah Thornton and Frank Whitney for providing CTD data collected in Saanich Inlet. Thanks to my officemates, Emma Murowinski, Di Wan, Ryan Clouston, Jeannette Bedard, and Wendy Calendar, for helping me understand physics and math.

Last, but definitely not least, I thank my parents and Wei-Cheng Wang for your invaluable support and having faith in me.

This work was supported by U.S. Office of Naval Research, NSERC Dicovery Grants, the Bob Wright Scholorship, and Dr. Arne H. Lane Graduate Fellowship, for which I am grateful.

Chapter 1

Introduction

Coupling between physical and biological processes in the ocean is subtle and complex. Not only do physical processes, such as shallow mixed layers or fronts, set the stage on which the biological play is enacted, but they can also influence biological processes in many direct ways. In this thesis, I focus on characterizing diel vertical migration, and turbulence and internal waves in Saanich Inlet, British Columbia, which together may potentially affect carbon cycling and predator-prey interactions.

1.1 Bio-physical coupling

Throughout Earth's history, the ocean has played a crucial role in modulating atmospheric carbon dioxide through a variety of physical, chemical and biological processes. The ocean has absorbed nearly half of the anthropogenic carbon dioxide emitted into the atmosphere since pre-industrial times (Sabine et al., 2004). About 70% of the pre-industrial surface-to-deep ocean gradient in dissolved inorganic carbon originates from organic matter exported through the biological pump (Gruber and Sarmiento, 2002), which transports carbon fixed by photosynthesis from the euphotic layer to the deep ocean through gravitational settling and active biotransport. Both physical and biological processes affect the efficiency of the biological pump. Physical mixing can supply nutrients to the euphotic zone, thereby increasing photosynthesis and enhancing carbon fixation. Diel vertical migration of zooplankton can actively increase the magnitude of the downward export of organic material, by feeding near the surface at night and descending to depth during the day, where the material is metabolized (Longhurst and Harrison, 1988). Estimates of carbon transport by vertical move-

ment of zooplankton range from $4 - 34\%$ of the gravitational flux of organic particles (Hernández-León et al., 2010). The magnitude of this active transport further depends on the biomass and size of the migrating organisms, the temporal duration over which migrations occur, and the vertical extent of the migration.

Water movement can contribute to migrations of plankton. It is frequently hypothesized that the diel vertical migration of zooplankton enables self-recruitment to populations in upwelling zones by retaining organisms in the region (Peterson, 1998). For example, in the California Current system, there are equatorward and offshore currents at the surface, and poleward and onshore currents at depth. Consequently, relatively small vertical migrations (on the order of $10 - 100$ m) allow zooplankton to utilize currents flowing opposite directions, and can reduce the along- and cross-shore transport of organisms (Wroblewski, 1982; Batchelder et al., 2002).

Turbulence influences trophic transfers at all levels from dissolved nutrients to fish. Turbulence affects the uptake of nutrients by phytoplankton, by enhancing or inhibiting depending on the level of turbulence (e.g., Pasciak and Gavis, 1975; Thomas and Gibson, 1990, 1992). Encounter rates between fish larvae and their zooplankton prey are also influenced by turbulence; feeding is enhanced by increasing contact rates with food particles at low levels of turbulence, while the process of food handling may be disrupted (leading to a reduced feeding rate) at higher levels of turbulence (reviewed by Dower et al., 1997). The optimum level of turbulence differs for various species, and there is a complex interaction of turbulence intensity with food density and its patchiness.

1.2 Diel vertical migration

Many freshwater and marine organisms undergo daily patterns of vertical movement, termed diel vertical migration, which is ultimately a predator avoidance strategy (Hays, 2003). This phenomenon has been known since early nineteenth century (Cuvier 1817, cited in Bayly, 1986). Of the three general patterns, the most common is a nocturnal migration characterized by a single daily ascent towards the surface at sunset and a descent to a maximum depth at sunrise. Twilight migration involves an ascent to the surface at sunset, a descent to deeper water around midnight (called the midnight sink), followed by a second ascent to the surface and then descent to deeper water at sunrise. Reverse migration involves an ascent to shallow water at sunrise followed by a descent to deeper water at sunset. Nocturnal and twilight migrations

provide a daytime refuge from visual predation in dark conditions at depth, and most commonly observed in zooplankton (Hutchinson, 1967; Zaret and Suffern, 1976; Forward, 1988). Reverse migration provides protection from nocturnally migrating predators. This situation has been clearly observed for the marine copepod *Pseudocalanus* sp., which undergo reverse diel vertical migration when predatory copepods and chaetognaths migrate nocturnally (Ohman et al., 1983).

A number of biological and environmental factors can affect diel vertical migration behavior. Light is thought to be the major factor controlling migration behavior (Forward, 1988), serving as an endogenous cue and involving phototactic behavior of organisms. Phototactic responses of zooplankton and the time spent at the surface can be further modified by food availability (Huntley and Brooks, 1982; Johnsen and Jakobsen, 1987; Pearre, 2003; Van Gool and Ringelberg, 2003). Response to a light stimulus can also be modified by chemical cues released by predators (Forward and Rittschof, 2000; Cohen and Forward, 2005). Differences in predation risk between species and size-bias in predation risk within species also cause variations in migration timing (De Robertis et al., 2000; Tarling et al., 2001; Tarling, 2003). The vertical extent of migrations can also be affected by food availability (Dagg et al., 1997), lunar phases (Benoit-Bird et al., 2009), and oxygen minimum zones (Beveridge, 2007; Parker-Stetter and Horne, 2009). Despite the traditional view of diel vertical migration as a vertically migrating single scattering layer regulated by light availability, the process can be quite complex and thus studying all of the interacting mechanisms simultaneously has proven challenging.

Although various forcing factors have been studied in the laboratory and over short periods in the field, long-term *in situ* observations of diel vertical migration remain few (Tarling, 2003; Lorke et al., 2004; Jiang et al., 2007). Consequently, variability in migration behavior (e.g., migration timing, speed and migrating biomass) *in situ* is poorly understood. Variability in migration timing can potentially affect encounter rates with predators, and changes in migrating biomass can affect the efficiency of the biological pump. One of the difficulties in unraveling the mechanisms driving diel vertical migration is the generally low resolution of biological oceanographic data compared to physical data. Previous studies have heavily relied on net sampling to identify migrating species, but nets provide very low temporal and spatial resolution. Similarly, optical techniques have limited range due to strong attenuation of light in water. Because of the ability to collect high-resolution data with low attenuation underwater, acoustic techniques have emerged as vital tools for exploring animal

behavior underwater.

Ship-mounted and moored echosounders have been used to monitor distribution and behavior of zooplankton and fish (e.g., Pieper et al., 1990; Lawson et al., 2008; Benoit-Bird et al., 2009), but they are not able to provide long time-series due to the limited power supply. The Victoria Experimental Network Under the Sea (VENUS) cabled observatory enabled us to collect bioacoustic data with a coverage and resolution comparable with physical data, due to unlimited power availability. One of the VENUS cabled observatory arrays lies in Saanich Inlet, which is a naturally hypoxic basin and is one of the best-studied anoxic fjords in the world (Tunnicliffe et al., 2003). Euphausiids (primarily *Euphausia pacifica*) are the dominant vertically migrating species in the inlet, with densities range from $10 - 10{,}000$ ind. m^{-3} in the scattering layers (Bary, 1966; Pieper, 1971; Mackie and Mills, 1983; Jaffe et al., 1998). The underwater cabled observatory located in the area with abundant populations of vertically migrating zooplankton offers the opportunity to further unravel the variability in migration behavior.

1.3 Turbulence in the ocean

The ocean has a large heat capacity relative to the atmosphere, so that the changes in atmospheric heat content can be absorbed by the ocean with relatively small temperature change (Thorpe, 2005). Turbulence is one of the mechanisms for transferring heat from the surface into the body of the ocean, playing an important role in controlling global temperature changes. In addition, turbulent transports of momentum, mass, nutrients and chemicals play major roles in a range of processes such as the ocean's stratification, sediment resuspension, primary production, and pollutant dispersion.

Turbulence is often produced by internal wave or unstable stratification (Tennekes and Lumley, 1972; Thorpe, 2005). In coastal regions, internal wave is typically generated by winds, tides, surface waves, and baroclinic flows. Unstable stratification results from surface processes such as surface cooling, evaporation and freezing. Turbulent energy is transferred from large-scale eddies to smaller eddies until their energy is eventually dissipated into heat by molecular viscosity. Turbulence in the ocean affects biological processes in a variety of ways. In the euphotic zone, dissolved inorganic nutrients are often the limiting factors for primary production and turbulence can be a mechanism of re-supplying nutrients from the deep-ocean reservoir (Gargett, 1997). Turbulence also affects encounter rates between planktonic predators and their prey,

as well as their feeding rates (Rothschild and Osborn, 1988).

Interactions between physics and biology are not entirely in one direction. Marine organisms have been recognized as capable of generating turbulence (Wiese and Ebina, 1995; Yen, 2000; Yen et al., 2003), but previous studies have focused primarily on the energetic consequences for the animal instead of the energetic consequences for the fluid medium. The ability of marine organisms to generate turbulence has been debated. Huntley and Zhou (2004) considered the energy produced by schooling animals and predicted dissipation rates of O(10^{-5} W kg^{-1}) for organisms ranging from zooplankton to cetaceans. Visser (2007) disagreed with these estimates, arguing that, by itself, elevated dissipation rate is insufficient proof of substantial biogenic mixing, because much of the turbulent kinetic energy of small animals is injected below the Ozmidov buoyancy length scale. Dissipation rates of $10^{-5} - 10^{-4}$ W kg^{-1} associated with euphausiid diel vertical migration have been reported from Saanich Inlet (Kunze et al., 2006), but no recurrence of turbulent bursts coincident with diel vertical migration was observed in follow-up field observations in Saanich Inlet (Rousseau et al., 2010) nor other regions (Rippeth et al., 2007).

Discovery of biologically generated turbulence in Saanich Inlet was solely based on the timing of increased turbulent mixing and zooplankton vertical migration (Kunze et al., 2006). Without knowledge of the physical environment, however, the relative contributions of marine organisms cannot be isolated from other sources of mixing. In addition, common techniques for measuring ocean turbulence using vertical profilers are extremely labor-intensive (hence expensive). As a result, these techniques are not suitable for the long-term monitoring that is essential for biologically-generated turbulence studies, because of the heterogeneity associated with the patchiness of schooling animals and the intermittent nature of turbulence generation. By deploying Acoustic Doppler velocimeter and Acoustic Doppler Current Profiler in proximity to the VENUS cabled observatory equipped with an echosounder, simultaneous measurements of physical and biological parameters can be achieved in Saanich Inlet, where dense aggregations of vertically migrating euphausiids are known to reside.

1.4 Outline of the thesis

This thesis consists of two components, quantifying biological and physical variability in Saanich Inlet. The first component (Chapter 2) uses bioacoustic data from the VENUS cabled observatory to characterize diel vertical migration timing of euphausi-

ids and identify factors responsible for this variability. This chapter is published in Marine Ecology Progress Series (Sato et al., 2013). The second part (Chapter 3) uses data collected in a one-month mooring deployment to characterize turbulence and internal waves in Patricia Bay of Saanich Inlet, and examine the possibility of biologically generated turbulence. Since these two chapters have been prepared as separate manuscripts, there is some overlap in their respective Materials and methods sections. The thesis concludes with a brief summary of the major results and offers some suggestions for future research.

Chapter 2

Second-order seasonal variability in diel vertical migration timing of euphausiids in Saanich Inlet

2.1 Introduction

Many planktonic species migrate away from food-rich surface waters during the day to avoid visual predators (Zaret and Suffern, 1976). Quantifying the variability in such diel vertical migration is essential to understand predator-prey interactions, and assess the least-known component of the biological pump (Steinberg et al., 2000). Euphausiids play a key role in pelagic food webs, being a grazer on phytoplankton, a predator on microzooplankton, and a key prey item for invertebrate, fish and marine mammals (Mauchline, 1980; Mackas et al., 1997). Variations in migration timing can influence encounters with both predators and food, so are a key factor for survival. Diel vertical migration also serves as a vector connecting deep-water and pelagic communities by actively transporting carbon and nutrients from the surface to deep waters (Longhurst and Harrison, 1988). However, its global contribution to biogeochemical cycles remains unresolved.

If diel vertical migration behavior is primarily a consequence of the conflicting requirements of feeding and predator avoidance (Bollens and Frost, 1989), the time at which organisms migrate between deep and surface waters should reflect this trade-off. Light has long been known to be the dominant factor controlling the timing of diel vertical migration (Forward, 1988). Since migrating zooplankton typically

reside at depth during the day, the light intensity that they experience can vary with the attenuation and spectral characteristics of light which, in turn, are affected by the presence of dissolved and suspended material (Hulburt, 1945; Tyler, 1975). In addition to the ambient light level, food availability and predator density are also thought to be factors affecting diel vertical migration. According to the hunger-satiation hypothesis (Pearre, 2003), diel vertical migration is asynchronous within the population; animals leave the surface waters during the night when they are satiated, and may go back for a second meal before dawn after digesting their early-night meal (e.g., Simard et al., 1985; Sourisseau et al., 2008). Differences in predation risk between and within species also cause variations in migration timing (e.g., De Robertis et al., 2000; Tarling et al., 2001).

Although these various factors have been studied in the lab and over short periods in the field, long-term *in situ* observations of diel vertical migrations remain few. Previous studies based on long time-series have shown changes in migration timing due to the seasonal shift in daylight length (Tarling, 2003; Lorke et al., 2004; Jiang et al., 2007) at first order. However, second-order variability (variability in migration timing relative to civil twilight times) has received little attention due to low sampling resolution and short record length. One of the few examples is consideration of variations in migration timing with euphausiid body size (De Robertis et al., 2000). High sampling resolution and long time-series are essential for understanding behavior driven by factors whose relative importance can change temporally. For example, Sato and Jumars (2008) demonstrated the value of high temporal and spatial sampling resolution by showing a shift in the dominant rhythm of mysid emergence patterns from diel in summer to semidiurnal in fall.

If diel vertical migration is a trade-off between energy gain and mortality risk (Bollens and Frost, 1989), then migration timing should not be tied solely to civil twilight times. Rather, variability in migration timing due to light intensity, food availability, predator density and predation risk should be expected. The goal of this study is to examine second-order variability in migration timing relative to civil twilight, and to identify the factors responsible for this variability. Here, I present data from a two-year 200-kHz echosounder time-series collected in Saanich Inlet by the Victoria Experimental Network Under the Sea (VENUS) cabled observatory.

2.2 Materials and methods

2.2.1 Study site

Data were collected in Saanich Inlet (48° 39.1'N, 123° 29.2'W), British Columbia, during June 2008 − May 2010 (Fig. 2.1). Saanich Inlet is a fjord, with a 75-m sill at its mouth and maximum depths exceeding 200 m (Herlinveaux, 1962). It is a reverse estuary with its major supply of fresh water outside the inlet mouth. The Cowichan River in winter and the Fraser River freshet in summer produce a year-round stabilizing salinity gradient in the upper water column. Wind and tidal forcing in Saanich Inlet are generally weak (Gargett et al., 2003). The estuarine circulation is normally too weak to permit flushing of deeper waters below the sill, so that a secondary halocline exists at sill depth (Herlinveaux, 1962). High primary production (~ 475 g C m^{-2} yr^{-1}), combined with infrequent deep-water replenishment, contribute to the formation of deep-water anoxia during much of the year (Timothy and Soon, 2001; Grundle et al., 2009). There are typically two renewal events per year in Saanich Inlet where dense oxygenated waters enter the mouth at the sill depth, shoaling the deep anoxic waters upward: (i) deep-water renewal (below the sill depth but not reaching the bottom) during spring and (ii) bottom-water renewal during fall (Anderson and Devol, 1973; Manning et al., 2010). The oxycline plays a major role in Saanich Inlet in determining the daytime depth of the scattering layer, posing a physiological barrier for euphausiids (Pieper, 1971; Devol, 1981; Mackie and Mills, 1983).

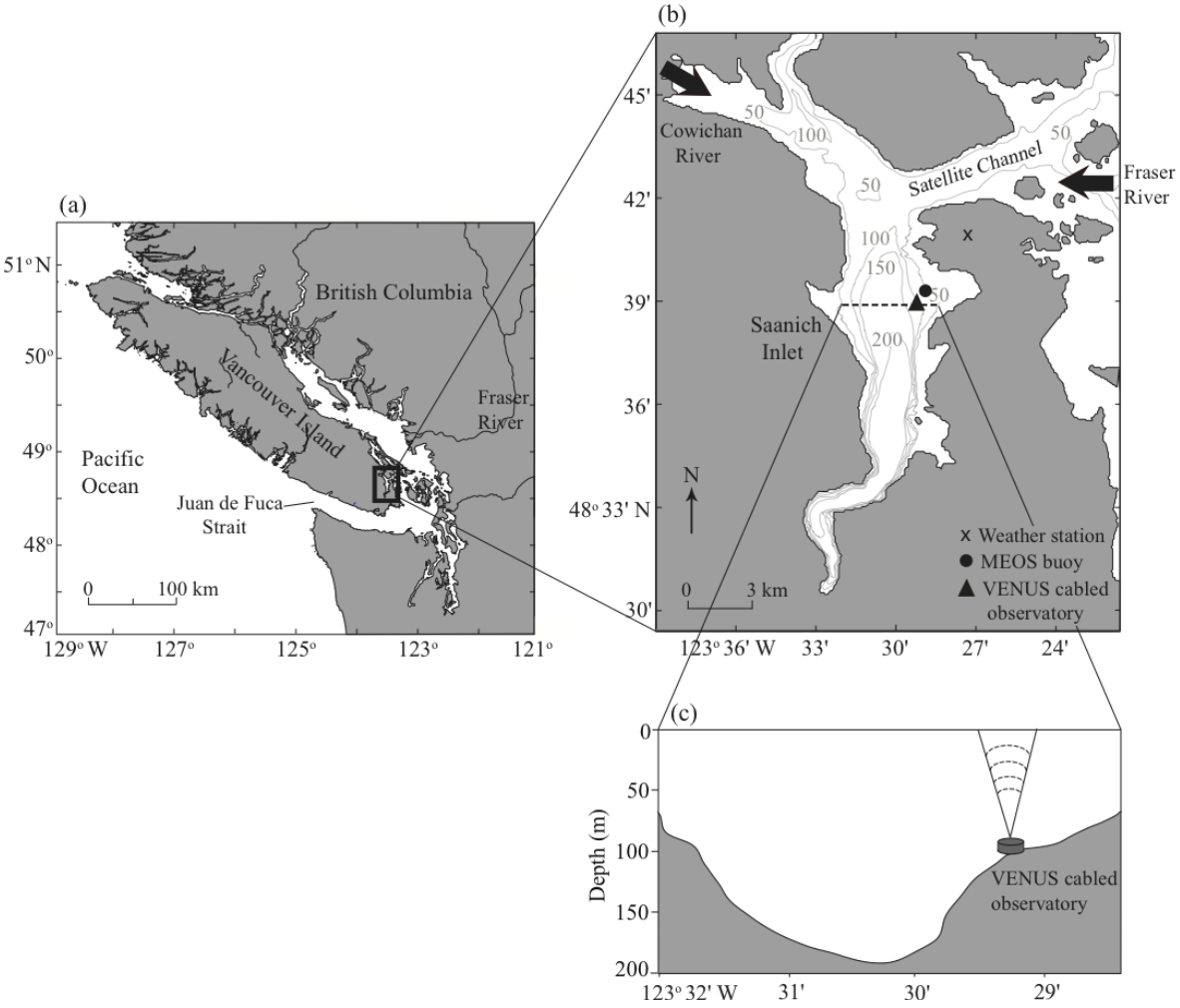

Figure 2.1: (a) Study site on the southeastern tip of Vancouver Island, British Columbia. (b) Locations of the Victoria Experimental Network Under the Sea (VENUS) cabled observatory, the Marine Ecosystem Observatories (MEOS) buoy 46134, and the shore-based weather station (from which insolation data were gathered) in Saanich Inlet. Bold arrows indicate major sources of freshwater input from the Cowichan River (winter) and Fraser River (summer). (c) Vertical section, showing the change in bathymetry across Saanich Inlet near the VENUS cabled observatory.

2.2.2 Potential acoustic scatterers of a 200-kHz echosounder

Year-round dominance of euphausiids in Saanich Inlet is supported by previous studies through optical images (Jaffe et al., 1998), visual observations (Mackie and Mills, 1983), and sampling using a 10-net MOCNESS (Multiple Opening/Closing Net and

Environmental Sensing System; De Robertis, 2001). Densities of euphausiids within the scattering layers range from $10 - 10{,}000$ ind. m^{-3} (Bary et al., 1962; Bary, 1966; Pieper, 1971; Mackie and Mills, 1983), accounting for $\sim 70\%$ of the daytime and $\sim 76\%$ of the night-time scattering layers based on the forward problem predictions of acoustic scatterers (Holliday and Pieper, 1995; De Robertis, 2002). *Euphausia pacifica* is the most abundant euphausiid throughout the year, constituting $77 - 100\%$ of all euphausiids followed by *Thysanoessa spinifera* and *T. raschii* (Bary et al., 1962; Pieper, 1971; De Robertis, 2001). *E. pacifica* live $1 - 2$ years (Tanasichuk, 1998) with their main spawning period from early May to mid-July, coinciding closely with the periods of higher phytoplankton abundance (Parsons et al., 1967; Heath, 1977).

The gammarid amphipod *Orchomene obtusus* is also abundant in Saanich Inlet (Bary et al., 1962; De Robertis, 2001), but resides at $100 - 125$-m depth and does not migrate (De Robertis et al., 2000; De Robertis, 2001). Since this study focuses on diel vertical migration behavior in upper 50 m of the water column, *O. obtusus* is unlikely to contribute to the major acoustic scatterers. The low biomass of copepods (Bary et al., 1962) and their low target strength (TS) values at 200-kHz due to their small body size (Trevorrow et al., 2005) suggest that their contribution to volume backscattering strength (S_v) is also minimal. Decapods, mysids, shrimps, physonectid siphonophores, gastropods, hydromedusae, ctenophores, chaetognaths and cephalopods have been observed in previous studies, but their rare occurrence and low density in scattering layers suggest insignificance as acoustic scatterers (Bary et al., 1962; Pieper, 1971; Mackie and Mills, 1983; De Robertis, 2001). Although the thecosome pteropod *Limacina helicina* and the gas-filled pneumatophores of siphonophores are strong acoustic targets (Stanton et al., 1994), scattering model calculations of *L. helicina*, which are less than 2 mm in diameter, indicate that their contribution to echoes is not significant at 445-kHz (De Robertis, 2001). Since theoretical TS value of the pteropods is predicted to be lower at 200-kHz than at 445-kHz (Stanton et al., 1994), their contribution is not significant at 200-kHz either. The density of physonectid siphonophore in Saanich Inlet is not known. In this study, I assumed that their contributions to S_v were minimal.

Other possible biological acoustic targets include Pacific herring (*Clupea pallasi*), hake (*Merluccius productus*), walleye pollock (*Theragra chalcogramma*), rockfish (*Sebastodes* spp.), myctophids (*Lampanyctus leucopsarus*), eulachon (*Thaleichthys pacificus*), smooth-tongue (*Leuroglossus stilbius*), and spiny dogfish (*Squalus acanthias*) (Bary et al., 1962; Bary, 1966; Pieper, 1971; De Robertis, 2002). Among these fish,

herring and young hake are the principal species associated with the scattering layers (Bary, 1966). Based on the minimal effect of fish schools on migration timing detection [see 2.2.9 Data Analysis (iv) Application of threshold], they are not likely to affect estimates of euphausiid migration timing which is the focus of this study. Sediments and bubbles are unlikely to contribute to the backscattering observed in my record. Given the weak tidal forcing in Saanich Inlet ($5 - 10$ cm s^{-1}), sediments are unlikely to be stirred more than 2 meters above bottom (mab). Bubbles are largely confined to the surface layer under breaking waves, which are not common in Saanich Inlet due to shelter from prevailing winds.

2.2.3 Identification of acoustic scatterers

Net sampling of the zooplankton community was carried out for ~ 3 hours near the VENUS cabled observatory around sunset on 15 April, 10 June, 15 July 2010, and sunrise on 14 October, 16 December 2011, 9 February 2012 to confirm dominance of euphausiids in the scattering layer. A Tucker trawl (1-m^2 mouth opening when towed at 45°, 1-mm mesh size) equipped with a double-release mechanism (Ocean Test Equipment Inc.) was towed at $\sim$ 80-, 40- and 10-m depths to compare the species composition inside and outside the diel migratory scattering layer. These depths were chosen to capture the scattering layer located at the daytime depth before the migration started, mid-depth during the migration, and near the surface after the upward migration was completed. Samples from outside the scattering layer were collected by towing these depths before the scattering layer reached or after it passed by. A pressure sensor (Minilog-TD; AMIRIX Systems Inc.) on the Tucker trawl monitored tow depth. Each sample consisted of $\sim$ 5-min horizontal tow at ~ 1 m s^{-1}. Samples were fixed in 5% formalin on deck, and displacement volume determined ashore after removal of jellyfish because they are weak acoustic targets compared to non-gelatinous zooplankton (Stanton et al., 1996). Animals were subsequently sorted, counted, and the total lengths of dominant euphausiids (tip of eye to tip of telson) measured under a dissecting microscope. Juvenile euphausiids were not identified in species level due to the difficulty in recognizing developing characteristics. Since a flow meter could not be mounted in the net mouth due to the mechanical limitations of using a double-release mechanism, abundance and displacement volume were normalized to 5-min tows to compare between samples. Copepods and fish were not collected in representative numbers by the 1-mm mesh

of the Tucker trawl but, as already argued, are unlikely to contribute to migration timing detection.

2.2.4 VENUS instruments

Diel vertical migration of zooplankton was monitored with an upward-looking 200-kHz echosounder (Acoustic Water Column Profiler; ASL Environmental Sciences Inc.) mounted on a metal frame at 100-m depth ($\sim$ 2 mab) above the oxycline throughout most of the year. Therefore, I could not quantify the seasonal change in daytime depth of the scattering layer in this study. A CTD (conductivity, temperature, depth) (SBE 16plus; Sea-Bird Electronics Inc.) was deployed on the same frame. All instruments were linked to the VENUS cabled observatory (http://venus.uvic.ca) and were serviced and cleaned twice a year to remove biofouling.

Backscattered acoustic signals from particles in the water column were digitized (8-bit resolution) into 12.5-cm depth bins, with a sampling interval of 2 s, pulse duration of 300 μs and beam width of 8°, then converted to S_v using the standard sonar equation (e.g., Urick, 1983)

$$S_v = 20log_{10}N_r + 20log_{10}r + 2\alpha r - SL - OCV - G - 10log_{10}(\frac{c\tau\Psi}{2}) \qquad (2.1)$$

where N_r is received signal output by the 8-bit A/D converter between 0 and 255, r the range of the target sensed by the transducer (m), α the absorption coefficient of the medium (dB m^{-1}), SL the source level of the transmitted signal (dB re 1 μPa at 1 m), OCV the transducer receiving response (dB re 1 V per 1 μPa), G the time-varying gain of the echosounder (dB), c the sound speed (m s^{-1}), τ the pulse duration (s), and Ψ the equivalent beam angle (sr). The range of S_v detectable was approximately -80 $-$ -43 dB re 1 m^{-1} at 50-m range, and -72 $-$ -41 dB re 1 m^{-1} at 100-m range. The resolution depends on the signal strength, varying 0.03 $-$ 1.9 dB at 50-m range and 0.03 $-$ 1.2 dB at 100-m range. Two identical echosounders (AWCP 1007, 1009) were deployed alternately to ensure continuous time-series data.

2.2.5 Calibrations

Both echosounders were calibrated using a 38.1-mm-diameter tungsten carbide sphere as prescribed by Vagle et al. (1996). Calibrations were conducted at the buoy of the Ocean Technology Test Bed, an underwater engineering laboratory operated by

the University of Victoria in Saanich Inlet (Proctor et al., 2007), on 9 February 2010 for AWCP 1007, and 31 January 2011 for AWCP 1009. Due to the technical difficulties in calibrating bottom-mounted echosounders at the operating depth of 100 m, calibrations were conducted near the surface. The transducer was mounted at $\sim$ 0.7-m depth facing downward, and calibration measurements were conducted at 22.66-, 24.69-, 30.76- and 36.83-m range for AWCP 1007, and 19.46-, 21.48-, 23.49-, 25.53-, 30.46- and 35.28-m range for AWCP 1009 to ensure calibration in the far field. On average, the mean adjustment needed in G was -0.34 dB for AWCP 1007, and -0.38 dB for AWCP 1009. Since the measured TS values were within 0.4 dB of the theoretical TS and depth dependency of transducer sensitivity could affect the calibration results (Ona, 1999), no correction was applied to G in this study (for more details of the calibration methods and associated results, see Appendix).

2.2.6 Additional data

Chlorophyll a concentration was monitored hourly by a WET Labs WETStar fluorometer deployed at 8-m depth on the Marine Ecosystem Observatories (MEOS) buoy 46134 (48° 39.6'N, 123° 28.8'W) (Fig. 2.1b). Chlorophyll a concentration, estimated using factory calibration values, was provided by J. Gower (personal communication; Gower et al., 1999; Gower, 2001). The fluorometer was cleaned once a month to remove biofouling. Insolation data monitored at Deep Cove Elementary School (48° 40.8'N, 123° 27.4'W), approximately 4 km northeast of the study site (Fig. 2.1b), were obtained through the University of Victoria's school-based weather station network (http://www.victoriaweather.ca). Times of sunrise, sunset and civil twilight (sun zenith angle = 96°) for the study site were obtained from the United States Naval Observatory (http://aa.usno.navy.mil/data/).

Vertical profiles of fluorescence and photosynthetically available radiation (PAR; 400 − 700 nm) were measured near the VENUS cabled observatory, using a WET Labs WETStar fluorometer and a Biospherical Instruments Inc. QSP-200L sensor, respectively. These data were analyzed to characterize the effect of phytoplankton blooms on underwater light intensity. Data were collected on three days in January (21 January 2009, 25 January 2010, and 25 January 2011), and two days in June (9 June 2010, and 10 June 2011) with one vertical cast per day whose sampling time varied between 10:11 PST and 14:10 PST. Since the spectral sensitivity of euphausiids has a narrower peak at 480 − 490 nm (Frank and Widder, 1999; Widder and Frank,

2001), my PAR data overestimate the true irradiance value available to the euphausiid eye.

To characterize vertical and seasonal variability of sound speed and absorption coefficient, CTD (SBE 19plus; Sea-Bird Electronics Inc.) profiles collected near the VENUS cabled observatory during January, May, June and July 2007 − 2011 were examined. Each month contained 2 − 7 vertical profiles.

2.2.7 Data processing

Two years (June 2008 − May 2010) of echosounder profile time-series were analyzed. Data gaps (2.6% of all data) due to mechanical problems and maintenance cruises were linearly interpolated to form a continuous data set. Based on the mean temperature (8.8 °C) and Absolute Salinity (31.0 g kg^{-1}) measured by the CTD at 100-m depth for two years, a constant sound speed 1482 m s^{-1} and absorption coefficient 0.05 dB m^{-1} were applied to calculate S_v throughout the water column. Based on seasonal and depth variations in sound speed of less than 1%, uncertainties in S_v, range and bin size were minimal. The use of a constant absorption coefficient results in less than 0.5 dB re 1 m^{-1} error in S_v at 100-m range. Raw S_v values were averaged into 1-min × 1-m bins. The detected ocean surface was used as a reference for analysis of migration timing and speed [see 2.2.9 Data Analysis (iii) Effect of reference point]. Time-series of fluorometer data measured hourly from the MEOS buoy were averaged over one day to be consistent with the number of occurrences of diel vertical migration.

2.2.8 3-D data cube concept

The two-year echosounder time-series sampled every 2 s with 12.5-cm depth bins generated ∼ 60-GB data. Analysis of such large datasets can be challenging. To deal with this problem, we utilize the data cube concept (Jiang et al., 2007; Sourisseau et al., 2008; Borstad et al., 2010; Cisewski et al., 2010) whereby echosounder data can be imaged in [time of day] × [day] × [depth] (Fig. 2.2a). By slicing this data cube vertically or horizontally, different aspects of diel vertical migration can be examined. To center the nocturnal diel vertical migration, each day begins at 12:00 PST (local noon) and ends at 12:00 PST of the following day. The first day in the time-series is 1 June 2008 and the last 1 June 2010. The cube was truncated at 3-m depth to present variation in ascent and descent timings of diel vertical migration without contamination by the surface. The seasonal variation in diel vertical migration regulated by the

seasonal shift in daylight length is evident as an hourglass shape on the top surface of the cube (Fig. 2.2a). A vertical slice parallel to the xz plane shows the diel vertical migration pattern on 19 April 2009 (Fig. 2.2b). This pattern represents typical nocturnal diel vertical migration; upward movement of the scattering layer towards the surface at dusk and downward movement to deeper waters at dawn. Examples of more complicated scattering layer patterns are presented in the Discussion.

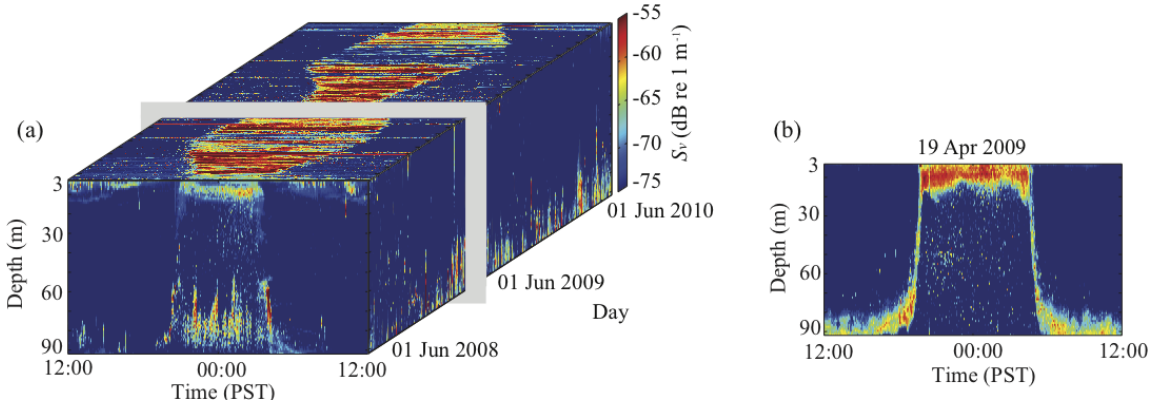

Figure 2.2: (a) Two-year time-series of volume backscattering strength S_v (1-min × 1-m bin averages), visualized as a 3-D data cube: [time of day] × [day] × [depth]. Hourglass shape on the top surface of the cube shows the first-order variability, which is the seasonal variation in diel vertical migration regulated by seasonal shift in daylight length. (b) An example of nocturnal diel vertical migration with a single scattering layer, corresponding to the vertical slice of the 3-D data cube shown in (a).

2.2.9 Data Analysis

(i) Migration timing

Using the acoustic sea surface as a reference, S_v were further smoothed by taking 11-min running × 5-m bin averages. Daily variability of S_v at 8-m depth, corresponding to the horizontal slice of the 3-D data cube in Fig. 2.3a, was used to detect migration timing; S_v within the upper 20 m gives a similar pattern as that at 8-m depth, indicating that S_v at 8-m depth is representative of near-surface conditions. Differences of S_v [$\Delta S_v = S_v(t+\Delta t)$ - $S_v(t)$, with time lag Δt = 20 min] were calculated to show the timing of increases/decreases in ΔS_v. Various Δt values were tested for estimating migration timing. By visually inspecting how well the estimated migration timing captured migration timing in echograms, I settled on Δt = 20 min

to calculate differences of S_v. Timing of diel vertical migration was estimated by detecting the maximum and minimum values of ΔS_v. The presence of non-migratory scatterers near the surface can contaminate migration timing detection. Based on visual examination, 35% of ascent and 29% of descent migration timings resulted in detection of such non-migratory scatterers. However, removal of those data points does not change the pattern of seasonally varying migration timing.

Detected migration timing was compared with the times of civil twilight to examine seasonal variability in ascent and descent migration timings. I also examined the migration timing relative to sunset and sunrise to find the effect of reference times. Seasonal variations in migration timing lags differ by less than 1 min between the two reference times. Since civil twilight times match migration timings more closely than sunset and sunrise times, civil twilight was used as a reference point in this study (e.g., Blaxter, 1973). Periodicities of variability in migration timing were determined by estimating the power spectral density (describing how the power of a signal is distributed with frequency).

(ii) Migration speed

In order to maintain the relatively high vertical resolution required to estimate migration speed, S_v were further smoothed by taking 11-min running $\times$ 2-m bin averages. The lag in migration timings between 19- and 50-m depths was used to estimate migration speed for each day. These depths were chosen to avoid the nearly exponential ascent and descent curves of the scattering layer in deep waters (Fig. 2.2b), and to include nocturnal sub-surface scattering layers that were occasionally located at $\sim$ 20-m depth. Owing to the differences in variance, Welch's t-test was used to test the null hypotheses of no differences in mean lag time among seasons assuming normal distributions.

(iii) Effect of reference point

Particle movement, as detected by echosounders, can be affected by vertical tidal motion. Therefore, the effect of choosing surface vs. bottom referencing on the migration timing analysis was examined. Spectral analysis of migration timing at 8-m depth, based on the 2-m bin-averaged bottom-referenced data, showed tidal components, indicating particle movement due to tidal heaving. Tidal surface displacements in Saanich Inlet vary from $2 - 3$ m over the spring-neap cycle based on the VENUS

pressure record. In order to avoid tidal effects on migration timing analysis near the surface, surface-referenced data smoothed over 11-min running × 5-m bin averages were used [see 2.2.9 Data Analysis (i) Migration timing]. Spectral analysis of migration timing at 19- and 50-m depths showed no apparent tidal components, regardless of the reference point. This spectral characteristic suggests little effect of tidal displacements on migration timing at these depths.

(iv) Application of threshold

The presence of fish in my single-frequency echosounder data can be recognized as a plume shape for fish schools and a crescent-moon shape for individual fish. The potential effect of fish presence on migration timing detection was examined by applying an upper threshold in S_v (1-min × 1-m bin averages) to remove fish schools from the acoustic time-series. A representative probability density function of S_v in the presence of both the zooplankton scattering layer and fish schools showed bi-modal characteristics with peaks located at ∼ -70 and -50 dB re 1 m^{-1}. Therefore, an upper threshold of -60 dB re 1 m^{-1} was chosen to filter out fish school echoes. Individual fish targets cannot be entirely extracted by thresholding; assuming that the TS of a 15-mm euphausiid is -79.8 dB re 1 m^2 at 200 kHz (Trevorrow et al., 2005) and that their densities within scattering layers in Saanich Inlet range from 10 − 10,000 ind. m^{-3} (Bary et al., 1962; Bary, 1966; Pieper, 1971; Mackie and Mills, 1983), the expected S_v varies from -69.8 − -39.8 dB re 1 m^{-1} which overlaps with the detected S_v of individual fish. This overlap suggests that a -60 dB re 1 m^{-1} threshold would remove S_v due to the scattering layer comprised of euphausiids, in addition to fish schools. Given these limitations, a threshold approach could not be used to quantify predator density. A lower threshold to remove noise was not applied because its application masks the weak diel vertical migration patterns during December 2009 − February 2010. Detected migration timings were indistinguishable from those timings without thresholds. Thus, the results below are presented without an upper threshold as well.

2.3 Results

2.3.1 Species composition from Tucker trawl samples

Euphausiids, shrimp larvae, amphipods and chaetognaths accounted for most of the zooplankton collected in the migratory scattering layers. Euphausiids (mostly *Eu-*

phausia pacifica) were the dominant acoustic scatterers throughout the year, constituting more than 84% of individuals within the scattering layer in April (more than 78% of total displacement volume), 91% in June (64%), 59% in July 2010 (67%), 98% in October (86%), 90% in December 2011 (99%), and 83% in February 2012 (78%). Fewer organisms were captured outside of the scattering layers, with very few euphausiids. Displacement volumes outside the scattering layers were $9 - 32\%$ of those inside the scattering layers. Although the period of Tucker trawl sampling did not exactly match that of the echosounder time-series, the numerical and displacement volume dominance of *E. pacifica* in the scattering layers in Saanich Inlet is well-supported by numerous previous studies (e.g., Bary et al., 1962; Mackie and Mills, 1983; De Robertis et al., 2000). Moreover, although the dominance of euphausiids did decrease during the summer, the remainder of the samples was never dominated by any species known to be a strong backscatterer. Given its dominance in the scattering layers, and that thresholding for fish schools did not affect migration timings, I hereafter assume that *E. pacifica* dominates diel vertical migration signals throughout the year.

2.3.2 Diel vertical migration timing

Nocturnal diel vertical migration, defined as a significantly higher S_v near the surface at night than during the day, occurs throughout the record (Fig. 2.3b), the only exception being low nocturnal S_v during December 2009 − February 2010. First-order variability is characterized by the seasonal change in migration timing associated with the seasonal shift in daylight length; scattering layers remain near the surface at night longer during winter than summer (Fig. 2.3b). Migration timing is closely related to civil twilight times (Fig. 2.3b), corresponding to the maximum and minimum values of ΔS_v (Fig. 2.3c).

Superimposed on this light-regulated pattern is seasonal and intraseasonal variability in migration timing relative to civil twilight times. Seasonal variability is characterized by the difference in offset between civil twilight and dusk ascent/dawn descent migration timings (Fig. 2.3d). Referenced to civil twilight times, early dusk ascent and late dawn descent occur during spring − fall, while late dusk ascent and early dawn descent are observed during winter (Fig. 2.4). There is a positive correlation ($r = 0.71$, $p < 0.0001$) between dusk ascent and dawn descent migration timings relative to civil twilight times (Fig. 2.5a). On average, dusk ascent occurs 14.3 ± 14.1

min before civil twilight during spring − fall, and 8.6 ± 11.9 min after civil twilight during winter, while dawn descent occurs 8.2 ± 15.1 min after civil twilight during spring − fall, and 15.2 ± 12.4 min before civil twilight during winter. Spectral analysis of the two-year time-series of migration timing shows a clear peak at an annual period for both dusk ascent and dawn descent migration timings (Fig. 2.5b).

Intraseasonal (shorter than 100 d) variability in the timing of the dusk ascent and dawn descent is of similar amplitude, with fluctuations in both signals being larger during summer than winter (Fig. 2.3d). However, there is no consistent correlation between dusk ascent and dawn descent migration timings on these timescales. Power spectral densities at intraseasonal timescales are nearly flat and have no significant peaks (Fig. 2.5b). Non-migratory scatterers are often detected during summer − fall but intraseasonal variability remains after removal of these data points, though interpretation becomes difficult because of increased data gaps. Because a Fourier transform smears out any detailed information on the changing processes, the intraseasonal variability will not be considered further in this study.

Figure 2.3 *(following page)*: (a) Two-year time-series of volume backscattering strength S_v (1-min × 1-m bin averages) in the 3-D data cube, with a horizontal slice at 8-m depth. (b) Daily variability of S_v (11-min running × 5-m bin averages) at 8-m depth. (c) Daily variability of 20-min difference of S_v at 8-m depth: $\Delta S_v = S_v(t+\Delta t)$ - $S_v(t)$, with time lag Δt = 20 min. (d) Timing of diel vertical migration relative to civil twilight times. Curves are 5-d running averages to remove day-to-day scatter. Positive values indicate migration timing in minutes before civil twilight time for dusk ascent migration, and after civil twilight time for dawn descent migration. (e) Time-series of chlorophyll *a* concentration at 8-m depth with 5-d running averages shown by curve. Data gaps (gray vertical bars) are due to the maintenance cruises or mechanical failure of instruments.

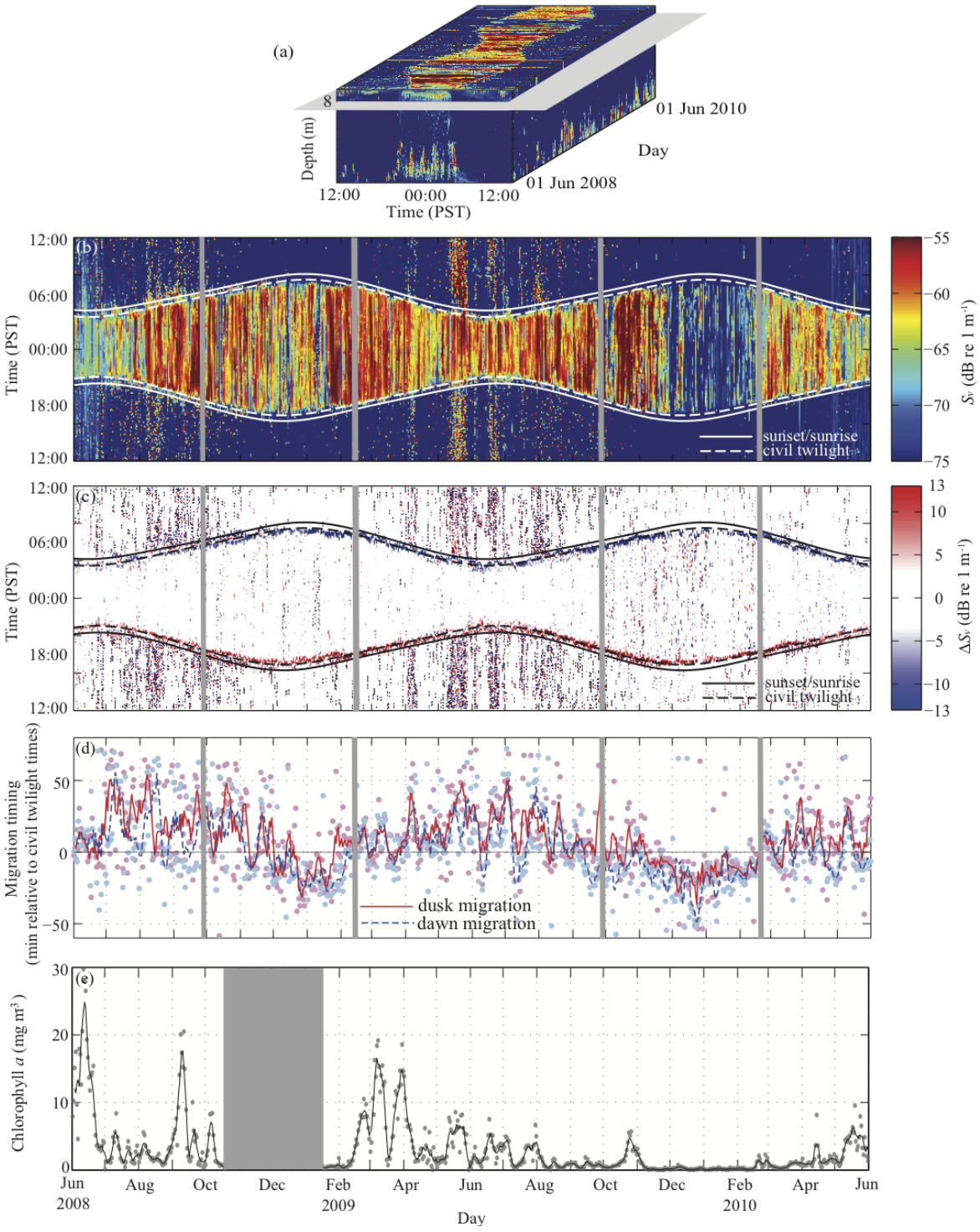
(a)
8
Depth (m)
01 Jun 2010
Day
01 Jun 2008
12:00
00:00
12:00
Time (PST)
(b)
12:00
06:00
00:00
18:00
12:00
Time (PST)
sunset/sunrise
civil twilight
−55
−60
−65
−70
−75
S_v (dB re 1 m^{-1})
(c)
12:00
06:00
00:00
18:00
12:00
Time (PST)
sunset/sunrise
civil twilight
13
10
5
0
−5
−10
−13
ΔS_v (dB re 1 m^{-1})
(d)
Migration timing
(min relative to civil twilight times)
50
0
−50
dusk migration
dawn migration
(e)
30
20
10
0
Chlorophyll a (mg m^3)
Jun
2008
Aug
Oct
Dec
Feb
2009
Apr
Jun
Aug
Oct
Dec
Feb
2010
Apr
Jun
Day

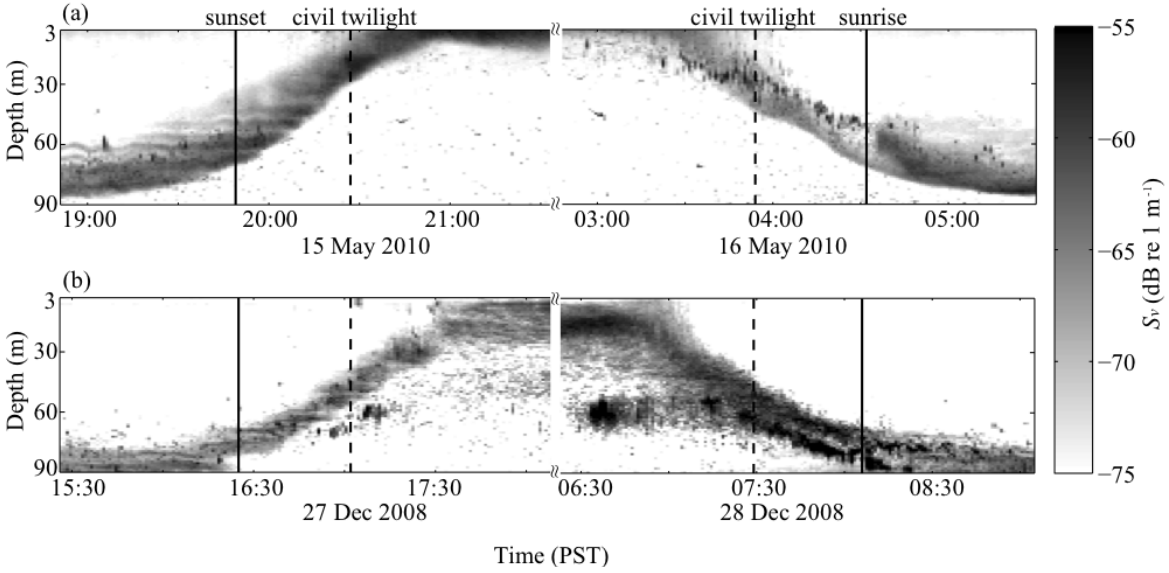

Figure 2.4: Examples of second-order seasonal variability in dusk ascent and dawn descent migration timings during (a) summer and (b) winter. Second-order seasonal variability in migration timing shows that the lag between civil twilight times and dusk ascent/dawn descent migration timings near the surface is larger during winter than spring − fall; early dusk ascent and late dawn descent occur during spring − fall, while late dusk ascent and early dawn descent are observed during winter.

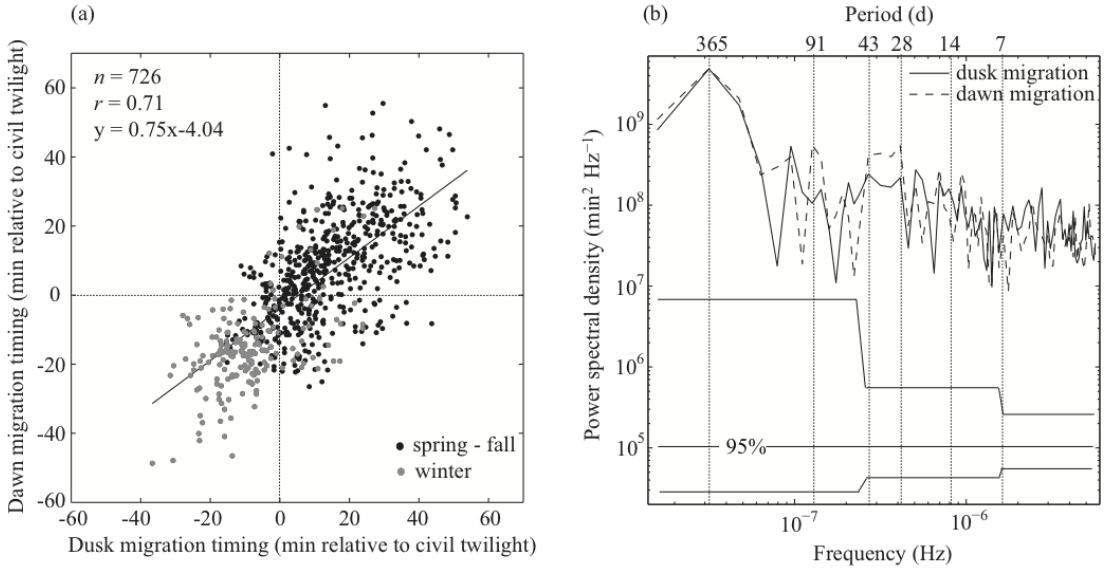

Figure 2.5: (a) Scatterplot of dusk ascent vs. dawn descent migration timings at 8-m depth with 5-d running averages for the two-year time-series. Positive values indicate migration timing in minutes before civil twilight time for dusk ascent migration, and after civil twilight time for dawn descent migration. (b) Power spectral density of dusk ascent and dawn descent migration timings at 8-m depth for the two-year time-series. Lines are the 95% confidence interval.

2.3.3 Factors affecting diel vertical migration timing

(i) Shadow effect of phytoplankton

Light intensity at depth is modified by dissolved and suspended material in the water column as well as seasonal change in insolation. Insolation at Saanich Inlet varies seasonally by over an order of magnitude, from a winter minimum of less than 50 W m^{-2} to a summer maximum of $\sim$ 1000 W m^{-2}. Despite the stronger insolation in summer, PAR deeper than 10-m depth is weaker in June than January (Fig. 2.6a) because it is below the depth of the chlorophyll maximum during phytoplankton blooms (Fig. 2.6b). Phytoplankton blooms in Saanich Inlet occur in spring – fall, with chlorophyll *a* concentrations often exceeding 15 mg m^{-3} at 8-m depth (Fig. 2.3e).

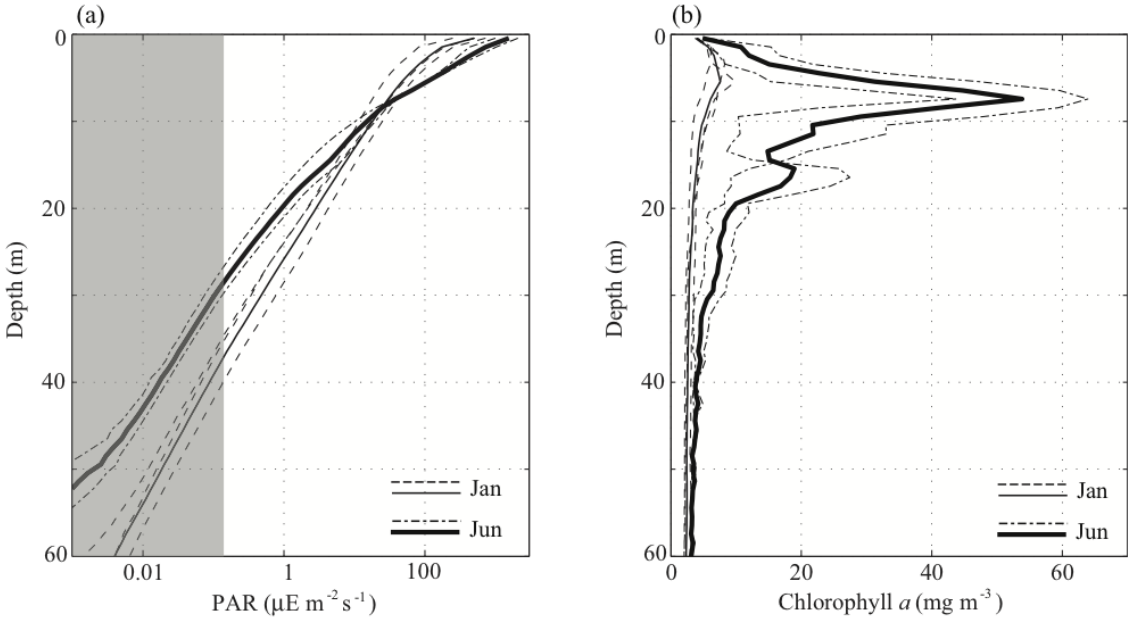

Figure 2.6: Vertical profiles of daytime (a) PAR and (b) chlorophyll *a* concentration in Saanich Inlet during January (21 January 2009, 25 January 2010, 25 January 2011) and June (9 June 2010, 10 June 2011). Data were averaged into 1-m bin. Dotted lines represent vertical profiles collected each day, and solid lines are monthly-averaged. The range of values below the manufacture's dynamic range is filled by gray.

(ii) Body size of euphausiids

Juvenile euphausiids dominate the Saanich population in summer while adults dominate in winter − spring. The size distribution of euphausiids collected from the surface scattering layers in Saanich Inlet shows a seasonal shift in average body length: 18.1 mm in April, 7.4 mm in June, 8.5 mm in July 2010, 12.9 mm in October, 15.2 mm in December 2011, and 15.1 mm in February 2012 (Fig. 2.7).

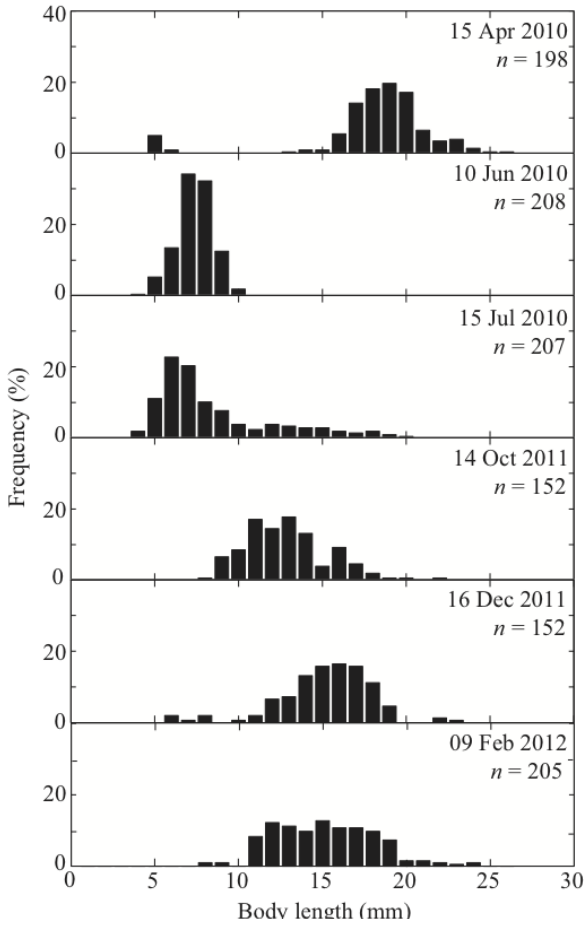

Figure 2.7: Size distribution of euphausiids (mostly *Euphausia pacifica*) collected from the surface scattering layers during April, June, July 2010, October, December 2011, and February 2012. n represents number of individuals counted.

(iii) Migration speed

Since I base migration timings on near-surface signals, migration speed can affect the dusk arrival timing near the surface. Seasonally averaged migration speeds at

dusk ascent/dawn descent are 2.0/2.1 cm s^{-1} during spring, 2.7/1.6 cm s^{-1} during summer, 3.0/2.3 cm s^{-1} during fall, and 2.0/1.5 cm s^{-1} during winter. Because the histograms of lag in migration timing, but not velocities, have normal distributions, the statistical significance of mean lag times between seasons is examined. There are no significant differences ($p > 0.05$) in dusk ascent mean lag time during spring and winter, or during summer and fall. Similarly, there are no significant differences ($p > 0.05$) in dawn descent mean lag time during spring and fall, or during summer and winter. Significant differences ($p < 0.05$) in mean lag times were observed in other seasons. If migration speed were a major cause of the late dusk ascent timing during winter, significant differences in dusk ascent mean lag times during winter and spring − fall would be expected. Since dusk ascent mean lag time during winter is not significantly different from spring, migration speed is unlikely a cause of the seasonal variability in migration timing and not considered further.

2.4 Discussion

2.4.1 Summary

The goal of this study was to characterize second-order variability in migration timing relative to civil twilight times, and to identify factors regulating this variability. To address this goal, I used an upward-looking echosounder mooring to monitor the migrating scattering layer, a fluorometer to measure chlorophyll *a* concentration near the surface to estimate the shadow effect of phytoplankton, and an insolation record. In addition, six sampling campaigns for zooplankton were conducted to confirm the identity of animals dominating the scattering layer and characterize their size distribution with season. The primary results in this study are;

- Migration timing of euphausiids exhibits second-order variability at seasonal timescales; early dusk ascent is associated with late dawn descent during spring − fall, and late dusk ascent is associated with early dawn descent during winter.
- Ascent timing appears to be controlled by a combination of shadowing by phytoplankton blooms and the seasonal change in the average body size of euphausiids affecting the phototaxis behavior.
- Descent timing appears to be controlled by the seasonal change in the average body size of euphausiids which affects phototactic behavior.

- These results support the size-dependent migration timing hypothesis (De Robertis et al., 2000), whereby more visually conspicuous larger-bodied euphausiids enter surface waters later and leave earlier than smaller-bodied individuals, with a two-year time-series covering a life cycle of the dominant euphausiids *Euphausia pacifica*.

2.4.2 Factors affecting diel vertical migration timing

Light is the major control of diel vertical migration timing. Both the absolute and relative rate of change in light intensity have been reported to initiate migration (reviewed by Cohen and Forward, 2005). However, these effects could not be examined directly in this study because the sensitivity of the irradiance sensor was too low to measure insolation before/after civil twilight times. Instead, I consider the following factors that can affect either underwater light intensity or phototactic behaviors of diel vertical migration so may regulate the observed second-order seasonal variability in migration timing: (i) shadowing by phytoplankton blooms, (ii) food availability, (iii) predator density, and (iv) zooplankton body size (Table 2.1).

Table 2.1: Possible factors affecting second-order seasonal variability in diel vertical migration timing. Each factor has an effect (+)/no effect (−) on dusk ascent and dawn descent migration timings. Ascent: arrival at surface, Descent: departure from surface. N/A: factor is not applicable for this study.

		This study		
Factors	Previously observed/proposed mechanisms (References)	Ascent	Descent	Exceptions
Shadowing by phytoplankton blooms	Shadow effect of phytoplankton changes underwater light intensity (Kaartvedt et al., 1996; Frank and Widder, 2002)	+	−	Spring - fall when chl *a* is low
Food availability	Response to light stimulus and duration at surface are modified by food concentration (Huntley and Brooks, 1982; Johnsen and Jakobsen, 1987; Pearre, 2003; Van Gool and Ringelberg, 2003)	N/A	N/A	−
Predator density	Response to light stimulus is modified by chemical cues released by predators (Forward and Rittschof, 2000; Cohen and Forward, 2005)	N/A	N/A	−
Body size	Larger-bodied zooplankton ascend later, and descend earlier than smaller ones to minimize risk of visual predation (De Robertis et al., 2000)	+	+	Pre-spawning period (Feb - Apr)

(i) Shadowing by phytoplankton blooms

Changes in light attenuation due to phytoplankton blooms can affect diel vertical migratory behavior. Kaartvedt et al. (1996) reported that euphausiids and mesopelagic fish ascended by $\sim$ 100 m during the day during periods of decreased light penetration associated with increased chlorophyll concentrations. Similarly, Frank and Widder (2002) found that the daytime depth of euphausiids shoaled by more than 100 m during an influx of turbid water relative to their depth before or after the turbidity event. In a very productive ecosystem like Saanich Inlet, high concentrations of phytoplankton in spring − summer inhibit light penetration (Fig. 2.6), reducing light intensity at 20-m depth to levels comparable to winter conditions (Watanabe, 1978).

Although phytoplankton shadowing is evident in Saanich Inlet, the daytime depth of the euphausiid scattering layer is unlikely to be affected because the oxycline determines their maximum daytime depth. However, it is still possible that phytoplankton shadowing could affect the timing of departure from the daytime depth contributing to the observed seasonal variability in dusk ascent migration timing. Assuming that migration timing is controlled by absolute light intensity, zooplankton may depart their daytime depth earlier during spring − fall (i.e., when phytoplankton are abundant) because light intensity falls below the threshold level earlier. Conversely, during winter, light intensity at the daytime depth is stronger (even with the low insolation) due to the lack of phytoplankton, thereby possibly delaying departure from the daytime depth. These expectations are consistent with the observed early dusk ascent during spring − fall and late ascent during winter. This phytoplankton shadowing effect assumes that the vertical distribution of phytoplankton is similar at dusk as it is during the day, which seems likely given that centric diatoms (which lack locomotory structures) dominate blooms in Saanich Inlet (Takahashi et al., 1978; Grundle et al., 2009). Another assumption is that the daytime depth of the euphausiid scattering layer is constant across seasons, which could not be verified due to the echosounder being deployed shallower than the daytime scattering layer depth. However, it is unlikely a cause of delayed arrival near the surface during winter, because the upward movement of the scattering layer associated with oxygen renewal events in fall (Anderson and Devol, 1973; Manning et al., 2010) should decrease the migration distance. Although local topography might also affect migration timing relative to civil twilight, this possibility could not be assessed in this study due to a lack of continuous irradiance measurements at the VENUS site.

(ii) Food availability

The phototactic response of zooplankton can be modified by food availability. When exposed to low food concentrations, *Daphnia* spp. show an increased phototactic response to decreasing light intensity (Van Gool and Ringelberg, 2003), triggering early ascent. Their response to an increase in relative rate of change in light intensity increases with food concentration (Van Gool and Ringelberg, 1995), predicting that well-fed animals will more readily descend at sunrise (Pearre, 2003). This hunger-satiation hypothesis is also supported by euphausiid species; the continuing downward movement of fed euphausiids *Meganyctiphanes norvegica* and *Thysanoessa rachii* was observed soon after the ascent (Sourisseau et al., 2008). Therefore, time spent in upper layers can be minimized when food availability is high, whereas zooplankton spend more time near the surface when food availability is low (e.g., Huntley and Brooks, 1982; Johnsen and Jakobsen, 1987). This hypothesis could be the case in this study, since winter nights are considerably longer than summer nights, more than compensating for the late dusk ascent and early dawn descent during winter. However, my data show no correlation between migration timings and chlorophyll *a* concentration. Another possibility is that the earlier ascent during spring − fall results from increased competition for food with other migratory species that are more abundant during that period. One difficulty in assessing the effect of food availability is that the depth of the chlorophyll maximum varies between $5 - 20$ m in Saanich Inlet and is not always detected by the fluorometer positioned at a single depth. In addition, euphausiids can switch their diets among phytoplankton, microzooplankton, and suspended organic matter (Mauchline and Fisher, 1969; Dilling et al., 1998; Nakagawa et al., 2004; Pinchuk and Hopcroft, 2007), so chlorophyll *a* concentration is only a proxy of food availability. Thus, the effect of food availability on migration timings remains inconclusive.

(iii) Predator density

Phototactic responses can be modified by chemical cues exuded by predators (i.e., kairomones). In the coastal copepod *Calanopia americana*, the threshold of relative rate of change in light intensity to induce an ascent increases in the presence of kairomones (Cohen and Forward, 2005), suggesting later ascent when predator abundance is high. Similarly, the photoresponse threshold required to initiate descent in larvae of the estuarine crab *Rhithropanopeus harrisii* decreases in the presence

of kairomones (Forward and Rittschof, 2000), resulting in an earlier descent of larvae at sunrise to lower their predation risk. The abundant euphausiids are common prey items for planktivorous fish in Saanich Inlet (Bary et al., 1962; Mauchline, 1980; Mackas et al., 1997). Adult migratory stocks of Pacific herring move into the Strait of Georgia from November until early March before spawning (Haist and Stocker, 1985), and some likely enter Saanich Inlet. Juvenile coho salmon also migrate from the lower Fraser River and Puget Sound into Saanich Inlet by July and August (Holtby et al., 1992). Fish predation pressure therefore varies seasonally due to different species spawning and moving into Saanich Inlet, as well as ontogenic shifts in their diets (Holtby et al., 1992; Adams et al., 2007). Although predation risk likely plays some role in regulating the second-order variability in migration timing, quantification of predator density could not be explored in this study [see 2.2.9 Data Analysis (iv) Application of threshold in Materials and methods].

(iv) Zooplankton body size

Size-dependent migration timing to avoid visual predators contributes to the observed seasonal variability in both dusk ascent and dawn descent migration timings; larger euphausiids during winter ascend later and descend earlier than smaller individuals during summer (Figs. 2.4, 2.7). In Saanich Inlet, juvenile *E. pacifica* ascend as much as 30 min earlier and descend up to 45 min later than adults (De Robertis et al., 2000). Size-dependent migration timing can explain the observed seasonal variability between summer and winter when the euphausiid population is dominated by different size classes (Fig. 2.7). However, early dusk ascent and late dawn descent during late February − April cannot be explained by this hypothesis since the population is dominated by adults at this time. One possible explanation is the energy demand related to the euphausiid reproduction cycle. Spring − summer is a period of intense spawning activity for *E. pacifica* (Parsons et al., 1967; Heath, 1977). Ovarian development and maturation occur over a period of several months prior to spawning (Ross and Quetin, 2000) and euphausiids invest large amounts of energy into reproduction (Virtue et al., 1996; Shaw et al., 2010). Tarling (2003) observed that the greater energy demand required to fuel reproduction appears to drive females to riskier diel vertical migration than males in the northern krill *M. norvegica*. High energy demand for reproduction can thus result in early dusk ascent and late dawn descent to maximize time spent at the food-rich surface during phytoplankton blooms.

2.4.3 More complicated diel vertical migration patterns

Multiple small targets and fewer large targets can result in similar S_v values, because a single-frequency echosounder only measures S_v and cannot distinguish individuals. Thus, my migration-timing detection assumes the arrival/departure of a single scattering layer (dominated by euphausiids) at/from the surface. However, my two-year echosounder time-series also reveals more highly variable and complex patterns, including two-layer upward migration where two layers migrate parallel to each other (Fig. 2.8a) or divergence of a single scattering layer into two or three layers (Fig. 2.8b), two-layer downward migration where divergence of a scattering layer into two layers (Fig. 2.8c) or convergence of two layers into one (Fig. 2.8d), and partial upward (Fig. 2.8e) or downward (Fig. 2.8f) migrations. Establishing a classification scheme of these complex patterns proved difficult due to the presence of confusing migration patterns, variability in thickness and strength of the scattering layers, as well as changes in spatial and temporal separations of multiple scattering layers. The occurrence of these patterns was examined in relation to seasonality, tidal cycle, moon phases and cloud cover, but no clear correlation was found. I suggest that such complex migration patterns are likely comprised of multiple species or multiple life history stages of a single species. They may be regulated by the feeding success of the migrators (Pearre, 2003). For example, a two-layer migration pattern (similar to Fig. 2.8a) comprised of the euphausiid *M. norvgica* and pteropod *Cavoliania inflexa* in discrete bands was observed in the Ligurian Sea (Tarling et al., 2001). A large fraction of the population of *Calanus pacificus* females did not migrate into the surface layer at night, but stayed below the chlorophyll maximum in the $25 - 50$ m range in Dabob Bay, Washington (Dagg et al., 1997). Sourisseau et al. (2008) observed the continuing downward movement of fed euphausiids *M. norvegica* and *T. raschii* soon after the ascent in the St. Lawrence Estuary. Understanding complex migration structures requires tracking not only mass transfer but also the interchange of individuals which is beyond the scope of this study.

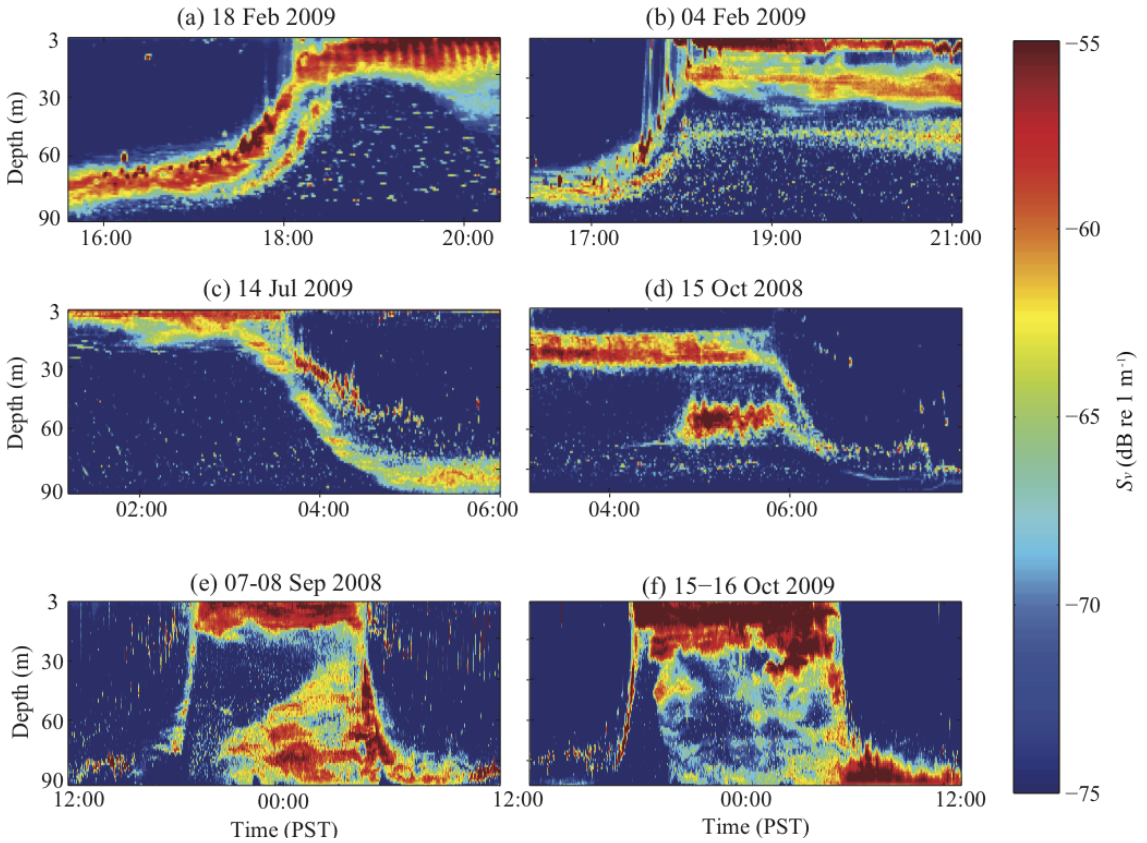

Figure 2.8: Sample echograms of volume backscattering strength S_v (1-min × 1-m bin averages), showing more complicated diel vertical migration patterns including (a, c) two-layer, (b) divergence, (d) convergence, (e) partial upward, and (f) partial downward migrations.

2.4.4 Conclusions

I conclude that a combination of phytoplankton bloom shadowing and the seasonal cycle in average euphausiid body size affect phototaxis behavior determining dusk ascent timing. Seasonal variability in dawn descent timing is most likely regulated by euphausiid body size. It is tempting to suppose that the seasonal correspondence in lags between dusk ascent and dawn descent migration timings (Fig. 2.3d) suggests a common driving mechanism. However, previous studies suggest that the photobiological control of diel vertical migration behavior may differ between ascent and descent phases within a species (Forward et al., 1984; Forward, 1985). The observations suggest that phytoplankton concentration can have higher impact on determining light intensity at daytime depth of the scattering layer than insolation, and likely affects

dusk ascent timing. Two-year time-series also supports the size-dependent migration timing hypothesis (De Robertis et al., 2000), whereby more visually conspicuous larger-bodied euphausiids enter surface waters later and leave earlier than smaller-bodied individuals. However, the pre-spawning period may be an exception to this hypothesis; rather than minimizing visual predation risk, migration timing may be timed to maximize energy gain. The hunger-satiation hypothesis could not be addressed in this study, because I did not include variability in migration timing other than dusk and dawn, such as midnight sinking. Instead of the traditional view of diel vertical migration timing, which is only correlated with civil twilight, this study suggests that euphausiids also adapt their migration timings seasonally to accommodate changes in environmental cues as well as their growth pattern.

Chapter 3

Turbulence and internal waves in Saanich Inlet

3.1 Introduction

The circulation of the oceans plays an important role in the world's climate by moving immense amounts of heat from tropical to polar regions at rates comparable to atmospheric transports (Bryden and Imawaki, 2001). This circulation is maintained by external mixing processes. Such physical processes in the ocean are also important to biology. For example, physical mixing can re-supply nutrients to the euphotic zone, potentially enhancing carbon fixation through photosynthesis. This process is particularly important for the carbon cycle in coastal waters, whose primary production accounts for $\sim 20\%$ of global ocean primary production (Liu et al., 2000; Walsh, 1988) and where most of the organic carbon burial in marine sediments occurs (Hedges and Keil, 1995; Middelburg et al., 1997; Muller-Karger et al., 2005). Ocean currents disperse planktonic organisms, which is a key determinate of the dynamics and structure of marine populations and communities.

In order to understand the role of coastal regions in carbon and nutrient cycling, descriptions from many settings are necessary due to the heterogeneity of the coastal ocean (Liu et al., 2000). Saanich Inlet, located in southern Vancouver Island, is an inverse estuary with its dominant freshwater supply outside the inlet mouth (Herlinveaux, 1962). In addition to infrequent deep-water renewals due to the sill located at the inlet mouth (e.g., Anderson and Devol, 1973), large settling fluxes of organic matter arising from high primary production (Timothy and Soon, 2001; Grundle

et al., 2009) cause deep-water anoxia for most of the year. Much of the primary production is by diatoms (Takahashi et al., 1978; Grundle et al., 2009), which are significant vectors of carbon flux in coastal settings (e.g., Waite et al., 1992; Kiørboe et al., 1994; Kemp et al., 2000). Zooplankton play a key role in the biological pump through grazing of phytoplankton and subsequent egestion of larger and hence more rapidly sinking fecal pellets (Ducklow et al., 2001; Turner, 2002). Vertically migrating zooplankton can further increase the efficiency of the biological pump, by consuming organic particles at the surface at night and excreting inorganic nutrients below the mixed layer during the day (Longhurst and Harrison, 1988, 1989; Longhurst et al., 1990). Saanich Inlet has an unusually abundant population of vertically migrating euphausiids, principally *Euphausia pacifica*, whose scattering layer densities are 10 − 10,000 ind. m^{-3} (Bary et al., 1962; Bary, 1966; Pieper, 1971; Mackie and Mills, 1983).

Due to productive populations of phytoplankton and zooplankton, Saanich Inlet appears to serve as a nursery for stocks of herring, hake and dogfish (Barraclough and Herlinveaux, 1961). Understanding of population dynamics and recruitment success of zooplankton is essential, because they (especially euphausiids) are a key prey item for these fish (Mauchline, 1980; Mackas et al., 1997). Copepods, early life-stages of euphausiids and larval fish are non-migratory (e.g., Brinton, 1962; Lu et al., 2003), suggesting that they are likely transported and dispersed by currents. Although observations of consistently high euphausiid population since 1960's (Bary et al., 1962; Pieper, 1971; De Robertis, 2001) suggest that the population is likely retained within the inlet, the retention mechanism cannot be addressed without characterization of currents.

Saanich Inlet has been considered to be a physically quiet environment (e.g., Gargett et al., 2003). However, no continuous measurement of currents and turbulence has been made to allow quantitative characterization. Sporadic measurements in previous studies suggest that typical turbulent dissipation rates in the inlet are O(10^{-9} W kg^{-1}), which correspond to diapycnal eddy diffusivities of O(2×10^{-6} m^2 s^{-1}) (Gargett et al., 2003; Kunze et al., 2006; Rousseau et al., 2010). This is too small to account for inferred vertical nitrate flux of O(4 mmol m^{-2} d^{-1}) in order to sustain significantly elevated primary production in the inlet (Gargett et al., 2003). Instead, Gargett et al. (2003) have shown that pressure gradient forces set up in the Strait of Georgia and the passages leading to Saanich Inlet, such as Haro Strait and Boundary Passage, cause intermittent upwelling of nutrient-rich waters throughout the inlet in

summer. However, without long time-series measurements, turbulent mixing within the inlet cannot be ruled out as a path of nutrient re-supply to the euphotic zone, because occurrence of high dissipation rates can easily be missed due to the intermittent nature of turbulence. Currents in Saanich Inlet have not been previously quantified, and their effects on dispersal of organisms are unknown. Gargett et al. (2003) suggest surface outflow and mid-depth ($\sim$ 50 m) inflow during spring tides, but the strengths of in- and outflows were not measured.

Characterization of the physical environment in Saanich Inlet is also motivated by the idea of a linkage between diel vertical migration and biologically generated turbulence. Kunze et al. (2006) reported one turbulent burst of O($10^{-5} - 10^{-4}$ W kg^{-1}) in two dusk microstructure time-series. Based on the similar timing of increased turbulent mixing and zooplankton vertical migration, they suggested that the school of vertically migrating euphausiid was the cause of the observed turbulent burst, and the burst could potentially mediate transport of nutrients toward the euphotic zone. No recurrence of turbulent bursts coincident with diel vertical migration was observed in follow-up field observations in Saanich Inlet (Rousseau et al., 2010) nor other regions (Rippeth et al., 2007). Clearly, not all dusk ascents and dawn descents of euphausiids produce intense turbulence, and the strong turbulence observed by Kunze et al. (2006) may have been caused by physical processes such as non-linear internal waves. Low temporal resolution based on ship-board microstructure measurements used in previous studies could have missed turbulent bursts, because of the heterogeneity associated with the patchiness of schooling animals and the intermittent nature of turbulence generation. This motivates a field experiment, which collects continuous records of turbulence, currents and acoustic backscatter, designed to isolate biological effects of turbulence from physical ones.

The goal of this study is to characterize turbulence and internal waves in Saanich Inlet, which allows us to examine (i) whether turbulent mixing can be a mechanism of nutrient re-supply to the euphotic zone, (ii) whether physical processes or diel vertical migration of euphausiids are likely the source of the turbulent burst reported by Kunze et al. (2006), and (iii) effects of currents in dispersing planktonic organisms. Here, I present 27-d time-series of turbulent dissipation rates estimated from a 6-MHz Acoustic Doppler velocimeter (ADV), and current velocities measured by a 300-kHz Acoustic Doppler Current Profiler (ADCP) deployed on two moorings. Echosounder data measured at the Victoria Experimental Network Under the Sea (VENUS) cabled observatory are used to examine the possibility of biological generation of turbulence.

3.2 Materials and methods

3.2.1 Study site

Data were collected in Saanich Inlet (48° 39.1'N, 123° 29.2'W), British Columbia (Fig. 3.1), during 3 − 30 September 2010. Saanich Inlet is a fjord, with a 75-m sill at its mouth and maximum depths exceeding 200 m (Herlinveaux, 1962). It is an embayment with its major supply of freshwater outside the inlet mouth. The Cowichan River in winter and the Fraser River freshet in summer produce a year-round stabilizing salinity gradient in the upper water column (Herlinveaux, 1962). In 2010, the Fraser River had a maximum discharge of O(6000 m^3 s^{-1}) in June and reduced to O(2000 m^3 s^{-1}) in September, and the Cowichan River had a maximum discharge of O(200 m^3 s^{-1}) in December − January. Wind and tidal forcing in Saanich Inlet are generally weak (Gargett et al., 2003). The estuarine circulation is normally too weak to permit flushing of deeper waters below the sill, so that a secondary halocline exists at sill depth (Herlinveaux, 1962). High primary production ($\sim$ 475 g C m^{-2} yr^{-1}), combined with infrequent deep-water replenishment, contribute to the formation of deep-water anoxia during much of the year (Timothy and Soon, 2001; Grundle et al., 2009). There are typically two renewal events per year in Saanich Inlet where dense oxygenated waters enter the mouth at the sill depth, shoaling deep anoxic waters upward; deep-water renewal (well below the sill depth, but not renewing the bottom) during spring, and bottom-water renewal during fall (Anderson and Devol, 1973; Manning et al., 2010).

Resident euphausiid populations show diel vertical migration behavior (Sato et al., 2013), and their schooling behavior might be a source of turbulence (Kunze et al., 2006). Year-round dominance of euphausiids in Saanich Inlet is documented in previous studies through optical images (Jaffe et al., 1998), visual observations (Mackie and Mills, 1983), and net samplings (De Robertis, 2001; Sato et al., 2013). *Euphausia pacifica* is the most abundant euphausiid throughout the year, constituting 77 − 100% of all euphausiids (Bary et al., 1962; Pieper, 1971; De Robertis, 2001). Densities of euphausiids within the scattering layers range from 10 − 10,000 ind. m^{-3} (Bary et al., 1962; Bary, 1966; Pieper, 1971; Mackie and Mills, 1983), accounting for $\sim$ 70% of the daytime and $\sim$ 76% of the night-time scattering layers (Holliday and Pieper, 1995; De Robertis, 2002).

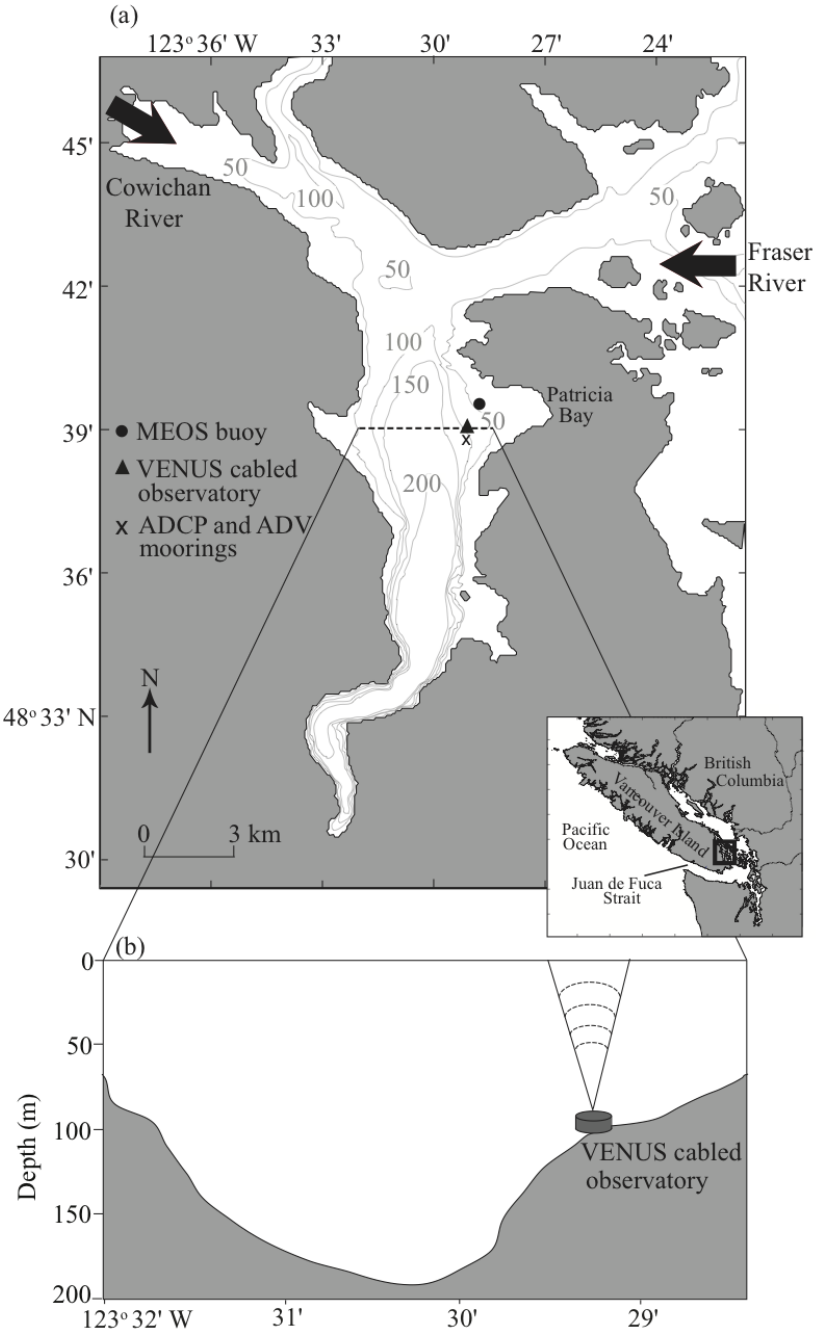

Figure 3.1: (a) Locations of the Marine Ecosystem Observatories (MEOS) buoy 46134, the VENUS cabled observatory, and the moorings of an ADCP and ADV in Saanich Inlet, located on the southeastern tip of Vancouver Island, British Columbia (inset). Bold arrows indicate major sources of freshwater input from the Cowichan River (winter) and Fraser River (summer). (b) Vertical section, showing the change in bathymetry across Saanich Inlet near the VENUS cabled observatory.

3.2.2 Instrumentation and data processing

Two moorings and the VENUS cabled observatory were located in Patricia Bay on the eastern shelf which is $\sim$ 100-m deep. They were 4.6 km south of the sill and 1.1 km east of the main channel. Both moorings were deployed within 200 m of the VENUS cabled observatory (Fig. 3.1).

ADCP

Current velocities throughout the water column were measured by a 300-kHz ADCP (Workhorse Sentinel; Teledyne RD Instruments), with a vertical bin size of 2 m and sampling frequency of 1 Hz. The ADCP was deployed on a metal frame at $\sim$ 96-m depth during 3 $-$ 30 September 2010 (Fig. 3.2a). Based on relatively constant temperature (9.5 $\pm$ 0.03 °C) and Absolute Salinity (31.3 $\pm$ 0.02 g kg^{-1}) measured by the VENUS CTD at 95-m depth during 3 $-$ 30 September 2010, a constant sound speed of 1485 m s^{-1} was applied to calculate ranges and velocities throughout the water column. Temporal changes in sound speed at the ADCP transducer depth was very small ($< 0.1\%$), so their effect on measured velocities was minimal. Sound speed computed from the CTD vertical profiles varied between 1484 $-$ 1502 m s^{-1} with depth, resulting in up to 0.22-m error in range estimates at 96-m range. The variation of sound speed with depth does not affect measurement of horizontal currents. Raw velocity values were averaged into 1 min, where the uncertainty in horizontal velocity measurements in terms of standard deviation was 0.01 m s^{-1}.

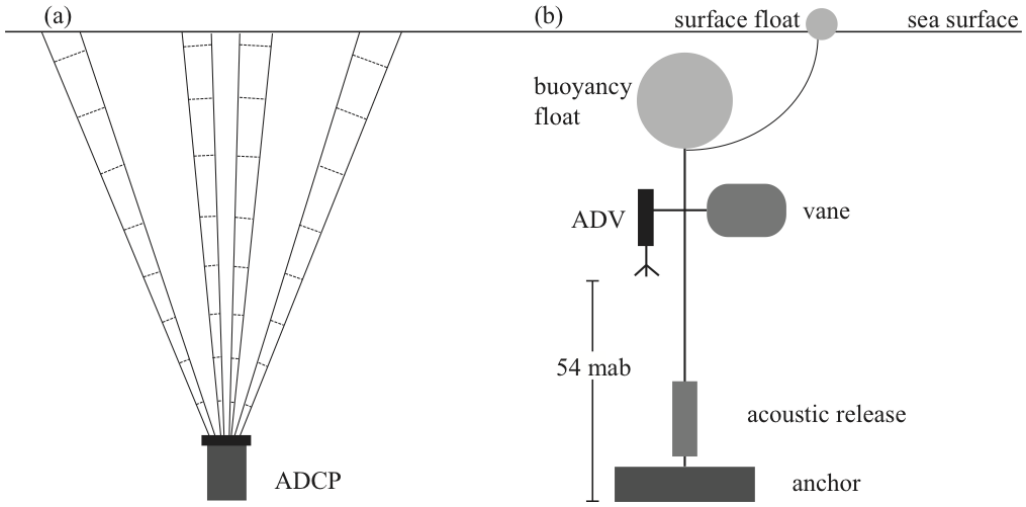

Figure 3.2: Schematic of two moorings with (a) an ADCP and (b) ADV. The orientation of the ADV was downward during 3 − 16 September (shown in b), and upward during 17 − 30 September 2010 (not shown).

ADV

Turbulent dissipation rates were estimated based on velocity measurements at a single point from a 6-MHz ADV (Vector; Nortek AS). The vertical location of the ADV sensing volume is 0.16 m from the transducer. In addition to three components of velocity (u, v, w), the ADV returned signal-to-noise ratio (SNR) and correlation on each of the three beams at 8 Hz. Heading, pitch and roll of the ADV were measured at 1 Hz. The ADV was located $\sim$ 54 meters above bottom (mab) in $\sim$ 96-m water column (Fig. 3.2b). A vane on the mooring oriented the ADV into the currents. If diel vertical migration of euphausiids is a source of turbulence, turbulence measurements can be affected by the orientation of the ADV because of the directional movement of the schooling euphausiids at dawn and dusk. In order to examine possible such effects of the ADV's vertical orientation on turbulent dissipation estimates, the ADV was deployed downward during 3 − 16 September (pitch = 2°, roll = 8°) and upward during 17 − 30 September 2010 (pitch = -20°, roll = 16°). The ADV data were marked bad when the SNR $<$ 6 dB and correlation $<$ 70% at any of the three acoustic beams (Elgar et al., 2005; Feddersen, 2010; Bryan et al., 2003). Data rejected according to these criteria were 5% of the time-series during 3 − 16 September and 12% during 17 − 30 September. Those data were removed and replaced by linear interpolation.

Horizontal velocities (u, v) were contaminated by mooring motions, but not w.

Therefore, turbulent measurements were estimated from w. Effects of mooring motion, recognized in the compass record, on the measured velocity data were examined. Mooring motion was likely caused by changes in tension of the mooring wire due to surface waves, or vibration of the vane attached to the ADV (Fig. 3.2b). In order to quantify its effect on the velocity measurements, variations in heading, pitch and roll were examined by taking the first difference ($\frac{d\theta}{dt}$). Values of $\frac{d\theta}{dt}$ in heading were much larger than those of pitch and roll, likely due to the 2° accuracy of the compass compared to the 0.2° for the tilt sensor. Variations in heading were sometimes larger, suggesting rotational jitter of the sensor.

Time-series of mooring motion ($u_{vibration}$, $v_{vibration}$) were estimated to examine whether there was correlation with measured velocities (u, v, w), using cross-spectral analysis. Mooring motion in u and v directions was estimated based on heading [$\theta(t)$] and distance between the ADV and mooring wire (r);

$$u_{vibration} = -r \sin\theta(t) \frac{d\theta(t)}{dt} \tag{3.1}$$

$$v_{vibration} = r \cos\theta(t) \frac{d\theta(t)}{dt}. \tag{3.2}$$

The velocities (u, v, w) measured at 8 Hz were downsampled to 1 Hz to match with the sampling frequency of the estimated vibration velocities ($u_{vibration}$, $v_{vibration}$). Cross-spectral analysis was conducted during periods of vibration and non-vibration for comparison. Velocity spectra of 1536-pt (25.6-min) were calculated based on block-averaging of five segments, with each segment using 512-pt (8.5-min) FFT with 50% overlap. The strength of the correlation was given by the coherence spectrum, $\gamma^2(f)$, ranging between $0 - 1$.

Mooring motion affected the ADV heading sporadically throughout its deployment. When mooring motion was present, spectra of u, v, $u_{vibration}$ and $v_{vibration}$ showed peaks at (3-6) $\times 10^{-2}$ Hz, while there were no such peaks in w (Fig. 3.3 a1). When u and v were not affected by mooring motions, these spectral peaks were absent (Fig. 3.3 a2). Velocity spectra sometimes showed other peaks at higher frequencies such as 3 Hz. Correlation of the high-frequency peaks with mooring motion could not be examined based on heading data, because the Nyquist frequency of heading measurements (0.5 Hz) were lower than these frequencies. Coherence spectra between the horizontal velocities (u, v) and estimated vibration velocities ($u_{vibration}$, $v_{vibration}$) during vibration periods showed $\gamma^2(f) = \sim 0.75$ at (3-6) $\times 10^{-2}$ Hz (Fig. 3.3 b1, c1), suggesting contamination of the horizontal velocities by mooring motion. Coherence

values between w and $u_{vibration}$ or $v_{vibration}$ during mooring motion periods were much lower (Fig. 3.3 d1), which is similar to those during non-vibration period (Fig. 3.3 b2-d2). Effects of mooring motion on horizontal velocity measurements were also observed in the time-series record. For example, when the ADV moved from north to south (decrease in $v_{vibration}$), currents appeared to move from south to north, resulting in an increase in measured v (Fig. 3.4b). This relationship confirmed that rotational vibration of the ADV was the cause of some of the horizontal velocity fluctuations observed.

Similarly, effects of mooring motion in w were estimated based on pitch and roll. Values of $\frac{d\theta}{dt}$ in pitch and roll were mostly within $\pm$ 0.3° so the estimated $w_{vibration}$ was significantly smaller than measured w. Therefore, turbulent measurements were estimated from w to avoid vibrational contamination.

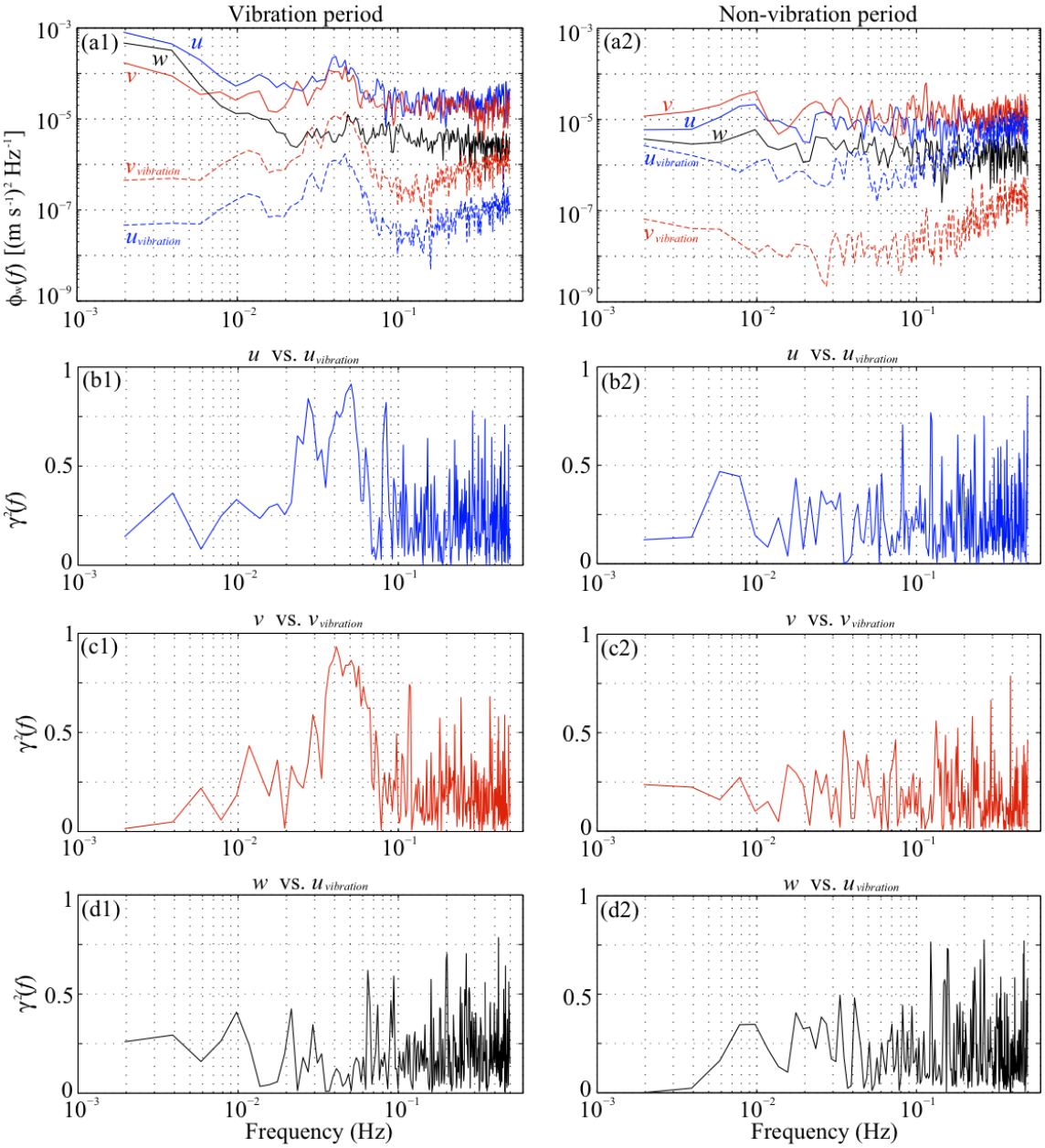

Figure 3.3: Examples of vibration effects on velocity measurements: (a1-d1) vibration period on 7 September vs. (a2-d2) non-vibration period on 18 September 2010. Power spectral densities of velocities (a), squared coherence between measured u and estimated vibration velocity $u_{vibration}$ (b), v and $v_{vibration}$ (c), and w and $u_{vibration}$ (d).

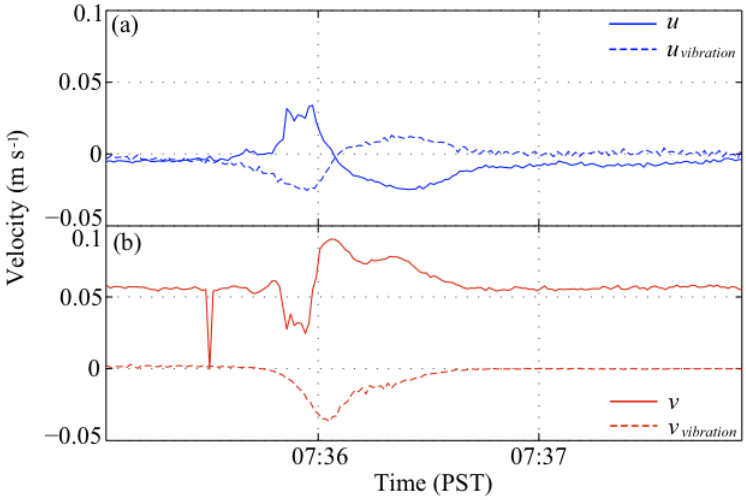

Figure 3.4: Comparison of measured and estimated mooring motion velocities in (a) u and (b) v, based on the heading data on 18 September 2010.

Echosounder

Diel vertical migration of zooplankton was monitored with an upward-looking 200-kHz echosounder (Acoustic Water Column Profiler; ASL Environmental Sciences Inc.) mounted on a metal frame at 95-m depth ($\sim$ 2 mab) (Fig. 3.1a). A CTD (SBE 16plus; Sea-Bird Electronics Inc.) was deployed on the same frame. Both instruments were linked to the VENUS cabled observatory (http://venus.uvic.ca), and were serviced and cleaned twice a year to remove biofouling. Backscattered acoustic signals from particles in the water column were digitized (8-bit resolution) into 12.5-cm depth bins, with a sampling interval of 2 s, pulse duration of 300 μs, and beam width of 8°, then converted to S_v using the standard sonar equation (e.g., Urick, 1983). The echosounder (AWCP 1007) was calibrated using a 38.1-mm-diameter tungsten carbide sphere as prescribed by Vagle et al. (1996) (see Appendix for details). Due to the mechanical problems, data gaps were present during 7 − 9 and 16 − 17 September 2010 in echosounder time-series.

Additional data

CTD (SBE 19plus; Sea-Bird Electronics Inc.) profiles were collected near the mooring sites on 3, 16, 17, 23 and 30 September 2010 with one vertical profile each day. A CTD profile collected at central part of Saanich Inlet (48° 35.6'N, 123° 30.0'W)

in deep water on 19 August 2010 was provided by F. Whitney (personal communication). Winds were monitored hourly $\sim$ 5 m above the sea level at the Marine Ecosystem Observatories (MEOS) buoy 46134 (48° 39.6'N, 123° 28.8'W; Fig. 3.1a). Daily discharge rates of the Fraser River and Cowichan River were obtained from the Archived Hydrometric database (Water Survey of Canada; http://www.wsc.ec.gc.ca/applications/H2O/index-eng.cfm).

3.3 Results

3.3.1 Physical environment

During September 2010, the water column in Saanich Inlet was well-stratified (Fig. 3.5). A surface mixed layer was only evident in the upper 4 m on 3 and 23 September. Temperature, salinity and density profiles on 16 − 30 September showed similar patterns, but the profile on 3 September showed warmer surface temperature, and lower salinity and density than other profiles in the upper 40 m. Due to the limited number of CTD casts, factors affecting the profile on 3 September could not be determined. Variation in buoyancy frequency among profiles at upper 10 m was due to a weak pycnocline. Relatively uniform stratification of 1.63×10^{-2} s^{-1} was observed over 10 − 82 m depth, decreasing to 0.89×10^{-2} s^{-1} in the bottom boundary layer at 82 − 100 m depth. Wind forcing within Saanich Inlet was generally weak, with wind speeds < 4 m s^{-1}. There was little difference in wind speeds between the deployment periods of the different ADV orientations; 2.41 ± 1.57 m s^{-1} during 3 − 16 September, and 2.30 ± 1.73 m s^{-1} during 17 − 30 September.

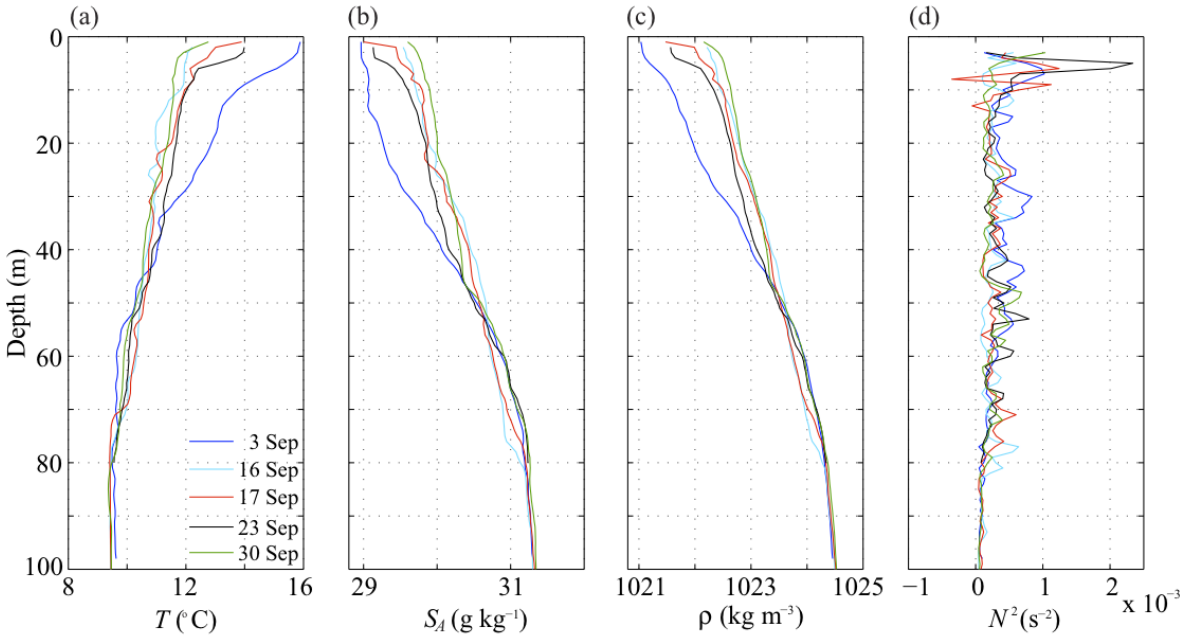

Figure 3.5: Vertical profiles (1-m bin averages) of (a) temperature T, (b) Absolute Salinity S_A, (c) density ρ, and (d) buoyancy frequency squared N^2 during September 2010 in Saanich Inlet.

3.3.2 Turbulence

(i) Estimates of turbulent dissipation rates

Assuming isotropy (e.g., Gargett et al., 1984), a single component of the velocity fluctuations, w, was used to estimate turbulent dissipation rate ϵ. The velocity wavenumber spectrum of turbulence is

$$\phi_w(k) = \alpha\epsilon^{2/3}k^{-5/3} \tag{3.3}$$

where α is a constant approximately equal to 0.5, and k wavenumbers (Thorpe, 2005). Estimates of wavenumber spectra can be converted to frequency spectra with the flow speed U

$$\phi_w(f) = \alpha\epsilon^{2/3}\left(\frac{2\pi}{U}\right)^{-2/3} f^{-5/3} = af^{-5/3} \tag{3.4}$$

where the amplitude a and flow speed U are defined as

$$a = \alpha\epsilon^{2/3}\left(\frac{2\pi}{U}\right)^{-2/3} \tag{3.5}$$

$$U = (< u >^2 + < v >^2)^{1/2}. \tag{3.6}$$

Amplitude is estimated from the velocity spectra multiplied by $f^{5/3}$, and the average is taken over a specified frequency range

$$a =< \phi_w(f)f^{5/3} > . \tag{3.7}$$

By converting the model wavenumber spectrum of turbulence (Eq. 3.3) to a frequency spectrum (Eq. 3.4), constant frequency range can be used to estimate a regardless of the changes in U. Therefore, dissipation rates can be estimated based on the amplitude

$$\epsilon = \left(\frac{a}{\alpha}\right)^{3/2}\left(\frac{2\pi}{U}\right). \tag{3.8}$$

Isotropy was confirmed by estimating turbulent dissipation rates based on u, v and w during a period of no vibration. During a period of strong turbulence, the velocity spectra were very similar among the horizontal and vertical velocities with the estimated ϵ varying between (1.2-1.6) $\times 10^{-7}$ W kg^{-1} (Fig. 3.6a). During a period

of weak turbulence, on the other hand, the estimated ϵ based on horizontal velocities was $5-7$ times higher than ϵ based on w (Fig. 3.6b). Gargett et al. (1984) provide a criterion for when ϵ may safely be estimated from a single measured component of the stress tensor

$$\epsilon > 50^{4/3}\nu N^2 \tag{3.9}$$

where ν is the kinematic viscosity. Assuming $\nu = 1.37 \times 10^{-6}$ m^2 s^{-1} (9.5°C, 31.3 g kg^{-1}) and $N = 1.63 \times 10^{-2}$ s^{-1}, $\epsilon > 7 \times 10^{-8}$ W kg^{-1}. Therefore, estimated ϵ values based on w likely underestimate turbulent dissipation rates ϵ weaker than 7×10^{-8} W kg^{-1}, though not necessarily the turbulent diffusivity K.

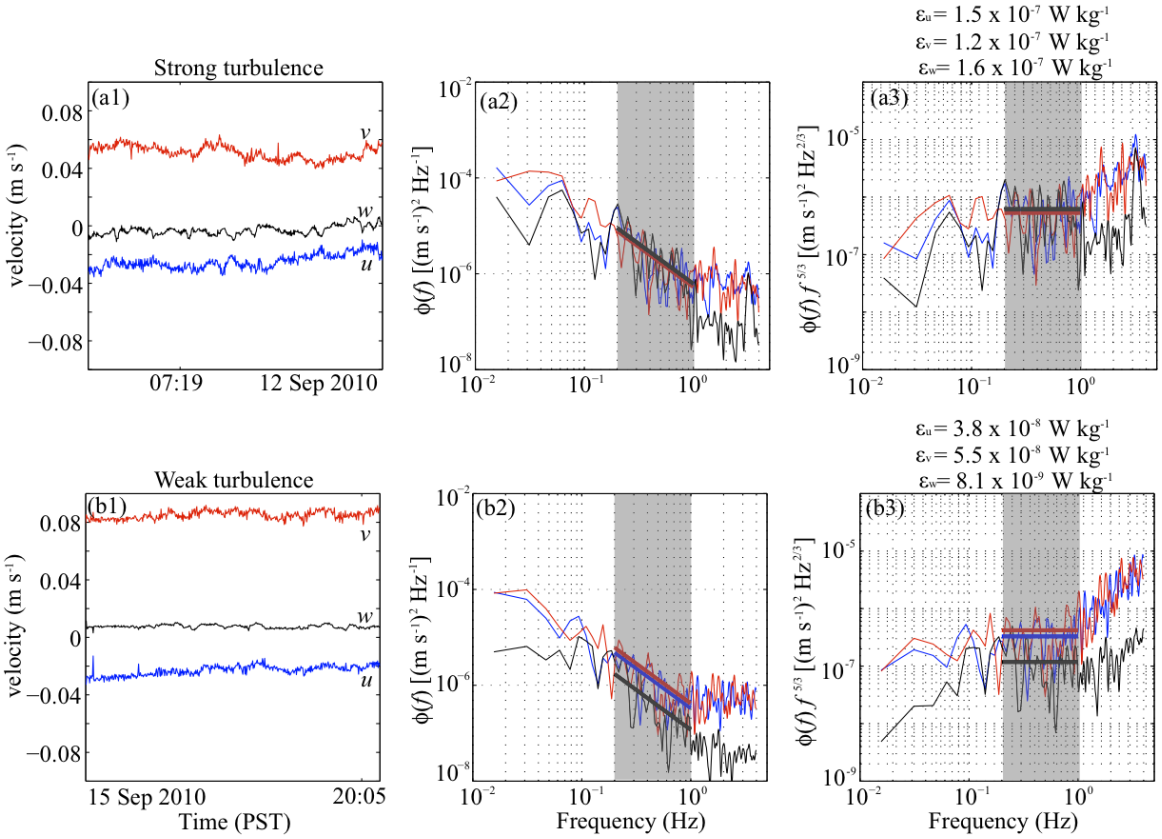

Figure 3.6: Examples of (a) isotropic and (b) non-isotropic turbulence; (a1, b1) time-series of velocities, (a2, b2) power spectral density of velocities with the -5/3 slope of Kolmogorov's law, and (a3, b3) the spectra multiplied by $f^{5/3}$ to estimate amplitude a shown in solid lines. The frequency range used to estimate amplitude a is shown in gray.

Velocity spectra were calculated based on 512-pt (64-s) FFT with 50% overlap. Assuming an average velocity of 5 cm s^{-1}, 64-s corresponds to a length-scale of 3.2 m. As the scattering layer is about $10 - 15$ m thick and lasts for $20 - 30$ min, a 64-s FFT should therefore be sufficient to capture any biologically generated turbulence. The frequency range to estimate amplitude was determined based on the velocity spectra showing turbulent characteristics over $0.2 - 1.0$ Hz. Estimated dissipation rates including all spectra were used to calculate upper-bound averages. Lower-bound averages were obtained by rejecting ϵ if the vertical velocity spectrum was not consistent with a -5/3 power law over the frequency range (Bryan et al., 2003; Jones and Monismith, 2008; Feddersen, 2010). For each spectra, the best-fit power-law exponent μ (with standard deviation $\pm\ \sigma$) was estimated by a least squares fit of $\log[\phi_w(f)]$ with $\log(f)$ over frequencies $0.2 - 1.0$ Hz, as in the examples (Fig. 3.7). The consistency of the estimated μ with -5/3 and the error of the fit σ was tested. Estimate of ϵ was rejected if the μ falls outside of the region

$$\mu - 0.6 \leqq -5/3 \leqq \mu + 0.6 \tag{3.10}$$

or σ falls outside of the region

$$\sigma \leqq 0.45. \tag{3.11}$$

Threshold values were determined through visual examination of spectra. Change of threshold value in Eq. 3.10 from 0.6 to 0.8 resulted in increase of lower-bound averages by 1.3 times. The effect of the choice of threshold value in Eq. 3.11 was minimal for the threshold larger than 0.4.

The first example ($\mu \pm \sigma$ = -1.75 $\pm$ 0.21; Fig. 3.7a) passes both μ and σ tests (Eqs. 3.10, 3.11), whereas the second example ($\mu \pm \sigma$ = -0.63 $\pm$ 0.37; Fig. 3.7b) fails the μ test, and the third example ($\mu \pm \sigma$ = -1.97 $\pm$ 0.50; Fig. 3.7c) fails the σ test. Values of μ fall within the range of -3 and 1.5 (Fig. 3.8). Increased μ values during $17 - 30$ September toward the expected power slope of noise ($\mu = 0$) suggest the increased noise level during this period. Differences in skewness between the two deployment periods (Fig. 3.8b, c) likely result from differences in the noise induced by the different orientations of the ADV. Values of σ fall within the range of 0.2 and 0.5, with very similar PDF patterns between $3 - 16$ and $17 - 30$ September (Fig. 3.9). Estimates of ϵ that failed those tests were replaced by zero to calculate lower-bound averages.

In addition to the μ and σ tests, magnitudes of the time-averaged velocity U were

examined because very small U values can result in high ϵ estimates (Eq. 3.8). In order to avoid this effect, ϵ estimates based on U where

$$U < 0.01 \quad [\text{m s}^{-1}] \tag{3.12}$$

were rejected and replaced by zero to calculate lower-bound estimates. Removal of these ϵ values resulted in decrease of lower-bound averages for 8% during $3 - 16$ September, and 44% during $17 - 30$ September. Taylor's frozen-turbulence hypothesis was also tested in its applicability for this study. The assumption states that the turbulent structures move as frozen entities transported by the mean velocity. It is only valid if

$$\frac{u}{U} << 1 \tag{3.13}$$

where u is the turbulent velocity signal (Tennekes and Lumley, 1972). By integrating the vertical velocity spectra in inertial subrange (e.g., Fig. 3.7a), u was estimated as

$$u = \left(\int_{0.125 \text{ Hz}}^{2 \text{ Hz}} \phi_w(f) df \right)^{1/2} \approx 2.5 \times 10^{-3} \text{ [m s}^{-1}\text{]}. \tag{3.14}$$

A few U values below this threshold were observed. Since this threshold is much lower than 0.01 m s^{-1} (a criteria for U to avoid overestimation of ϵ; Eq. 3.12), ϵ estimates which do not hold the Taylor's hypothesis were replaced by zero to calculate lower-bound averages. During $3 - 16$ September, 22% of the spectra pass all the tests, while only 4% of the spectra pass the tests during $17 - 30$ September.

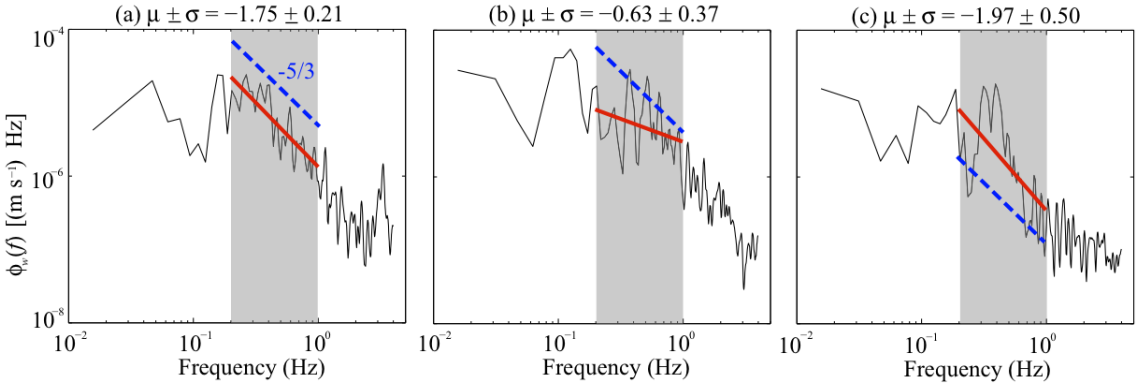

Figure 3.7: Examples of vertical velocity spectra $\phi_w(f)$ which (a) pass both the μ and σ tests, (b) fail the μ but pass the σ test, (c) pass the μ but fail the σ test. The frequency range used to estimate the power-law exponent μ (red solid line) is shown in gray and a -5/3 power slope in blue dotted line.

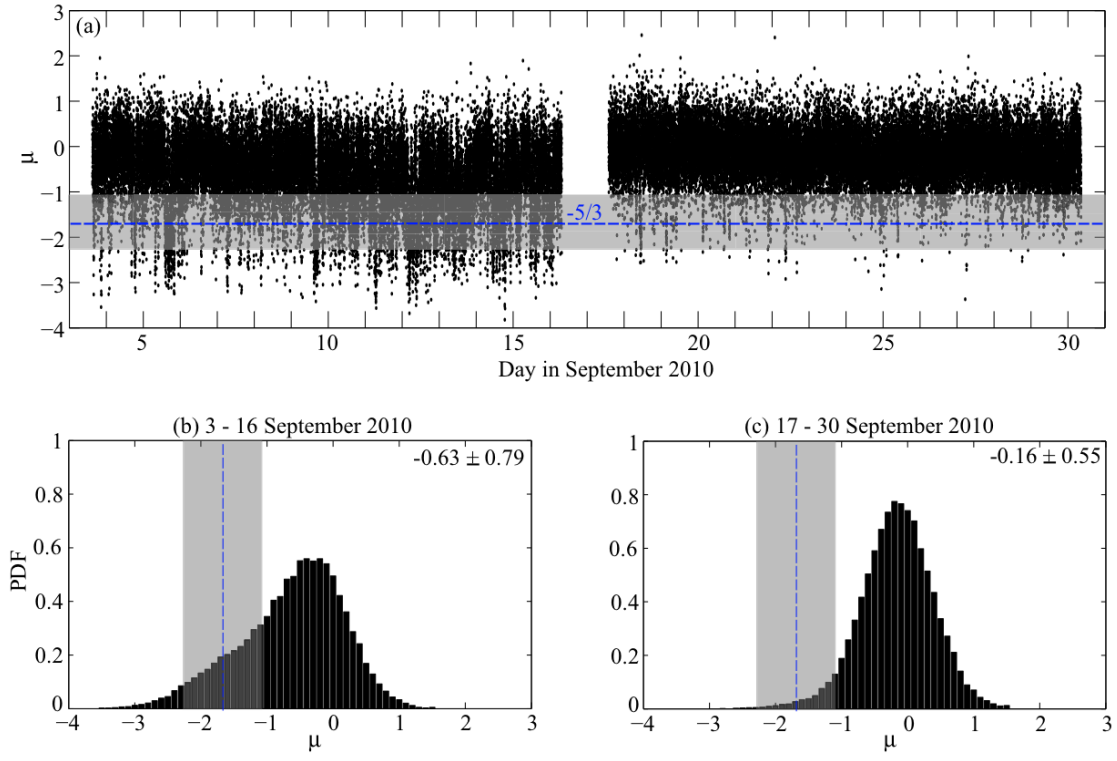

Figure 3.8: (a) Time-series of the power-law exponent μ. Total PDFs during (b) 3 − 16 September and (c) 17 − 30 September. Expected power slope in an inertial subrange (μ = -5/3) is shown in blue dotted line, and the passing range of μ values based on Eq. 3.10 in gray.

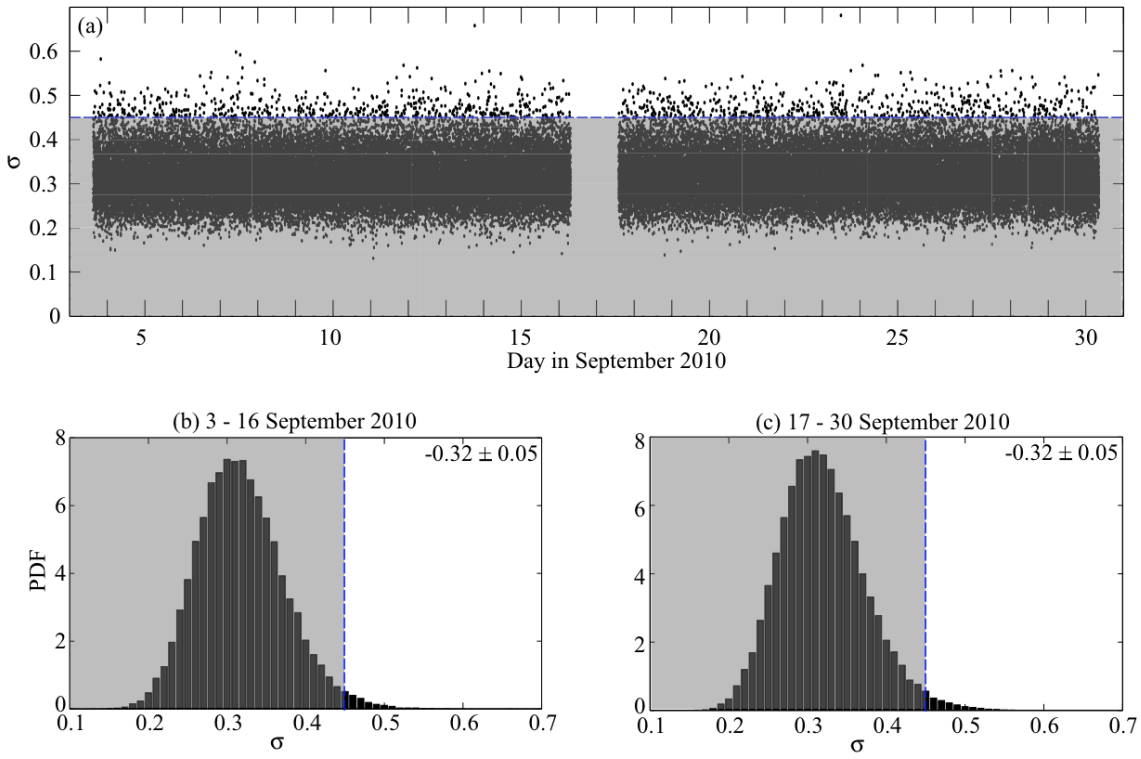

Figure 3.9: (a) Time-series of the standard deviation σ of power-law exponent μ. Total PDFs during (b) $3-16$ September and (c) $17-30$ September. Threshold value of 0.45 is shown in blue dotted line, and the passing range of σ values based on Eq. 3.11 in gray.

During $3-16$ September, average kinetic energy dissipation rates ϵ are (0.6-1.7) $\times\ 10^{-8}$ W kg^{-1} with the lower bound based on non-turbulent data zeroed out and the upper bound including all estimates (Fig. 3.10). During this period, 22% of the spectra were well-fit by the turbulence model. Based on lower-bound estimates of ϵ, the maximum value achieved is $2.3\ \times\ 10^{-6}$ W kg^{-1} and 1.3% of ϵ exceed 10^{-7} W kg^{-1}. These high dissipation rates last for a maximum of 4.8 min.

During $17-30$ September, average ϵ are (0.5-11.5) $\times\ 10^{-8}$ W kg^{-1} with only 4% of the data turbulent. The upper-bound estimate in this period is likely biased high due to the higher noise level (possibly due to the effect of the ADV orientation). Based on lower-bound estimates of ϵ, the maximum value achieved is $1.4\ \times\ 10^{-6}$ W kg^{-1}, and 1.9% of ϵ exceed 10^{-7} W kg^{-1}. These high dissipation rates last for a maximum of 6.9 min.

Diapycnal eddy diffusivity K is estimated as

$$K = \frac{\gamma\epsilon}{N^2} \tag{3.15}$$

where γ is a mixing efficiency of 0.2 following standard microstructure practice (Osborn, 1980; Oakey, 1982; St. Laurent and Schmitt, 1999). Using 12-d averages of lower- and upper-bound estimates of ϵ and vertically-averaged N of $1.63\ \times\ 10^{-2}$ s^{-1} at $10-82$ m (Fig. 3.5d), K = (4.7-12.5) $\times\ 10^{-6}$ m^2 s^{-1} during $3-16$ September, and K = (4.0-86.6) $\times\ 10^{-6}$ m^2 s^{-1} during $17-30$ September. Since the higher noise level allowed very few turbulence measurements, upper-bound estimates during $17-30$ September are not considered further.

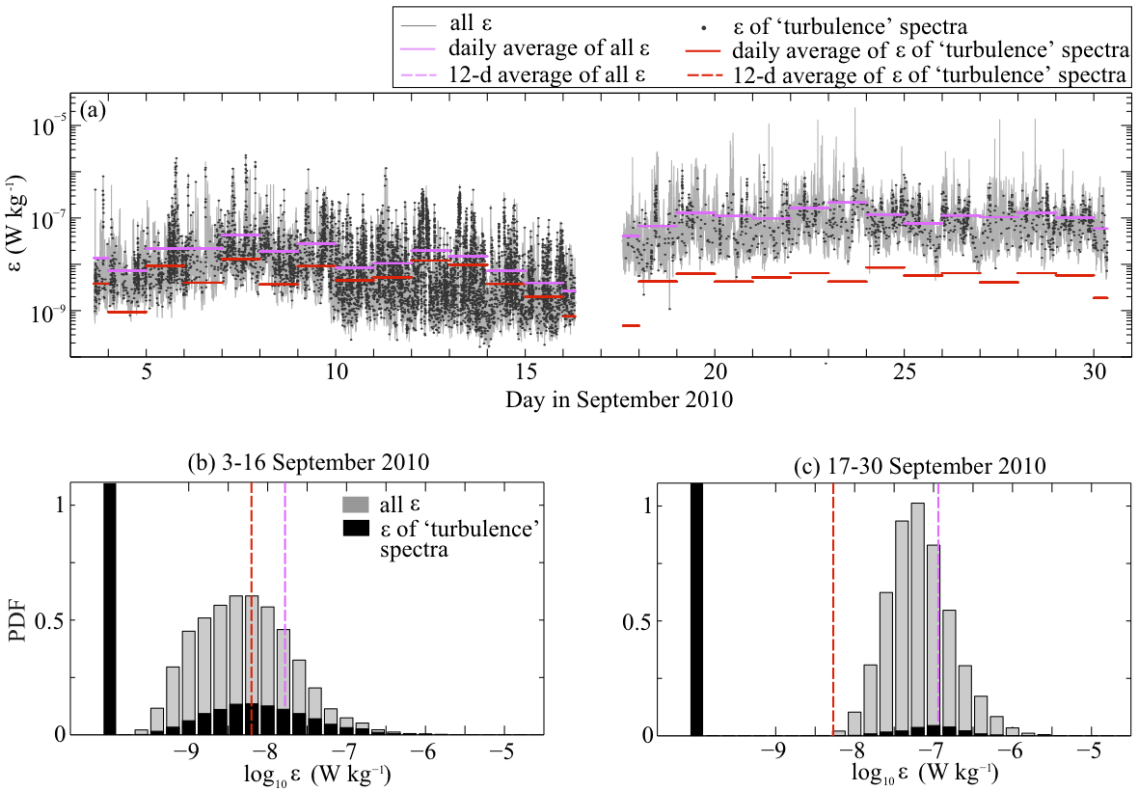

Figure 3.10: (a) Comparison between the two daily-averaged dissipation rates: all ϵ values included (upper-bound estimates) vs. ϵ of turbulent spectra only (lower-bound estimates). (b, c) Corresponding total PDFs for both estimates; the mean of each distribution was indicated with vertical dotted lines.

(ii) Biological generation of turbulence

I compare the observed turbulence with volume backscattering strength S_v from the 200-kHz echosounder at the VENUS cabled observatory, in order to determine if there is a correlation between diel vertical migration of zooplankton and turbulence at the study site. An example echogram shows typical nocturnal diel vertical migration (Fig. 3.11a); upward movement of the scattering layer towards the surface at dusk and downward movement to deeper waters at dawn. Diel vertical migration behavior was observed throughout the period of mooring deployment in September 2010. The S_v at $\sim$ 45 m (approximate ADV deployment depth) shows the peaks at dawn and dusk corresponding to diel vertical migration (Fig. 3.11b), but ϵ does not have the corresponding peaks (Fig. 3.11c). These patterns also apply to ϵ averaged over various timescales at 5-, 10-, 20-, 40- and 60-min. Since diel vertical migration typically

lasts for about 20 min at $\sim$ 45 m, 40-min averaging should capture increased S_v associated with migration events. Comparing 40-min averaged ϵ at noon, midnight, dusk and dawn, there is no significant difference in ϵ values (Fig. 3.12). If diel vertical migration were a significant source of turbulence, a positive correlation between ϵ and S_v would be expected. Instead, ϵ varies by up to three orders of magnitude regardless of S_v, thereby implying that diel vertical migration is not creating turbulence. Also, there is no correlation between S_v and ϵ when examining the entire time-series and the time-series averaged over timescaels from $5 - 60$ min. Based on observation of 24 dusk ascents and 23 dawn descents, the turbulent burst associated with euphausiid diel vertical migration reported by Kunze et al. (2006) is not found in this study, consistent with Rippeth et al. (2007) and Rousseau et al. (2010).

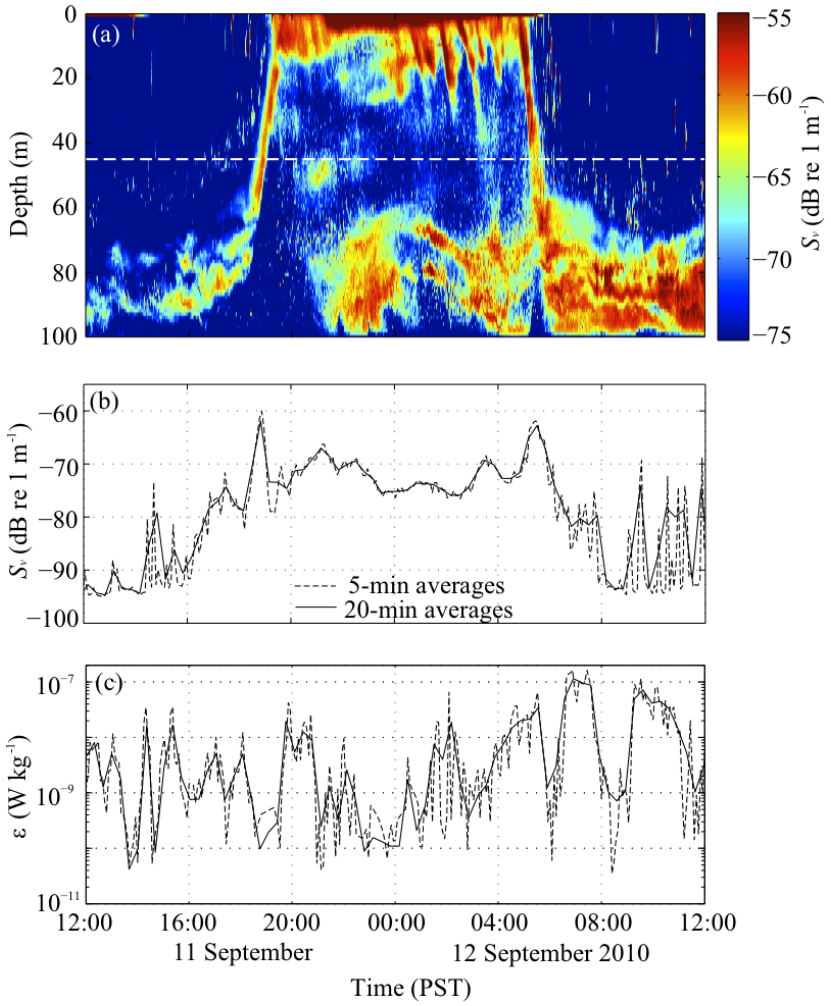

Figure 3.11: (a) Echogram of volume backscattering strength S_v (1-min × 1-m bin averages). (b) S_v (5-min/20-min × 10-m bin average) at ∼ 45 m, where the ADV was deployed corresponding to the dotted line in (a). (c) Lower-bound estimates of ϵ (5-min/20-min averages) observed by the ADV on 11 − 12 September 2010.

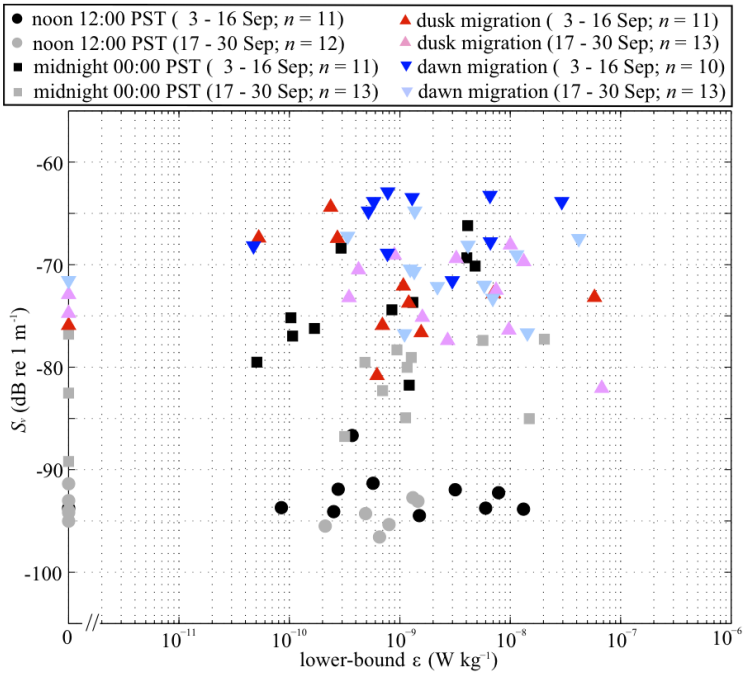

Figure 3.12: Scatterplot of ϵ (lower-bound estimates; 40-min averages) vs. volume backscattering strength S_v (40-min $\times$ 10-m bin averages) during 3 $-$ 30 September 2010. Data at 12:00 PST (local noon), 00:00 PST (midnight), dusk and dawn were plotted.

3.3.3 Currents

Despite the fact that Saanich Inlet is one of the best-studied anoxic fjords in the world (Tunnicliffe et al., 2003), current velocities have not been quantified. Previous studies described the inlet as a physically quiet environment without any detailed quantification (Herlinveaux, 1962; Gargett et al., 2003). Here, currents near the VENUS site are characterized and compared with the turbulent dissipation rates.

(i) Low-frequency flow

Spring/neap modulation in tidal flows produces strong modification in the v but not u component (Fig. 3.13). This is likely because Saanich Inlet is oriented north/south (Fig. 3.1b). Low-frequency v velocity shows southward surface flow, and northward mid-depth flow during 4 $-$ 6, 11 $-$ 17, and 28 $-$ 30 September corresponding to spring tides, with the strongest northward velocities at mid-depth during 10 $-$ 15 September. Northward surface flow and southward mid-depth flow during 19 $-$ 27

September correspond to neap tides. Note that this is the opposite sense of the flow implied by Gargett et al. (2003), who predicted southward flow at mid-depth during spring tides as mixed water from the north intrudes into the inlet.

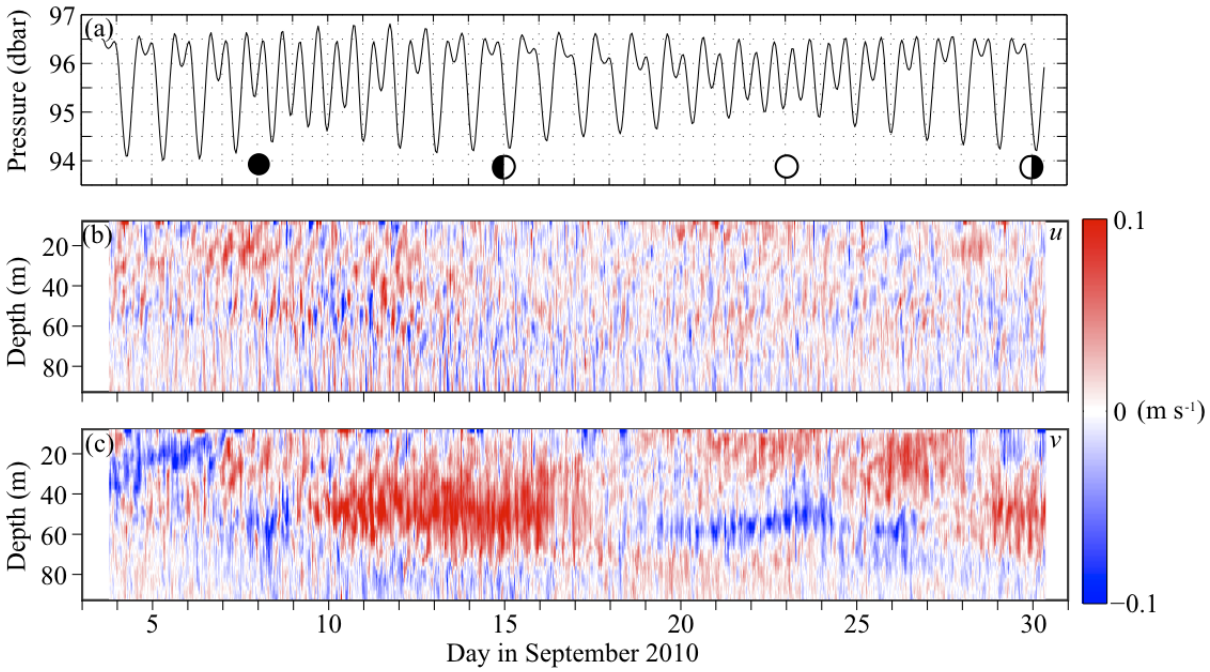

Figure 3.13: Time-series of (a) pressure, (b) u and (c) v velocities observed by ADCP (10-min average × 2-m bin). Moon phases are shown in (a).

(ii) Barotropic velocities

Saanich Inlet has mixed tides with both diurnal (O_1, K_1) and semidiurnal (M_2, S_2) components (Fig. 3.14a, b). Generally, the fortnightly cycle in tidal range on the outer coast of B.C. is closely linked to the moon phases. However, this does not apply to tides within protected waters, because the shape of the basin into which the tidal wave propagates and bottom friction play a role in determining the response of sea level to the tidal wave (Thomson, 1981), creating phase lags as well as harmonics. During the September 2010 mooring period, Saanich Inlet spring tides correspond to the first and third quarters (Fig. 3.14a) rather than the full and new moons.

Barotropic flow shows a positive mean v-component (i.e., northward flow) during $10 - 15$ September, with $\langle v \rangle = 2.4$ cm s^{-1} during this 6-d period (Fig. 3.14c). The spectrum of barotropic v-component is dominated by M_2, followed by O_1/K_1, MK_3, M_4 and $2MK_5$ (Fig. 3.14d). Variation in u-component is smaller than v-component,

with M_2/S_2 dominating. Current velocities in the Strait of Georgia, Haro Strait and Juan de Fuca Strait computed from XTide (D. Flatter, available at http://www.flaterco.com/xtide/) show similar spectral patterns as Saanich Inlet pressure data (Fig. 3.14b, 3.15), supporting the idea of forced response from signals outside. The $2MK_5$ harmonic appears in Haro Strait (Fig. 3.15a) but not in Juan de Fuca Strait (Fig. 3.15b).

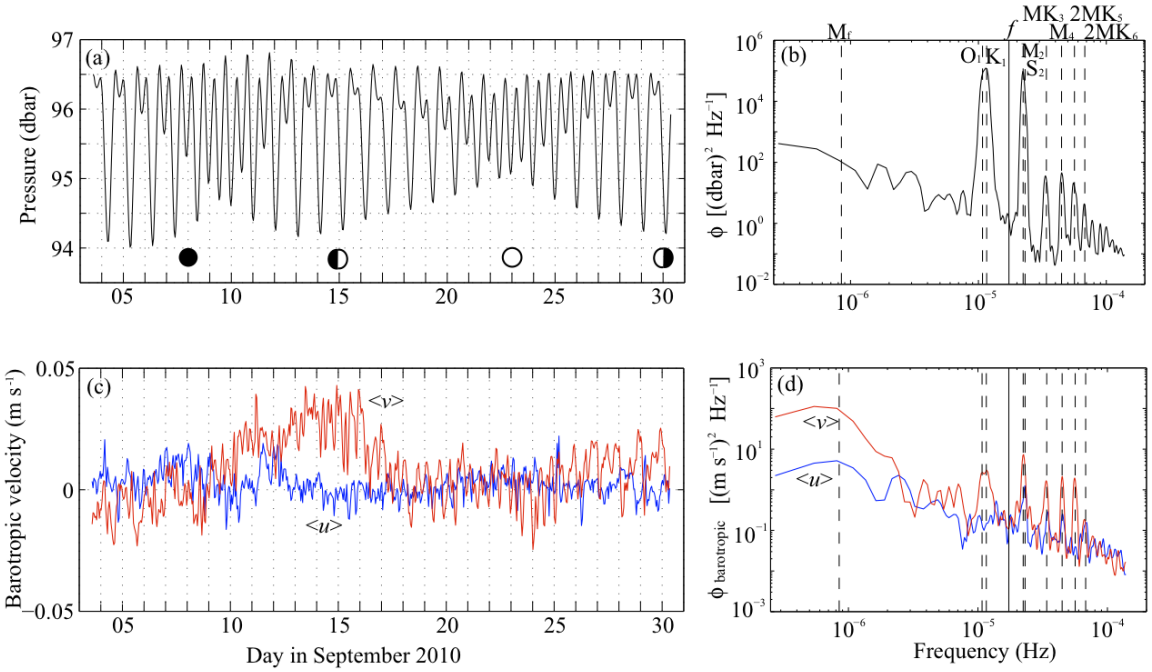

Figure 3.14: Time-series and spectra calculated from 26.8 days of data (1-hr average) during $3-30$ September 2010: (a) pressure time-series and (b) spectra, (c) barotropic velocity time-series and (d) spectra. The vertical dashed lines in (b) and (d) indicate M_f (13.66 d), O_1 (25.82 h), K_1 (23.93 h), the Coriolis ($f = 1.7 \times 10^{-5}$ Hz), M_2 (12.42 h), S_2 (12.00 h), MK_3 (8.18 h), M_4 (6.21 h), $2MK_5$ (4.93 h), and $2MK_6$ (4.17 h) frequencies.

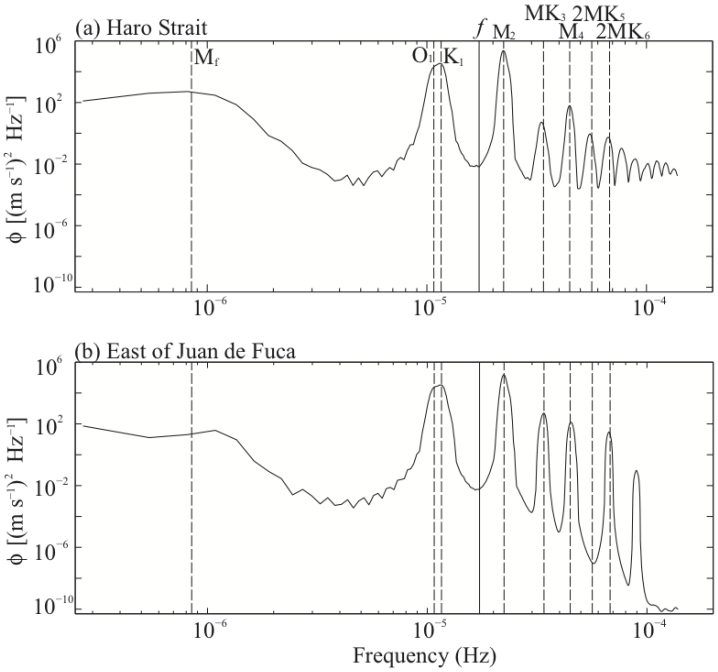

Figure 3.15: Current velocity spectra calculated on 28 days of data (1-hr sampling interval) during $2 - 30$ September 2010 in (a) Haro Strait (48° 35.0'N, 123° 14.0'W) and (b) east of Juan de Fuca Strait (48° 13.9'N, 123° 31.8'W). The vertical dashed lines indicate M_f (13.66 d), O_1 (25.82 h), K_1 (23.93 h), the Coriolis ($f = 1.7 \times 10^{-5}$ Hz), M_2 (12.42 h), MK_3 (8.18 h), M_4 (6.21 h), $2MK_5$ (4.93 h), and $2MK_6$ (4.17 h).

(iii) Baroclinic velocities

Similar to the low-frequency flow, spring/neap modulation in tidal flows produces strong modification of the v-component in the baroclinic velocities, but not in the u-component (Fig. 3.16, 3.17). Low-frequency baroclinic flow shows surface southward flow and mid-depth northward flow during spring tides, and the reverse during neap tides (Fig. 3.17b). Bandpass-filtered signals in baroclinic velocities show the dominance of semidiurnal and M_4 components in u' (Fig. 3.16c-e) and semidiurnal in v' (Fig. 3.17c-e). Kinetic energy densities of the baroclinic velocities are larger than those of barotropic flows in both u and v components (Fig. 3.16g, Fig. 3.17g). Since the barotropic tidal velocities are likely the source of energy for the baroclinic velocities, this implies that energy is being fed into the baroclinic flows until they saturate.

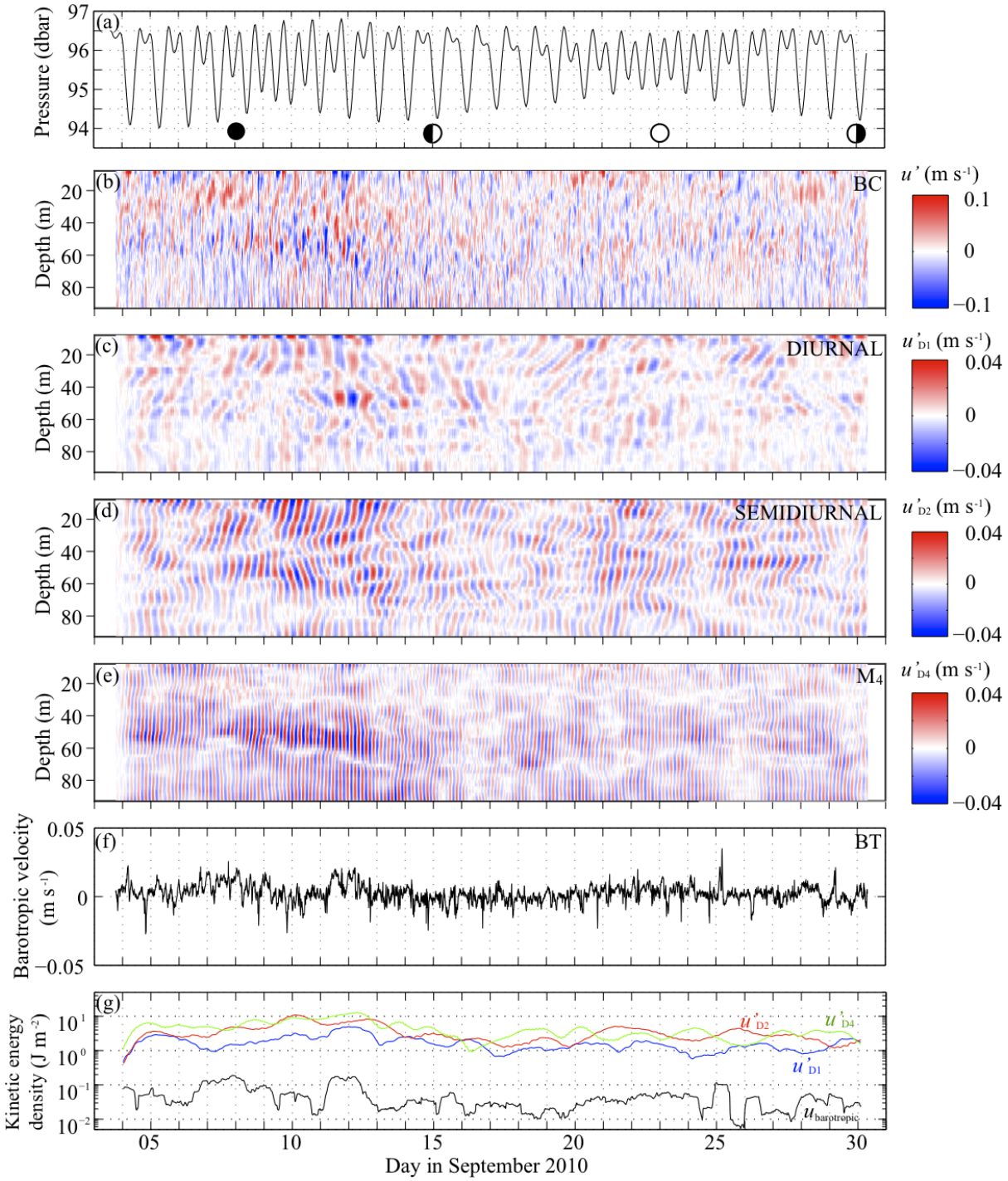

Figure 3.16: Time-series of (a) pressure, (b) u-component of baroclinic velocity (u'), (c) diurnal component of u' (u'_{D1}), (d) semidiurnal component of u' (u'_{D2}), (e) M_4 component of u' (u'_{D4}), (f) u-component of barotropic velocity, and (g) kinetic energy density of barotropic and baroclinic velocities. Bandpass filter was applied to obtain specified frequency range in ADCP data (10-min average × 2-m bin).

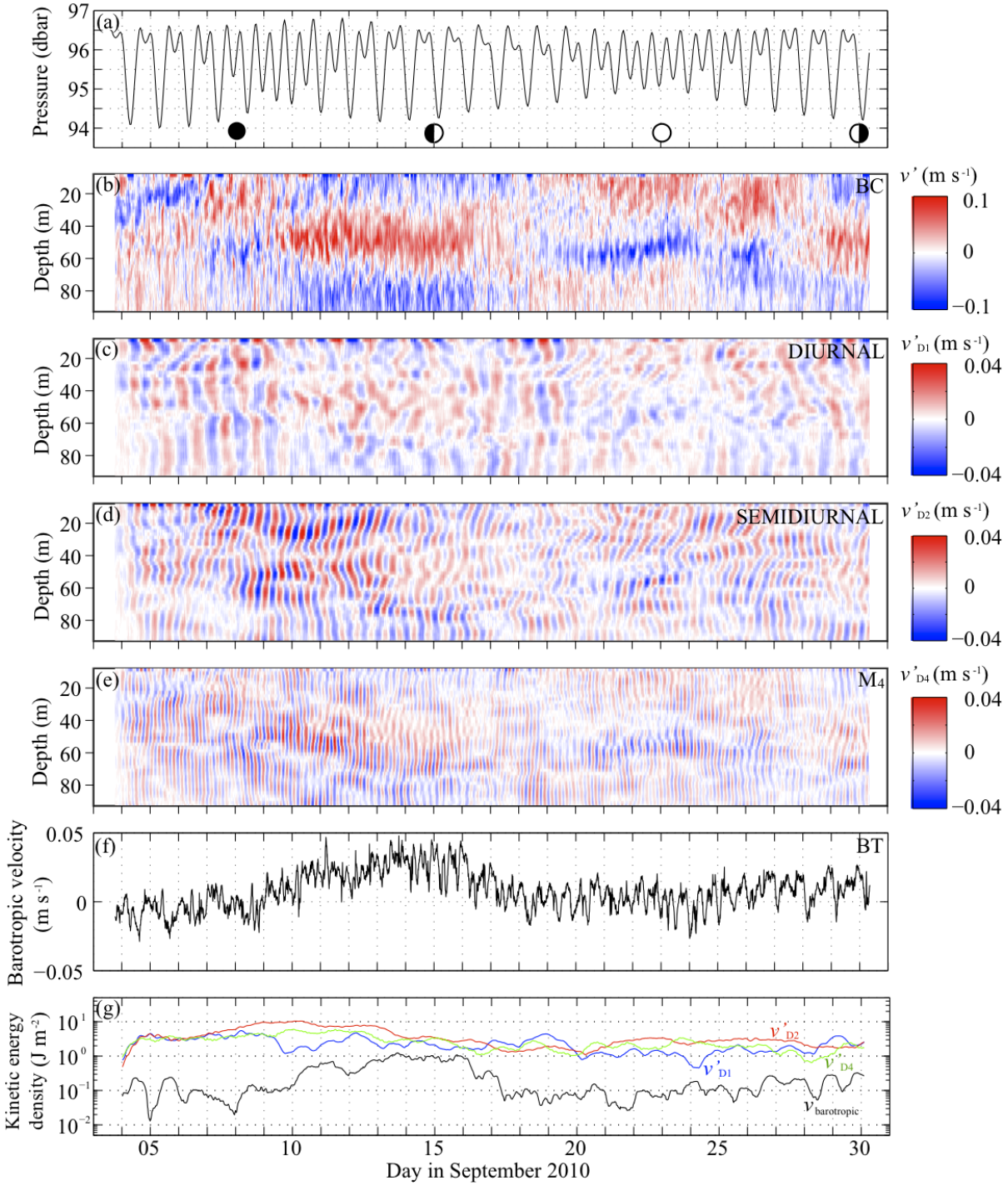

Figure 3.17: Time-series of (a) pressure, (b) v-component of baroclinic velocity (v'), (c) diurnal component of v' (v'_{D1}), (d) semidiurnal component of v' (v'_{D2}), (e) M_4 component of v' (v'_{D4}), (f) v-component of barotropic velocity, and (g) kinetic energy density of barotropic and baroclinic velocities. Bandpass filter was applied to obtain specified frequency range in ADCP data (10-min average × 2-m bin).

I compute spectra of the baroclinic velocities averaged in a 10-m window around the ADV deployment depth (Fig. 3.18a), in order to compare with the turbulent dissipation rates. At this depth, baroclinic velocities are dominated by M_4. Individual spectra for each depth bin show that M_4 dominates in u except in the upper 30 m. Its signal is weaker in the v-component. The spectral peak at M_2 is broader, but present throughout most of the water column in both u- and v-components (Fig. 3.18c, e). Shear spectra show a peak between the Coriolis and M_2 frequencies in both u and v (Fig. 3.18d, f), but the peak is not obvious at ~ 45 m where the ADV was deployed (Fig. 3.18b).

Understanding of the internal wave spectrum is primarily empirical, and based on fits to frequency (ω) and vertical wavenumber (m) spectra (Garrett and Munk, 1975; Cairns and Williams, 1976; Munk, 1981; Gregg and Kunze, 1991). The Garrett-Munk (GM) model spectrum (Garrett and Munk, 1972, 1975) was developed to kinematically describe the deep-ocean internal wave field. [GM76 refers to the form presented in Garrett and Munk (1975) modified by Cairns and Williams (1976).] The GM76 spectrum of horizontal velocity is

$$\phi_u(\omega, m) = \frac{b^2 N_0 N(\omega^2 + f^2)}{\omega^2} E(\omega, m) \tag{3.16}$$

where $b = 1300$ m is the e-folding scale of $N(z)$, $N_0 = 5.2 \times 10^{-3}$ s^{-1} the surface-extrapolated buoyancy frequency (Munk, 1981), $N = 1.63 \times 10^{-2}$ s^{-1} the average buoyancy frequency during the mooring period (Fig. 3.5), and $f = 1.09 \times 10^{-4}$ s^{-1} the Coriolis frequency at the study site (48° 38.9'N). $E(\omega, m)$ is a dimensionless energy density that is factored as follows;

$$E(\omega, m) = B(\omega) H(m) E_0 \tag{3.17}$$

$$B(\omega) = \frac{f}{\omega} \frac{1}{\sqrt{\omega^2 - f^2}} \tag{3.18}$$

$$H(m) = \frac{m_*}{(m + m_*)^2} \tag{3.19}$$

$$m_* = \frac{\pi}{b} \frac{N}{N_0} j_* \tag{3.20}$$

where $E_0 = 6.3 \times 10^{-5}$ the nondimensional internal spectral level and $j_* = 3$ a mode number (Munk, 1981). Shear spectra are computed from velocity spectra as

$$\phi_s(\omega, m) = m^2 \phi_u(\omega, m) \tag{3.21}$$

where $\phi_u(\omega, m)$ is given by Eq. 3.16.

Since the mooring site is only $\sim$ 100-m deep which is much shallower than the GM model generally applies, the GM76 spectra is integrated over the following wavenumber range (m_{min}, m_{max}) to take into account the shallow-water setting for this study;

$$m_{max} = \frac{2\pi}{10\text{ m}} \tag{3.22}$$

$$m_{min} = \frac{2\pi}{\lambda_{max}} \tag{3.23}$$

$$\lambda_{max} = 2H \times \frac{N}{N_0} \quad \text{where } H = 100\text{ m}. \tag{3.24}$$

Therefore, the modified GM76 spectra of horizontal velocity and shear (Fig. 3.18a, b) are

$$\phi_u(\omega) = \pi E_0 b j_* \frac{f(\omega^2+f^2)N^2}{\omega^3\sqrt{\omega^2-f^2}} \frac{1}{m_{min}+m_*} \tag{3.25}$$

$$\phi_s(\omega) = \pi E_0 b j_* \frac{f(\omega^2+f^2)N^2}{\omega^3\sqrt{\omega^2-f^2}} m_{max}. \tag{3.26}$$

Comparison with the GM spectra gives a sense of the internal wave energy level in the study site relative to the open ocean. Baroclinic kinetic energy and shear variance near the ADV deployment depth were normalized by the GM kinetic energy and shear variance given by

$$\int_{m_{min}}^{m_{max}} \int_{f}^{N} \phi_u(\omega, m) d\omega dm = \frac{3\pi}{2} E_0 N^2 \frac{b j_*}{m_{min}+m_*} = 7.2 \times 10^{-3} \quad [\text{m}^2\ \text{s}^{-2}] \tag{3.27}$$

$$\int_{m_{min}}^{m_{max}} \int_{f}^{N} \phi_s(\omega, m) d\omega dm = \frac{3\pi}{2} E_0 N^2 b j_* m_{max} = 1.9 \times 10^{-4} \quad [\text{s}^{-2}] \tag{3.28}$$

to understand their relation to the turbulent dissipation rates (Fig. 3.19). In this data, the baroclinic kinetic energy is an order of magnitude smaller than the modified GM76 model, while shear variance is about one third of the modified GM76 (Fig. 3.19b). Baroclinic kinetic energy and shear variance correlate with each other, peaking during $9-10$ September and dipping to minima on 16 September, then remaining relatively constant until the end of the month. Comparison with the time-series of dissipation rates suggests a weak correlation between turbulent dissipation rates and internal

wave field (Fig. 3.19c); $r = 0.43$ for baroclinic kinetic energy, and $r = 0.48$ for shear variance. If physical forcing is the source of turbulence, one would expect a positive correlation between dissipation rates and the internal wave field. In contrast, the observed weak correlation likely results from the small dynamic range in dissipation rates and the internal wave field which are near the detection limit of the instruments due to the physically quiet environment of Saanich Inlet.

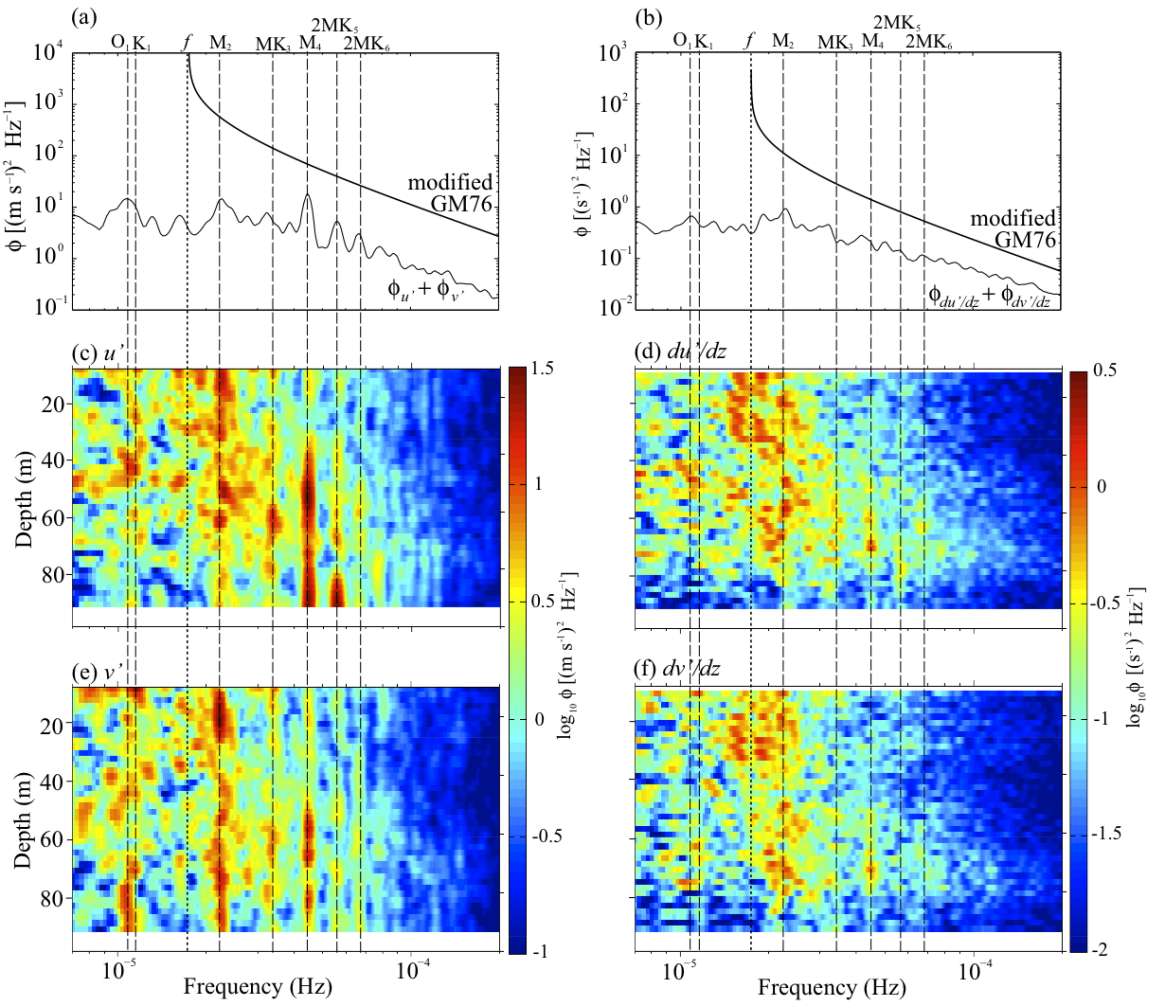

Figure 3.18: Baroclinic velocity ($\phi_{u'} + \phi_{v'}$) and shear spectra ($\phi_{du'/dz} + \phi_{dv'/dz}$) calculated from 26.81 days of ADCP data (1-min average × 2-m bin) during 3 − 30 September 2010. (a) Baroclinic velocity and (b) shear spectra averaged over the depth range 37.6 − 47.6 m, corresponding to the approximate deployment depth of the ADV, along with the modified GM76 model. Depth-frequency maps of (c) *u'*, (d) *du'/dz*, (e) *v'*, and (f) *dv'/dz*. The vertical dashed lines indicate O_1 (25.82 h), K_1 (23.93 h), the Coriolis ($f = 1.7 \times 10^{-5}$ Hz), M_2 (12.42 h), MK_3 (8.18 h), M_4 (6.21 h), $2MK_5$ (4.93 h), and $2MK_6$ (4.17 h) frequencies.

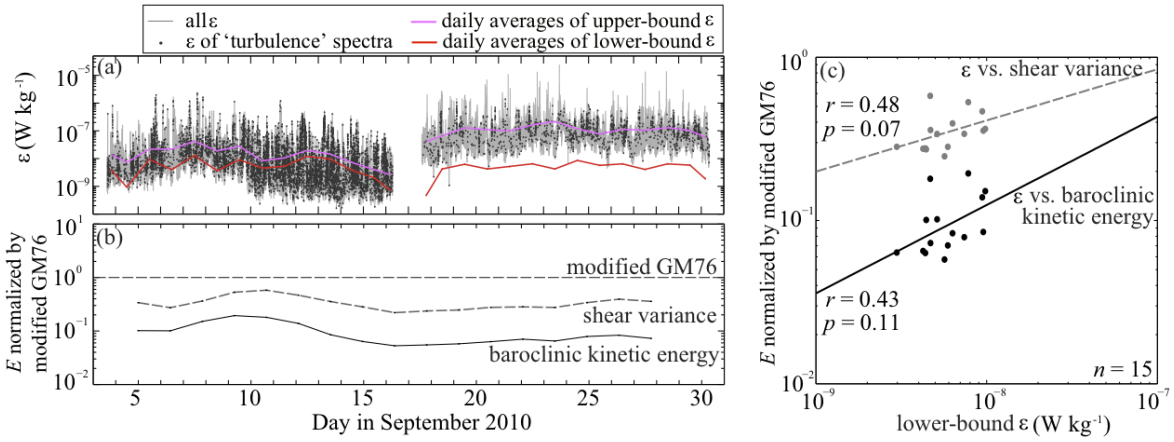

Figure 3.19: (a) Time-series of daily-averaged ϵ estimates. (b) Time-series of baroclinic kinetic energy and shear variance, normalized by the modified GM76 kinetic energy and shear variance. Spectral analysis of 4096-pt (2.84-d) of baroclinic velocities and shear with 50% overlap was conducted based on 1-min average $\times$ 2-m bin data. Spectra between 37.6 $-$ 47.6 m (corresponding to the approximate deployment depth of the ADV) were averaged before calculating the variance. (c) Scatterplot of lower-bound ϵ vs. the baroclinic kinetic energy/shear variance.

Distribution of energy between vertical modes

The distribution of energy between vertical modes has important implications for the magnitude and location of shear variance, as well as turbulence production. The vertical structure of each mode is governed by

$$\frac{d}{dz}\left(\frac{1}{N^2}\frac{d\Psi_n}{dz}\right) + \frac{1}{c_n^2}\Psi_n = 0 \tag{3.29}$$

where N is the buoyancy frequency, Ψ_n the vertical structure of the mode number n (0, 1, 2, ...), z the depth of the water column, and c_n the separation constant (eigenvalue) (Kundu and Cohen, 2008). Boundary conditions are imposed at the sea surface and sea floor, such that

$$\frac{d\Psi_n}{dz} = 0 \tag{3.30}$$

at $z = 0$ and -H, where H is the maximum depth of the water column (Kundu and Cohen, 2008). In practice, the vertical mode shapes, Ψ_n, presented here are calculated

from numerical solution of Eq. 3.29 using the average stratification profile collected near the mooring site at ∼100-m bottom depth (Fig. 3.5d). Note the main basin is deeper, at 200 m, and therefore basin modes must be converted to shelf modes, as I discuss below. The current velocity data can be described as

$$v(z,t) = \Psi(z,n)a(n,t) \tag{3.31}$$

where $v(z,t)$ is velocities observed by the ADCP, and $a(n,t)$ amplitudes of vertical structure of modes.

The most unique feature is that M_4 mode 2 in u has more energy than mode 1 at any other frequency (Fig. 3.20a, b). Since M_4 is usually a harmonic of the M_2 tide, it is unusual for it to have more energy than the M_2. Therefore, I investigate a possibility that the inlet is resonant to M_4 frequencies. Due to the sill located at the mouth of the inlet at 75 m, the basin can be considered either open or closed in along-channel direction, while closed in cross-channel direction;

$$\text{closed basin: } T_m = \frac{2L}{(m+1)c_n} \quad (m = 0,\ 1,\ 2,\ ...) \tag{3.32}$$

$$\text{open basin: } T_m = \frac{4L}{(2m+1)c_n} \quad (m = 0,\ 1,\ 2,\ ...) \tag{3.33}$$

where T is period (s), L length of the basin (m), m number of modal line presents, c_n wave speed (m s^{-1}) of the vertical mode number n which corresponds to the separation constant (eigenvalue) of Eq. 3.29. Although the ADCP was deployed at ∼ 100-m bottom depth, the bottom depth exceeds 200 m in the central part of Saanich Inlet (Fig. 3.1b). Considering the vertical structure of modes, mode 3 in the deep basin corresponds to mode 2 in shallow water (Fig. 3.21). Hence, based on $c_3 = 0.22$ m s^{-1} at deep-water, $L = 15$ km for the along-channel and $L = 4$ km for the cross-channel length of the basin, a resonant seiche period close to M_4 can be obtained (Eqs. 3.32, 3.33): $T_5 = 6.4$ hr for along-channel and $T_1 = 5.1$ hr for cross-channel seiches in closed basin, and $T_6 = 5.9$ hr for along-channel seiches in open basin. Since seiches with lower m contain more energy, cross-channel seiches of T_1 more likely cause amplification of the M_4 mode 2 in the u component rather than T_5 or T_6 for along-channel seiches.

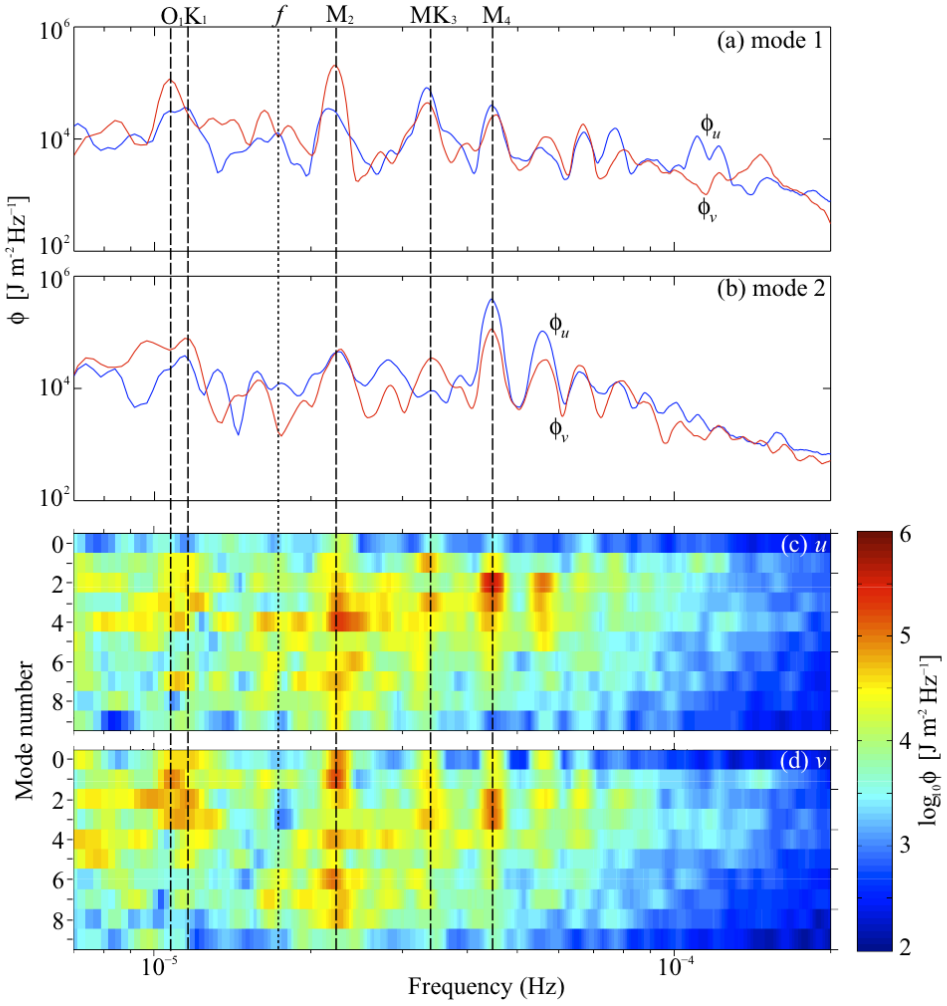

Figure 3.20: Spectra of $a(n,t)$ calculated based on decomposition of vertical modes of ADCP data (1-min average $\times$ 2-m bin) during 3 $-$ 30 September 2010. Example spectra of (a) mode 1 and (b) mode 2. Depth-frequency maps of (c) u and (d) v. The vertical dashed lines indicate the inertial ($f = 1.7 \times 10^{-5}$ Hz), buoyancy (N), M_f (13.66 d), O_1 (25.82 h), K_1 (23.93 h), M_2 (12.42 h), MK_3 (8.18 h), M_4 (6.21 h), and $2MK_5$ (4.93 h) frequencies.

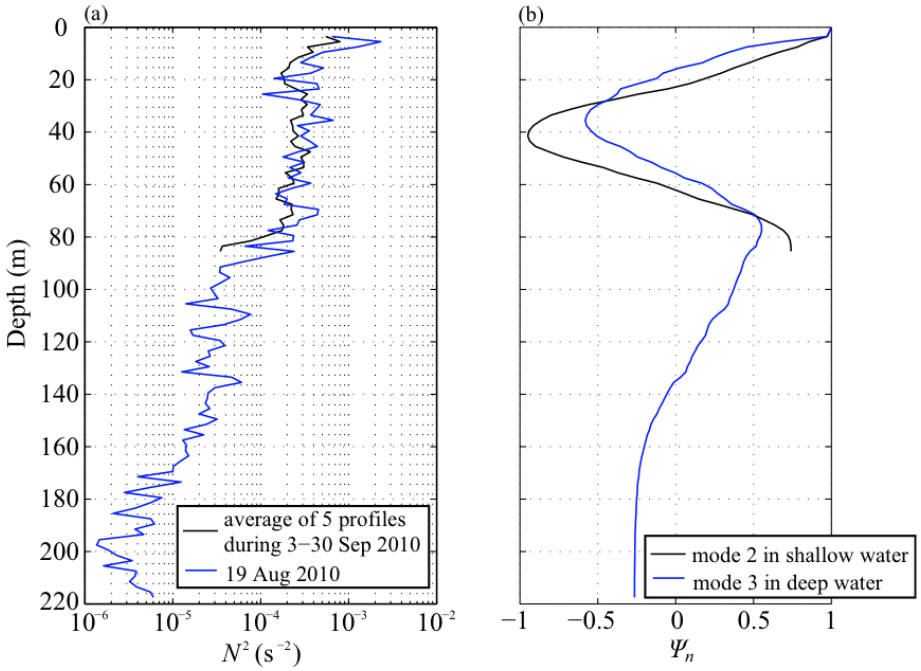

Figure 3.21: (a) Vertical profiles of buoyancy frequency squared N^2 at the mooring site (black) and central part of Saanich Inlet (blue). (b) Comparison of vertical structure of modes calculated in shallow and deep water.

Since the vertical structure of mode 1 has $\Psi_1 = 0$ at mid-depth corresponding to the deployment depth of the ADV, examination of kinetic energy level at the mid-depth (Fig. 3.19b) might not capture the internal wave energy present in the water column. Vertical modes fit through the water column give an estimate of depth-integrated energy

$$E_n = \frac{\rho}{2} \int_f^N \phi_n d\omega \int_{-H}^0 {\Psi_n}^2 dz \tag{3.34}$$

where ϕ_n is the power spectral density of the mode number n. Kinetic energy density of baroclinic low modes shows a peak during $9 - 12$ September, then decreases and remains constant until the end of the month, slightly higher energy density in u than v (Fig. 3.22). The pattern is very similar to the time-series of the baroclinic kinetic energy shown in Fig. 3.19b, suggesting that the kinetic energy level observed at the mid-depth of my study site does capture the internal wave energy field in the water column.

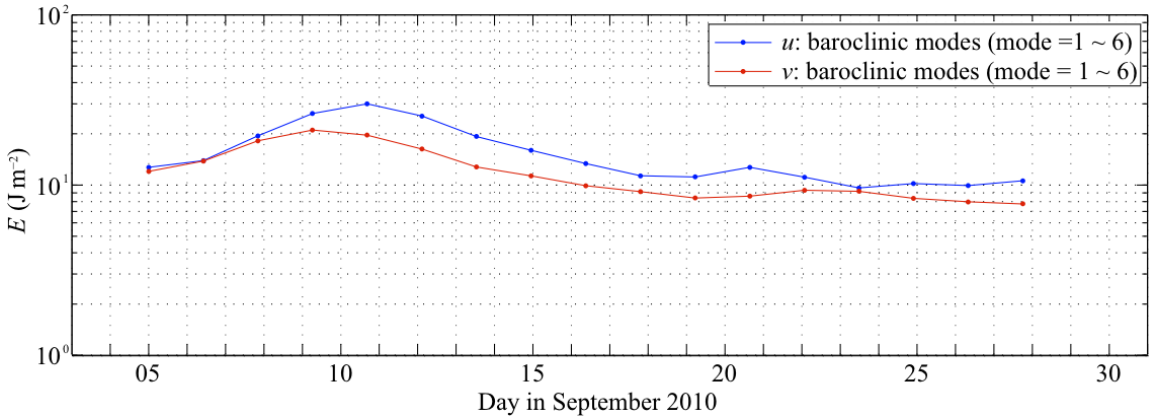

Figure 3.22: Time-series of kinetic energy density in baroclinic velocities depending on vertical structure of modes. Spectral analysis of 4096-pt (2.84-d) of *a(n, t)* with 50% overlap was conducted based on 1-min average × 2-m bin data.

3.4 Discussion

The goal of this study was to characterize the physical environment in Saanich Inlet in order to examine (i) whether turbulent mixing can be a mechanism of nutrient re-supply to the euphotic zone, (ii) whether physical processes or diel vertical migration of euphausiids are likely the source of the turbulent burst reported by Kunze et al. (2006), and (iii) effects of currents in dispersing planktonic organisms. To address this goal, I used an ADV to estimate turbulent dissipation rates, an ADCP to measure current velocities, and an upward-looking echosounder to monitor the migrating scattering layer as a biological source of turbulence. Barotropic, baroclinic and turbulent signals in Saanich Inlet were described, and the relationship between turbulence and internal waves/scattering layer examined. The primary results are

- During $3-16$ September, average ϵ are (0.6-1.7) $\times 10^{-8}$ W kg^{-1}, with the lower bound based on zeroing out data not deemed turbulent and the upper bound including all estimates. During this period, 22% of the spectra are turbulent. Corresponding diapycnal turbulent diffusivities K are (4.7-12.5) $\times 10^{-6}$ m^2 s^{-1}. During $17-30$ September, lower-bound average of ϵ is 0.5×10^{-8} W kg^{-1} with $K = 4.0 \times 10^{-6}$ m^2 s^{-1} and only 4% of the data turbulent. Upper-bound estimates during this period are not considered further, because the higher noise level allowed very few turbulence measurements. Turbulent dissipation

rates occasionally reach to O(10^{-7} – 10^{-6} W kg^{-1}), but are never as high as the 10^{-5} – 10^{-4} W kg^{-1} reported by Kunze et al. (2006).

- No relation between diel vertical migration at dusk/dawn and elevated turbulent dissipation rates is found.
- Low-frequency flow is southward at the surface and northward at mid-depth during spring tides, and the reverse during neaps.
- Barotropic velocities show forced responses to tides outside the inlet, such as in the Strait of Georgia and Haro Strait.
- The nondimensional spectral energy levels of baroclinic velocity and shear are below GM levels, even accounting for the shallow-water setting. They correlate weakly with turbulent dissipation rates; $r = 0.43$ for baroclinic kinetic energy and $r = 0.48$ for shear variance.

3.4.1 Turbulent mixing as a mechanism of nutrient re-supply to the euphotic zone

Dissipation rates ϵ in the open ocean vary strongly with buoyancy frequency squared N^2, while the turbulent diffusivities K are much more uniform at (5-10) $\times$ 10^{-6} m^2 s^{-1} (Gregg and Sanford, 1988; Gregg, 1989; Gregg et al., 2003). For the buoyancy frequency in Saanich Inlet $N^2 = 2.7 \times 10^{-4}$ s^{-2}, expected open-ocean ϵ is (0.7-1.3) $\times$ 10^{-8} W kg^{-1}. Therefore, lower- and upper-bound estimates of Saanich Inlet diffusivities and dissipation rates are within the range found in the stratified open ocean.

Average dissipation rates and diffusivity estimates in this study are higher than previously reported values using vertical profilers [ϵ = O(10^{-9} W kg^{-1}), K = O(2×10^{-6} m^2 s^{-1}); Gargett et al. (2003); Kunze et al. (2006); Rousseau et al. (2010)]. Although the 27-d measurements did not capture previously reported bursts of O(10^{-5} – 10^{-4} W kg^{-1}), the continuous measurements allow me to observe intermittent high dissipation rates of O(10^{-7} – 10^{-6} W kg^{-1}) which could have been missed by infrequent sampling. In addition, a few hours of sampling in previous studies are not long enough to estimate typical turbulent dissipation rates in the inlet. Conversely, diffusivities based on dissipation rates inferred here are an order of magnitude smaller

than those based on the time-series of bottom-water salinity and salinity depth gradient at 145 − 165 m [$(5.2 \pm 1.0) \times 10^{-5}$ m^2 s^{-1}; Manning et al. (2010)]. A possible explanation for this discrepancy is the potential for enhanced mixing at the basin walls and sill. Turbulence produced by diel vertical migration of euphausiids is unlikely, because the daytime depth of the euphausiid scattering layer in the inlet is shallower than 125 m throughout the year (Beveridge, 2007).

A weak correlation between turbulent dissipation rates, baroclinic kinetic energy and shear variance is observed. This is consistent with previous parameterizations for the deep (Gregg, 1989) and coastal (Carter and Gregg, 2002; MacKinnon and Gregg, 2003) ocean, where average dissipation rates are attributed to internal waves. Small dynamic ranges of both turbulent dissipation rates and internal wave energy in this study likely result in observed weak correlation between them. In fjords, internal waves generated by oscillating barotropic currents over sills seem to provide most of the power required for turbulence and diapycnal mixing in deep waters (Stigebrandt, 1976; Stigebrandt and Aure, 1989; Simpson and Rippeth, 1993; Tinis, 1995). However, how the barotropic to baroclinic energy conversion occurs at sills to create turbulent dissipation and diapycnal mixing at small scales is not well understood.

Because nitrate supply periodically limits summer phytoplankton growth in Saanich Inlet (Takahashi et al., 1977), a vertical nitrate flux produced by the observed turbulent mixing is estimated to examine whether turbulent mixing can be a mechanism of nutrient re-supply to the euphotic zone. Using a mean nitrate gradient of O(0.5 mmol m^{-3} m^{-1}) estimated based on discrete water samples, which is a typical mid-inlet value during summer (Gargett et al., 2003), averaged diffusivities observed during 3 − 16 September [K = (4.7-12.5) $\times 10^{-6}$ m^2 s^{-1}] would produce a vertical nitrate flux of O(0.2 − 0.5 mmol m^{-2} d^{-1}). Similarly, vertical nitrate flux on the same order is obtained for lower-bound averaged diffusivity during 17 − 30 September. These estimated vertical nitrate fluxes are too small to account for inferred fluxes of O(4 mmol m^{-2} d^{-1}) during a part of the fortnightly tidal cycle (Gargett et al., 2003). Although the average ϵ suggests weak turbulent mixing, enhanced mixing at the basin walls and sill can potentially increase vertical nitrate flux. Since the physical forcing is more likely stronger at the main channel than our study site, which is more sheltered, average turbulent dissipation rates at the main channel are expected to be larger than O(10^{-8} W kg^{-1}). In order to get the inferred vertical nitrate flux of O(4 mmol m^{-2} d^{-1}) as suggested by Gargett et al. (2003), ϵ needs to be O(10^{-7} W kg^{-1}) which corresponds to K = O(10^{-6} m^2 s^{-1}). In addition to the pressure gradients caused

by strong tidal mixing outside Saanich Inlet (Gargett et al., 2003) and biologically generated turbulence (Kunze et al., 2006), turbulent mixing by physical processes within the inlet might be a third mechanism by which nutrients are re-supplied to the euphotic zone.

3.4.2 Possible sources of a turbulent episode reported by Kunze et al. (2006)

The ability of marine organisms to generate turbulence has been debated both theoretically and observationally. Huntley and Zhou (2004) considered the energy produced by schooling animals and estimated ϵ of $\sim 10^{-5}$ W kg^{-1}. Observation of a turbulent burst of O($10^{-5} - 10^{-4}$ W kg^{-1}) associated with euphausiid diel vertical migration in Saanich Inlet (Kunze et al., 2006) appeared to be consistent with the predictions of Huntley and Zhou (2004). If diel vertical migration is a cause of the turbulent burst, as suggested by Kunze et al. (2006), high turbulent dissipation rates should be expected twice a day (i.e., dusk ascent and dawn descent). However, Kunze et al. (2006) observed the burst only in 1 of 2 dusk ascents. In order to generate statistics on biologically generated turbulence in Saanich Inlet, Rousseau et al. (2010) conducted turbulence measurements in 6 dusk ascents and 5 dawn descents. But no turbulent burst of the same intensity reported in Kunze et al. (2006) was observed. Biologically generated turbulence suggested by Kunze et al. (2006) was contested by Rippeth et al. (2007) as not being representative of coastal areas. Their measurements of turbulent dissipation rates on the western continental shelf of the British Isles showed no elevated turbulence during 11 migration periods.

Elevated levels of turbulent dissipation rates ϵ also do not necessarily mean that mixing is proportionally higher, because much of the turbulent kinetic energy of small animals is injected below the Ozmidov buoyancy length scale (Visser, 2007). Simultaneous measurements of dissipation rates and mixing efficiency showed horizontally-moving fish schools can generate elevated turbulent dissipation rates, but were not associated with elevated mixing (Gregg and Horne, 2009). Lorke and Probst (2010) estimated mixing efficiencies of $\gamma = 0.2$ and observed no correlation between γ and abundance of juvenile perch. Rousseau et al. (2010) suggested that mixing efficiency of biologically generated turbulence may depend on the synchronized movement of individuals within a school, which is not well understood.

This study obtained continuous measurements of turbulent dissipation rates by

deploying an ADV on a mooring. Although diel vertical migrations were observed throughout the 27-day mooring period (24 dusk ascents and 23 dawn descents), there was no recurrence of the turbulent burst reported by Kunze et al. (2006). Maximum ϵ corresponding to dusk ascent and dawn descent was O(10^{-7} W kg^{-1}), and no correlation was observed between dissipation rates and volume backscattering strength (Fig. 3.12). Possible factors accounting for the difference in observed ϵ between these two studies are (i) sampling season, (ii) location and (iii) measurement technique. Kunze et al. (2006) conducted their field measurements in April at the main channel using vertical profilers, while I deployed the ADV mooring in September in Patricia Bay which is shallower and more sheltered.

(i) Sampling season: Differences in sampling season suggest a difference in body size and biomass of *Euphausia pacifica*, the dominant migrator in the inlet. *E. pacifica* live $1 - 2$ years (Tanasichuk, 1998) with their main spawning period from early May to mid-July (Heath, 1977). Their average body size is 18.1 mm in April, which is their maximum size just before spawning, and 12.9 mm in October (Sato et al., 2013). Huntley and Zhou (2004) estimated ϵ for schooling animals to be 10^{-5} W kg^{-1}. Although effect of animal size in creating turbulence *in situ* remains unknown, the difference in average body size of $\sim$ 5 mm is unlikely a cause of 3 - 4 orders of magnitude difference in ϵ. Seasonal change in biomass is unlikely the cause of high ϵ either, because biomass of *E. pacifica* in September is more than twice as large as that in April (Heath, 1977).

(ii) Sampling location: Physical forcing might be expected to be stronger at the main channel than Patricia Bay because of the sill located at the mouth of the inlet. Although only a weak correlation was observed between turbulent dissipation rates and baroclinic velocity/shear in this study (Fig. 3.19), a possibility of stronger physical forcing at the main channel creating turbulence reported by Kunze et al. (2006) cannot be ruled out. In unpublished data collected during a different cruise, a turbulent burst was observed near the west shore of the deep channel that was not associated with diel vertical migration (E. Kunze, personal communication). As there was not corresponding ADCP data, physical mechanisms could not be examined. But this burst may have been associated with internal waves generated at the sill or by west bank bathymetry. However, its occurrence must be rare, because Rousseau et al. (2010) found no recurrence of an intense turbulent burst in 11 migration events collected in the main channel.

(iii) Measurement technique: Field measurements using vertical profilers to estimate turbulent dissipation rates may induce avoidance behavior of organisms in advance of a descending probe (e.g., Farmer et al., 1987). Although Kunze et al. (2006) observed only one turbulent episode and Rousseau et al. (2010) found no turbulent burst using the same methodology as Kunze et al. (2006), it may be a result of the avoidance behavior whose effects depend on swimming speed and densities of schools. The mooring approach taken in this study does not induce such artificial behavior. However, fish are known to get attracted to drifting objects and often associate with them (Kawamura et al., 1996), which could affect my velocity measurements.

No evidence of turbulent bursts associated with diel vertical migration was found in this study. The underlying mechanism of the burst reported by Kunze et al. (2006) remains unresolved. Physical forcing at the main channel can be a possible source of such very intermittent high turbulent episodes.

3.4.3 Effects of currents in dispersing planktonic organisms

Zooplankton, such as copepods and early life-stages of euphausiids, are highly susceptible to transport away from their source populations due to their weak swimming capability and non-migratory behavior (e.g., Brinton, 1962; Lu et al., 2003). Here, I examine a possible mechanism of dispersal of planktonic organisms through low-frequency currents observed in Saanich Inlet. Low-frequency flow shows southward surface flow and northward mid-depth flow during spring tides in September, and the reverse during neaps (Fig. 3.13). These patterns are likely due to circulations internal to Saanich Inlet, which can arise from tidal rectification over the topography (Codiga, 1997; Kunze and Toole, 1997). There is evidence of a counterclockwise eddy during neap tides associated with weak surface outflow on the eastern side of Saanich Inlet (Gargett et al., 2003), consistent with my observations of northward flow at the surface. The dispersal of plankton dominated by low-frequency flow is estimated by calculating the power spectral density of displacement in v-component, $\phi_v(f)/(2\pi f)^2$. The average displacement at M_f (13.66 d) frequency is thus estimated 1.4 km at 15-m depth and 7.3 km at 45-m depth. Since the measurements were taken in Patricia Bay, observed current velocities are likely capturing a circulation around the inlet, rather than in and out of its mouth.

Similar depth-dependent patterns of fortnightly-modulated currents are suggested

in the main channel of the inlet. During spring tides in summer, Gargett et al. (2003) observed surface outflow and mid-depth inflow driven by pressure gradients set up by strong tidal mixing in passages outside Saanich Inlet. Based on the estimates of average displacement at low-frequency currents, water within a few kilometers of the mouth are likely to be swept in and out regularly, but not those in Patricia Bay. This is supported by small numbers of *E. pacifica* occasionally caught in Satellite Channel (Heath, 1977). It is possible that euphausiids in the inlet form a distinct population with only limited exchange with populations in adjacent waters. This likely results in the observation of distinct physiological characteristics of Saanich Inlet *E. pacifica* populations. Boden and Kampa (1965) found that *E. pacifica* in Saanich Inlet are more sensitive to green light than to blue compared to individuals from the San Diego Trough. That is, *E. pacifica* in Saanich Inlet have adapted to environmental lighting which is greener in color and significantly brighter in intensity than those experienced at daytime depth of $\sim$ 250 m by the California population.

3.4.4 Remaining questions for future study

This study results in questions, some of which are attributed to the mooring location in Patricia Bay. Because the study site is more sheltered and shallower than the central part of the inlet, interpretation of the current velocity records is difficult.

- What is the mechanism of producing episodically higher turbulent dissipation rates of O($10^{-7} - 10^{-6}$ W kg^{-1})?
- Can physical forcing at the main channel of the inlet produce turbulent dissipation rates of O($10^{-5} - 10^{-4}$ W kg^{-1}) reported by Kunze et al. (2006)?
- Do seiches cause amplification of the M_4 mode 2 in the u component?
- What mechanism supplies nutrients for phytoplankton productivity?

3.4.5 Conclusions

This study characterizes and quantifies the physical environment in Saanich Inlet, which has long been considered quiet. Average dissipation rates are nearly an order of magnitude larger than the previously reported values of O(10^{-9} W kg^{-1}) (Gargett et al., 2003; Kunze et al., 2006; Rousseau et al., 2010). These dissipation rates are in the range of those found in the open ocean pycnocline for the same stratification.

Although diffusivity estimates based on average dissipation rates in Patricia Bay are insufficient to explain nutrient fluxes reported by Gargett et al. (2003), higher dissipation rates expected at the main channel could potentially supply nutrients to the euphotic zone to sustain high primary productivity in the inlet. A weak correlation was observed between turbulent dissipation rates and baroclinic velocity/shear, but the direct cause of the sporadic increase in dissipation rates remains unresolved. Previously reported turbulent bursts of $O(10^{-5} - 10^{-4}$ W kg$^{-1})$ associated with diel vertical migration of euphausiids (Kunze et al., 2006) are not observed in this study. Physical forcing at the main channel, which is likely stronger than at my study site, remains as a possible cause of the turbulent episode. Displacement due to low-frequency currents is $O(1 - 10$ km), whose effects on dispersal of planktonic organisms are likely confined to near the mouth of the inlet.

Chapter 4

Conclusions and future research

4.1 Overview of research

Simultaneous quantification of biological and physical properties of the ocean is key to understanding the behaviour of marine organisms. Likewise, simultaneous measurements are necessary to quantify biological effects on the physical properties of the ocean. The research presented here has focused on biological and physical processes in Saanich Inlet, which could affect both carbon cycling and predator-prey interactions.

4.1.1 Variability in diel vertical migration timing of euphausiids in Saanich Inlet (Chapter 2)

Diel vertical migration timing is closely tied to civil twilight times, but variability in migration timing superimposed on the seasonal shift in daylight length has received little attention to date. Capitalizing on the VENUS cabled observatory deployed in Saanich Inlet, I quantified the seasonal variability in migration timing of euphausiids relative to civil twilight using a two-year 200-kHz echosounder time-series. Early dusk ascent and late dawn descent occur during spring − fall, while late dusk ascent and early dawn descent occur during winter. Ascent timing appears to be regulated by (i) light availability at the daytime depth of the euphausiids which is modulated by phytoplankton bloom shadowing, and (ii) euphausiid size-dependent visual predation risk. Because (i) does not apply at dawn, descent timing appears to be regulated primarily by (ii). During the pre-spawning period, higher energy demands for reproduction may cause early dusk ascent and later dawn descent to maximize energy gain, even with larger body size.

The observed variability in migration timing could affect encounter rates between euphausiids and their predators. Although a seasonal signal of just 23 min may seem a small difference, quantifying such small-scale variability will help to improve our predictions of larger scale changes. Certainly, the very fact that a second-order seasonal signal in diel vertical migration even exists suggests that it confers a survival advantage. Therefore, and as zooplankton represent an important trophic linkage, understanding this phenomenon will contribute to the broader topic of energy flow in marine ecosystems. This study also highlights the utility of the sort of long-term continuous time-series observations that can only be collected via cabled observatories.

A natural follow-up to this work would be to deploy multi-frequency or split-beam echosounders on the VENUS cabled observatory to separate fish from zooplankton acoustic signals, which allow examination of how predator behavior affects the diel vertical migration pattern of their prey. Multi-frequency or split-beam echosounders would also provide quantitative estimates of zooplankton abundance in Saanich Inlet. Combined with excretion estimates of zooplankton, this would enable researchers to estimate the strength of the biological pump and its seasonal, inter- and intra-annual variability in Saanich Inlet. With VENUS's goal of providing at least 20 years of sustained ocean measurements (Tunnicliffe et al., 2003), the development of data visualization tools to provide an overview of such long time-series will become essential. This is particularly important for echosounders which sample acoustic backscatter throughout the water column, producing enormous datasets after only a few years. The 3-D data cube concept presented in this study provides one example of how the development of novel data visualization tools can result in a different perspective and enhanced understanding of diel vertical migration.

Euphausia pacifica is one of the dominant euphausiid species off B.C., accounting for more than 70% of the euphausiid biomass in the Strait of Georgia (Fulton and Le Brasseur, 1984). A commercial fishery on *E. pacifica* off western Canada began in 1970s, with fishing initially concentrated in Saanich Inlet, then Howe Sound, and recently in Jervis Inlet (Nicol and Endo, 1999; Heath, 1977). The annual catch has been set at 500 tonnes since 1976, with an open season from November − March. Although the methodology for acoustic estimation of euphausiid abundance has been refined (Romaine et al., 2002), very little is known on the local biomass of euphausiids and the inter-annual variability of the populations. Since euphausiids are a major food source for Pacific hake, Pacific herring, chinook and coho salmon (Mauchline, 1980; Mackas et al., 1997), a crash in euphausiid populations could be disastrous

to other commercial species production. Quantification of euphausiid biomass at various timescales using multi-frequency or split-beam echosounders on the VENUS nodes located in Saanich Inlet and the Strait of Georgia will help future fisheries management to adjust quotas as well as open seasons in the waters off B.C.

4.1.2 Turbulence and internal waves in Saanich Inlet (Chapter 3)

Characterization of the physical environment in Saanich Inlet was motivated partly by the idea of a linkage between diel vertical migration and biologically generated turbulence reported by Kunze et al. (2006). By deploying two moorings in September 2010, I was able to characterize turbulence and internal waves in Saanich Inlet. A 200-kHz echosounder at the VENUS cabled observatory was used to examine possible biological generation of turbulence. Although the average dissipation rates of O(10^{-9} – 10^{-8} W kg^{-1}) suggested only weak turbulent mixing, higher dissipation rates expected at the main channel could potentially supply nutrients to the euphotic zone to sustain high primary productivity in Saanich Inlet. I did not find any relationship between diel vertical migration and turbulent dissipation rates, and the internal wave field was only weakly correlated with turbulent dissipation rates. Because my mooring experiment was conducted on a shallow shelf in Patricia Bay [which is more confined than the central part of the inlet where Kunze et al. (2006) conducted their experiments], I would expect physical forcing to be weaker at the mooring site. Similar mooring experiments in the main channel of the inlet, where the strongest currents are expected, might verify whether physical forcing could be the source of the turbulent episodes that Kunze et al. (2006) attributed to biological effects. Low-frequency flow suggested the depth-dependent patterns of currents, whose direction changes fortnightly. Potential displacement due to these patterns is O(1 – 10 km), suggesting its effect on dispersal of planktonic organisms is limited near the mouth of the inlet.

4.2 Future directions

Extending quantification of variability in diel vertical migration behavior to a productive continental shelf will improve our understanding of this important yet poorly understood component of the biological pump. Upwelling systems support a large proportion of the world's fisheries by transporting nutrient-rich water into the photic

zones of coastal oceans and increasing their productivity (Pauly and Christensen, 1995). However, this productivity can also fuel high sedimentation and thus high levels of respiration in the already oxygen-poor water advected up onto the shelf, potentially resulting in hypoxic or anoxic conditions (Grantham et al., 2004; Chan et al., 2008). The strength of coastal upwelling is highly variable, depending on the magnitude and direction of the local wind (Bograd et al., 2008), affecting productivity as well as the development of hypoxia on the continental shelf. Many animals in upwelling regions undergo diel vertical migration (Pearcy et al., 1977; Lu et al., 2003), which plays an important role as a retention mechanism (Wroblewski, 1982; Peterson, 1998; Batchelder et al., 2002). However, how organisms change their migration behavior in seasonally varying upwelling systems and how upwelling-driven hypoxia alters their distributions are poorly understood. Understanding of the impact of hypoxia on coastal ecosystems will help future ecosystem-based management in regions undergoing hypoxia.

Hypoxia constrains the vertical and horizontal distribution of species (e.g., Bertrand et al., 2010). Hypoxia tolerance and threshold values are species- and stage-specific, and can vary enormously (Miller et al. 2002). For example, some fish larvae may suffer at oxygen values of less than 3 mL O_2 L^{-1}, while euphausiids may survive to 0.1 mL O_2 L^{-1} (Sameoto et al., 1987; Howell and Simpson, 1994). If predators and prey are both intolerant of hypoxic conditions, the two may be constrained to a smaller, shared region of the water column and result in high mortality of prey (Prince and Goodyear, 2006). When prey, but not predators, are tolerant of hypoxic conditions, hypoxia can lead to a decoupling of predator-prey interactions and change trophic fluxes through food webs (Taylor and Rand, 2003). A change in dissolved oxygen may thus have a significant impact on the survival of certain species with consequent changes in species composition, trophic relationships and productivity (e.g., Koslow et al., 2011). With future deployment of multi-frequency echosounders on the VENUS node below the oxycline, Saanich Inlet will constitute a model system to study responses of organisms to changing oxygen conditions and predator-prey interactions, because the seasonal cycle of the anoxic depth is predictable.

Hypoxia is becoming a major threat for marine ecosystem health in the world's coastal waters. Along the coast of North America, high rates of oxygen loss in waters between 100 and 500 m have been reported, resulting in the shoaling of groundfish habitat (Whitney et al., 2007; Bograd et al., 2008). In the California Current System, anoxia in the water column is expanding (Chan et al., 2008) and the upper bound-

ary of the oxygen minimum layer has shoaled by up to 90 m over the last 20 years (Bograd et al. 2008). In 2006, the continental shelf from Oregon to B.C. suffered the worst hypoxic event on record, causing massive mortality of demersal fish and benthic invertebrates (Grantham et al., 2004; Chan et al., 2008). Increasingly hypoxic conditions and the expansion of the oxygen minimum zone could lead to cascading effects on benthic and pelagic ecosystems, including habitat compression and community reorganization.

Cabled observatories located in upwelling regions will provide an opportunity to explore the links between changes in seasonally varying upwelling strength, predator-prey interactions, and upwelling-driven hypoxia. Examples of such cabled observatories include the NEPTUNE Canada node located in Barkley Canyon (the continental margin off the west coast of Vancouver Island) and the U.S. Ocean Observatories Initiative on the continental shelf of the Washington and Oregon coast. Euphausiids reside as dominant migrating species at these sites, playing a key role in the food web as both predator and prey (Pearcy et al., 1977; Lu et al., 2003; Dorman et al., 2005). The cabled observatories will continuously measure temperature, salinity, oxygen, fluorescence, current velocities, and acoustic backscattering at various frequencies. To supplement these spatially-discrete measurements, spatial surveys using gliders or ships equipped with echosounders can be conducted. This will provide a unique view of mesopelagic community distributions in relation to hypoxia on the continental shelf. Direct sampling of acoustic scattering layers using nets can provide species composition, allowing interpretation of the predator-prey interactions of acoustically observed zooplankton and micronekton.

Quantification of the variability in zooplankton behavior in range of temporal (e.g., seasonal, inter-annual, and decadal scales) and spatial scales (e.g., coastal waters, continental shelf, open ocean) is essential in developing a sophisticated behavioural-hydrodynamic model, which can be used to evaluate the biogeochemical consequences of diel vertical migration on the biological pump and nutrient cycling. In the long-term, a broader and deeper understanding of marine ecosystem will help us make more accurate predictions and forge relevant solutions for the effects of global climate change on ecosystems.

Bibliography

Adams, C. F., A. I. Pinchuk, and K. O. Coyle, 2007: Seasonal changes in the diet composition and prey selection of walleye pollock (*Theragra chalcogramma*) in the northern Gulf of Alaska. *Fisheries Research*, **84**, 378–389.

Anderson, J. J. and A. H. Devol, 1973: Deep water renewal in Saanich Inlet, an intermittently anoxic basin. *Estuarine and Coastal Marine Science*, **1**, 1–10.

Barraclough, W. and R. H. Herlinveaux, 1961: Midwater trawling through the echo scattering layer in Saanich Inlet, March 1-2, 1961. *Fisheries Research Board of Canada: Manuscript Report Series*, **712**.

Bary, B., 1966: Back scattering at 12 kc/s in relation to biomass and numbers of zooplanktonic organisms in Saanich Inlet, British Columbia. *Deep-Sea Research*, **13**, 655–666.

Bary, B., W. Barraclough, and R. Herlinveaux, 1962: Scattering of underwater sound in Saanich Inlet, British Columbia. *Nature*, **194**, 36–37.

Batchelder, H. P., et al., 2002: The GLOBEC Northeast Pacific California Current. *Oceanography*, **15**, 36–47.

Bayly, I. A. E., 1986: Aspects of diel vertical migration in zooplankton, and its enigma variations. *Limnology in Australia*, P. De Deckker and W. Williams, Eds., Springer Netherlands, Monographiae Biologicae, Vol. 61, 349–368.

Benoit-Bird, K. J., W. W. L. Au, and D. W. Wisdom, 2009: Nocturnal light and lunar cycle effects on diel migration of micronekton. *Limnology and Oceanography*, **54**, 1789–1800.

Bertrand, A., M. Ballon, and A. Chaigneau, 2010: Acoustic observation of living organisms reveals the upper limit of the oxygen minimum zone. *PLoS ONE*, **5**, e10 330.

Beveridge, I. A., 2007: Acoustic observations of zooplankton distribution in Saanich Inlet, an intermittently anoxic fjord. M.S. thesis, University of Victoria.

Blaxter, J., 1973: The vertical movements and light responses of herring and plaice larvae. *Journal of the Marine Biological Association of the United Kingdom*, **53**, 635–647.

Boden, B. P. and E. M. Kampa, 1965: An aspect of euphausiid ecology revealed by echo-sounding in a fjord. *Crustaceana*, **9**, 155–173.

Bograd, S. J., C. G. Castro, E. D. Lorenzo, D. M. Palacios, B. H., W. Gilly, and F. P. Chavez, 2008: Oxygen declines and the shoaling of the hypoxic boundary in the California Current. *Geophysical Research Letters*, **35**, L12 607.

Bollens, S. M. and B. W. Frost, 1989: Zooplanktivorous fish and variable diel vertical migration in the marine planktonic copepod *Calanus pacificus*. *Limnology and Oceanography*, **34**, 1072–1083.

Borstad, G., L. Brown, M. Sato, D. Lemon, R. Kerr, and P. Willis, 2010: Long zooplankton time series with high temporal and spatial resolution. *Proceedings of the OCEANS'10*, 1–9.

Brinton, E., 1962: The distribution of Pacific euphausiids. *Bulletin of the Scripps Institution of Oceanography*, **8**, 21–270.

Bryan, K. R., K. P. Black, and R. M. Gorman, 2003: Spectral estimates of dissipation rate within and near the surf zone. *Journal of Physical Oceanography*, **33**, 979–993.

Bryden, H. L. and S. Imawaki, 2001: Ocean heat transport. *Ocean circulation and climate: observing and modeling the global ocean*, G. Siedler and J. Church, Eds., Academic Press, San Diego, CA, 455–474.

Cairns, J. and G. Williams, 1976: Internal wave observations from a midwater float, 2. *Journal of Geophysical Research*, **81**, 1943–1950.

Carter, G. and M. Gregg, 2002: Intense, variable mixing near the head of Monterey Submarine Canyon. *Journal of Physical Oceanography*, **32**, 3145–3165.

Chan, F., J. A. Barth, J. Lubchenco, A. Kirincich, H. Weeks, W. T. Peterson, and B. A. Menge, 2008: Emergence of anoxia in the California Current large marine ecosystem. *Science*, **319**, 920–920.

Cisewski, B., V. H. Strass, M. Rhein, and S. Krägefsky, 2010: Seasonal variation of diel vertical migration of zooplankton from ADCP backscatter time series data in the Lazarev Sea, Antarctica. *Deep-Sea Research I*, **57**, 78–94.

Codiga, D. L., 1997: Physics and observational signatures of free, forced, and frictional stratified seamount-trapped waves. *Journal of Geophysical Research*, **102**, 23–23.

Cohen, J. H. and R. B. Forward, 2005: Photobehavior as an inducible defense in the marine copepod *Calanopia americana*. *Limnology and Oceanography*, **50**, 1269–1277.

Dagg, M. J., B. W. Frost, and J. A. Newton, 1997: Vertical migration and feeding behavior of *Calanus pacificus* females during a phytoplankton bloom in Dabob Bay, U.S. *Limnology and Oceanography*, **42**, 974–980.

De Robertis, A., 2001: Validation of acoustic echo counting for studies of zooplankton behavior. *ICES Journal of Marine Science*, **58**, 543–561.

De Robertis, A., 2002: Small-scale spatial distribution of the euphausiid *Euphausia pacifica* and overlap with planktivorous fishes. *Journal of Plankton Research*, **24**, 1207–1220.

De Robertis, A., J. S. Jaffe, and M. D. Ohman, 2000: Size-dependent visual predation risk and the timing of vertical migration in zooplankton. *Limnology and Oceanography*, **45**, 1838–1844.

Devol, A. H., 1981: Vertical distribution of zooplankton respiration in relation to the intense oxygen minimum zones in two British Columbia fjords. *Journal of Plankton Research*, **3**, 593–602.

Dilling, L., J. Wilson, D. Steinberg, and A. Alldredge, 1998: Feeding by the euphausiid *Euphausia pacifica* and the copepod *Calanus pacificus* on marine snow. *Marine Ecology Progress Series*, **170**, 189–201.

Dorman, J. G., S. M. Bollens, and A. M. Slaughter, 2005: Population biology of euphausiids off northern California and effects of short time-scale wind events on *Euphausia pacifica*. *Marine Ecology Progress Series*, **288**, 183–198.

Dower, J. F., T. J. Miller, and W. C. Leggett, 1997: The role of microscale turbulence in the feeding ecology of larval fish. *Advances in Marine Biology*, **31**, 169–220.

Ducklow, H. W., D. K. Steinberg, and K. O. Buesseler, 2001: Upper ocean carbon export and the biological pump. *Oceanography*, **14**, 50–58.

Elgar, S., B. Raubenheimer, and R. T. Guza, 2005: Quality control of acoustic Doppler velocimeter data in the surfzone. *Measurement Science and Technology*, **16**, 1889–1893.

Faran, J. J., 1951: Sound scattering by solid cylinders and spheres. *Journal of the Acoustical Society of America*, **23**, 405–418.

Farmer, D. D., G. B. Crawford, and T. R. Osborn, 1987: Temperature and velocity microstructure caused by swimming fish. *Limnology and Oceanography*, **32**, 1987.

Feddersen, F., 2010: Quality controlling surf zone acoustic Doppler velocimeter observations to estimate the turbulent dissipation rate. *Journal of Atmospheric and Oceanic Technology*, **27**, 2039–2055.

Foote, K. G., 1982: Optinimizing copper spheres for precision calibraiton of hydroacoustic equipment. *Journal of the Acoustical Society of America*, **71**, 742–747.

Forward, R. B., 1985: Behavioral responses of larvae of the crab *Rhithropanopeus harrisii* (Brachyura: Xanthidae) during diel vertical migraiton. *Marine Biology*, **90**, 9–18.

Forward, R. B., 1988: Diel vertical migration: Zooplankton photobiology and behavior. *Oceanography and Marine Biology: An Annual Review*, **26**, 361–393.

Forward, R. B., T. W. Cronin, and D. E. Stearns, 1984: Control of diel vertical migraiton: Photoresponses of a larval crustacean. *Limnology and Oceanography*, **29**, 146–154.

Forward, R. B. and D. Rittschof, 2000: Alteration of photoresponses involved in diel vertical migration of a crab larva by fish mucus and degradation products of mucopolysaccharides. *Journal of Experimental Marine Biology and Ecology*, **245**, 277–292.

Francois, R. E. and G. R. Garrison, 1982: Sound absorption based on ocean measurements. part II: Boric acid contribution and equation for total absorption. *Journal of the Acoustical Socienty of America*, **72**, 1879–1890.

Frank, T. and E. Widder, 1999: Comparative study of the spectral sensitivities of mesopelagic crustaceans. *Journal of Comparative Physiology A: Neuroethology, Sensory, Neural, and Behavioral Physiology*, **185**, 255–265.

Frank, T. E. and E. A. Widder, 2002: Effects of a decrease in downwelling irradiance on the daytime vertical distribution patterns of zooplankton and micronekton. *Marine Biology*, **140**, 1181–1193.

Fulton, J. and R. Le Brasseur, 1984: Euphausiids of the continental shelf and slope of the Pacific coast of Canada. *La Mer*, **22**, 268–276.

Gargett, A., D. Stucchi, and F. Whitney, 2003: Physical processes associated with high primary production in Saanich Inlet, British Columbia. *Estuarine, Coastal and Shelf Science*, **56**, 1141–1156.

Gargett, A. E., 1997: "Theories" and techniques for observing turbulence in the ocean euphotic zone. *Scientia Marina*, **61**, 25–45.

Gargett, A. E., T. R. Osborn, and P. W. Nasmyth, 1984: Local isotropy and the decay of turbulence in a stratified fluid. *Journal of Fluid Mechanics*, **144**, 231–280.

Garrett, C. and W. Munk, 1972: Space-time scales of internal waves. *Geophysical Fluid Dynamics*, **3**, 225–264.

Garrett, C. and W. Munk, 1975: Space-time scales of internal waves: A progress report. *Journal of Geophysical Research*, **80**, 291–297.

Gower, J., A. Peña, and A. Gargett, 1999: Biological monitoring with the western Canadian ODAS marine buoy network. *OCEANS'99 MTS/IEEE. Riding the Crest into the 21st Century*, IEEE, Vol. 3, 1244–1248.

Gower, J. F. R., 2001: Productivity and plankton blooms observed with Seawifs and in-situ sensors. *Geoscience and Remote Sensing Symposium, 2001. IGARSS'01. IEEE 2001 International*, IEEE, Vol. 5, 2181–2183.

Grantham, B. A., F. Chan, K. J. Nielsen, D. S. Fox, J. A. Barth, A. Huyer, J. Lubchenco, and B. A. Menge, 2004: Upwelling-driven nearshore hypoxia signals ecosystem and oceanographic changes in the northeast Pacific. *Nature*, **429**, 749–754.

Gregg, M., 1989: Scaling turbulent dissipation in the thermocline. *Journal of Geophysical Research*, **94**, 9686–9698.

Gregg, M. and E. Kunze, 1991: Shear and strain in Santa Monica basin. *Journal of Geophysical Research*, **96**, 16 709–16 719.

Gregg, M., T. Sanford, and D. Winkel, 2003: Reduced mixing from the breaking of internal waves in equatorial waters. *Nature*, **422**, 513–515.

Gregg, M. C. and J. K. Horne, 2009: Turbulence, acoustic backscatter, and pelagic nekton in Monterey Bay. *Journal of Physical Oceanography*, **39**, 1097–1114.

Gregg, M. C. and T. B. Sanford, 1988: The dependence of turbulent dissipation on stratification in a diffusively stable thermocline. *Journal of Geophysical Research*, **93**, 12 381–12 392.

Gruber, N. and J. L. Sarmiento, 2002: Large-scale biogeochemical-physical interactions in elemental cycles. *The Sea*, **12**, 337–99.

Grundle, D. S., D. A. Timothy, and D. E. Varela, 2009: Variations of phytoplankton productivity and biomass over an annual cycle in Saanich Inlet, a British Columbia fjord. *Continental Shelf Research*, **29**, 2257–2269.

Haist, V. and M. Stocker, 1985: Growth and maturation of Pacific herring (*Clupea harengus pallasi*) in the Strait of Georgia. *Canadian Journal of Fisheries and Aquatic Sciences*, **42**, 138–146.

Hays, G. C., 2003: A review of the adaptive significance and ecosystem consequences of zooplankton diel vertical migrations. *Hydrobiologia*, **503**, 163–170.

Heath, W., 1977: The ecology and harvesting of euphausiids in the Strait of Georgia. Ph.D. thesis, University of British Columbia, Vancouver, B.C.

Hedges, J. I. and R. G. Keil, 1995: Sedimentary organic matter preservation: an assessment and speculative synthesis. *Marine Chemistry*, **49**, 81–115.

Herlinveaux, R. H., 1962: Oceanography of Saanich Inlet in Vancouver Island, British Columbia. *Journal of the Fisheries Research Board of Canada*, **19**, 1–37.

Hernández-León, S., G. Franchy, M. Moyano, I. Menéndez, C. Schmoker, and S. Putzeys, 2010: Carbon sequestration and zooplankton lunar cycles: Could we be missing a major component of the biological pump? *Limnology and Oceanography*, **55**, 2503–2512.

Hickling, R., 1962: Analysis of echoes from a solid elastic sphere in water. *Journal of the Acoustical Society of America*, **34**, 1582–1592.

Holliday, D. and R. Pieper, 1995: Bioacoustical oceanography at high frequencies. *ICES Journal of Marine Science*, **52**, 279–296.

Holtby, L., R. Kadowaki, and K. Simpson, 1992: Factors affecting the vulnerability of juvenile coho (*Oncothynchus kisutch*) and chinook salmon (*O. tshawytscha*) in a saltwater sport fishery. *Canadian Journal of Fisheries and Aquatic Sciences*, **49**, 2164–2178.

Howell, P. and D. Simpson, 1994: Abundance of marine resources in relation to dissolved oxygen in Long Island Sound. *Estuaries*, **17**, 394–402.

Hulburt, E. O., 1945: Optics of distilled and natural water. *Journal of the Optical Society of America*, **35**, 698–705.

Huntley, M. and E. R. Brooks, 1982: Effects of age and food availability on diel vertical migraiton of *Calanus pacificus*. *Marine Biology*, **71**, 23–31.

Huntley, M. E. and M. Zhou, 2004: Influence of animals on turbulence in the sea. *Marine Ecology Progress Series*, **273**, 65–79.

Hutchinson, G. E., 1967: *A treatise on limnology, Vol. II Introduction to lake biology and the limnoplankton*. Wiley, New York.

Jaffe, J. S., M. D. Ohman, and A. D. Robertis, 1998: OASIS in the sea: measurement of the acoustic reflectivity of zooplankton with concurrent optical imaging. *Deep-Sea Research II*, **45**, 1239–1253.

Jiang, S., T. D. Dickey, D. K. Steinberg, and L. P. Madin, 2007: Temporal variability of zooplankton biomass from ADCP backscatter time series data at the Bermuda Testbed Mooring site. *Deep-Sea Research I*, **54**, 608–636.

Johnsen, G. and P. Jakobsen, 1987: The effect of food limitation on vertical migration in *Daphnia longispina*. *Limnology and Oceanography*, **32**, 873–880.

Jones, N. L. and S. G. Monismith, 2008: The influence of whitecapping waves on the vertical structure of turbulence in a shallow estuarine embayment. *Journal of Physical Oceanography*, **38**, 1563–1580.

Kaartvedt, S., W. Melle, T. Knutsen, and H. R. Skjoldal, 1996: Vertical distribution of fish and krill beneath water of varying optical properties. *Marine Ecology Progress Series*, **136**, 51–58.

Kawamura, G., T. Matsushita, M. Nishitai, and T. Matsuoka, 1996: Blue and green fish aggregation devices are more attractive to fish. *Fisheries Research*, **28**, 99–108.

Kemp, A. E. S., J. Pike, R. B. Pearce, and C. B. Kange, 2000: The "Fall dump" - a new perspective on the role of the "shade flora" in the annual cycle of diatom produciton and export flux. *Deep-Sea Research II*, **47**, 2129–2154.

Kiørboe, T., C. Kundsgaard, M. Olesen, and J. L. S. Hansen, 1994: Aggregation and sedimentation processes during a spring phytoplankton bloom: A field experiment to test coafulaiton theory. *Journal of Marine Research*, **52**, 297–323.

Koslow, J. A., R. Goericke, A. Lara-Lopez, and W. Watson, 2011: Impact of declining intermediate-water oxygen on deepwater fishes in the California Current. *Marine Ecology Progress Series*, **436**, 207–218.

Kundu, P. K. and I. M. Cohen, 2008: *Fluid mechanics*. 4th ed., Academic Press.

Kunze, E., J. F. Dower, I. Beveridge, R. Dewey, and K. P. Bartlett, 2006: Observations of biologically generated turbulence in a coastal inlet. *Science*, **313**, 1768–1770.

Kunze, E. and J. M. Toole, 1997: Tidally driven vorticity, diurnal shear, and turbulence atop Fieberling Seamount. *Journal of Physical Oceanography*, **27**, 2663–2693.

Lawson, G. L., P. H. Wiebe, C. J. Ashjian, and T. K. Stanton, 2008: Euphausiid distribution along the Western Antarctic Peninsula—Part B: Distribution of euphausiid aggregations and biomass, and associations with environmental features. *Deep-Sea Research II*, **55**, 432–454.

Liu, K. K., K. Iseki, and S. Y. Chao, 2000: *Continental margin carbon fluxes*. Cambridge University Press, Cambridge, 187–239 pp.

Longhurst, A. R., A. W. Bedo, W. G. Harrison, E. J. H. Head, and D. D. Sameoto, 1990: Vertical flux of respiratory carbon by oceanic diel migrant biota. *Deep-Sea Research*, **37**, 685–694.

Longhurst, A. R. and W. G. Harrison, 1988: Vertical nitrogen flux from the oceanic photic zone by diel migrant zooplankton and nekton. *Deep-Sea Research*, **35**, 881–889.

Longhurst, A. R. and W. G. Harrison, 1989: The biological pump: profiles of plankton production and consumption in the upper ocean. *Progress in Oceanography*, **22**, 47–122.

Lorke, A., D. F. Mcginnis, P. Spaak, and A. Wuest, 2004: Acoustic observations of zooplankton in lakes using a Doppler current profiler. *Freshwater Biology*, **49**, 1280–1292.

Lorke, A. and W. N. Probst, 2010: *In situ* measurements of turbulence in fish shoals. *Limnology and Oceanography*, **55**, 354–364.

Lu, B., D. L. Mackas, and D. F. Moore, 2003: Cross-shore separation of adult and juvenile euphausiids in a shelf-break alongshore current. *Progress in Oceanography*, **57**, 381–404.

Mackas, D. L., R. Kieser, M. Saunders, D. R. Yelland, R. M. Brown, and D. F. Moore, 1997: Aggregation of euphausiids and Pacific hake (*Merluccius productus*) along the outer continental shelf off Vancouver Island. *Canadian Journal of Fisheries and Aquatic Sciences*, **54**, 2080–2096.

Mackenzie, K. V., 1981: Nine-term equations for sound speed in the oceans. *Journal of the Acoustical Society of America*, **70**, 807–812.

Mackie, G. O. and C. E. Mills, 1983: Use of the Pisces IV submersible for zooplankton studies in coastal waters of British Columbia. *Canadian Journal of Fisheries and Aquatic Sciences*, **40**, 763–776.

MacKinnon, J. and M. Gregg, 2003: Mixing on the late-summer New England shelf - solibores, shear, and stratification. *Journal of Physical Oceanography*, **33**, 1476–1492.

MacLennan, D. N. and J. R. Dunn, 1984: Estimation of sound velocities from resonance measurements on tungsten carbide calibration spheres. *Journal of Sound and Vibration*, **97**, 321–331.

Manning, C. C., R. C. Hamme, and A. Bourbonnais, 2010: Impact of deep-water renewal events on fixed nitrogen loss from seasonally-anoxic Saanich Inlet. *Marine Chemistry*, **122**, 1–10.

Mauchline, J., 1980: The biology of mysids and euphausiids. *Advances in Marine Biology*, **18**, 1–681.

Mauchline, J. and L. Fisher, 1969: The biology of euphausiids. *Advances in Marine Biology*, **7**, 1–454.

Middelburg, J. J., K. Soetaert, and P. M. J. Herman, 1997: Empirical relationships for use in global diagenetic models. *Deep-Sea Research I*, **44**, 327–344.

Muller-Karger, F. E., R. Varela, R. Thunell, R. Luerssen, C. Hu, and J. J. Walsh, 2005: The importance of continental margins in the global carbon cycle. *Geophysical Research Letters*, **32**, L01 602.

Munk, W., 1981: Internal waves and small-scale processes. *Evolution of physical oceanography*, B. Warren and C. Wunsch, Eds., The MIT Press, Cambridge, MA, 264–291.

Nakagawa, Y., T. Ota, Y. Endo, K. Taki, and H. Sugisaki, 2004: Importance of ciliates as prey of the euphausiid *Euphausia pacifica* in the NW North Pacific. *Marine Ecology Progress Series*, **271**, 261–266.

Nicol, S. and Y. Endo, 1999: Krill fisheries: development, management and ecosystem implications. *Aquatic Living Resources*, **12**, 105–120.

Oakey, N., 1982: Determination of the rate of dissipation of turbulent energy from simultaneous temperature and velocity shear microstructure measurements. *Journal of Physical Oceanography*, **12**, 256–271.

Ohman, M. D., B. W. Frost, and E. B. Cohen, 1983: Reverse diel vertical migration: an escape from invertebrate predators. *Science*, **220**, 1404–1407.

Ona, E., 1999: Methodology for target strength measurements: with special reference to in situ techniques for fish and mikro-nekton. *International Council for the Exploration of the Sea*, **235**, 49–59.

Osborn, T. R., 1980: Estimates of the local rate of vertical diffusion from dissipation measurements. *Journal of Physical Oceanography*, **10**, 83–89.

Parker-Stetter, S. L. and J. K. Horne, 2009: Nekton distribution and midwater hypoxia: A seasonal, diel prey refuge? *Estuarine, Coastal and Shelf Science*, **81**, 13–18.

Parsons, T., R. LeBrasseur, and J. Fulton, 1967: Some observations on the dependence of zooplankton grazing on the cell size and concentration of phytoplankton blooms. *Journal of the Oceanographical Society of Japan*, **23**, 10–17.

Pasciak, W. J. and J. Gavis, 1975: Transport limited nutrient uptake rates in *Ditylum brightwellii*. *Limnology and Oceanography*, **20**, 604–617.

Pauly, D. and V. Christensen, 1995: Primary production required to sustain global fisheries. *Nature*, **374**, 255–257.

Pearcy, W. G., E. E. Krygier, R. Mesecar, and F. Ramsey, 1977: Vertical distribution and migration of oceanic micronekton off Oregon. *Deep-Sea Research*, **24**, 223–245.

Pearre, S., 2003: Eat and run? the hunger/satiation hypothesis in vertical migration: history, evidence and consequences. *Biological Reviews*, **78**, 1–79.

Peterson, W., 1998: Life cycle strategies of copepods in coastal upwelling zones. *Journal of Marine Systems*, **15**, 313–326.

Pieper, R., 1971: A study of the relationship between zooplankton and high-frequency scattering of underwater sound. Ph.D. thesis, University of British Columbia, Vancouver, B.C.

Pieper, R. E., D. V. Holliday, and G. S. Kleppel, 1990: Quantitative zooplankton distributions from multifrequency acoustics. *Journal of Plankton Research*, **12**, 433–441.

Pinchuk, A. I. and R. R. Hopcroft, 2007: Seasonal variations in the growth rates of euphausiids (*Thysanoessa inermis*, *T. spinifera*, and *Euphausia pacifica*) from the northern Gulf of Alaska. *Marine Biology*, **151**, 257–269.

Prince, E. D. and C. P. Goodyear, 2006: Hypoxia-based habitat compression of tropical pelagic fishes. *Fisheries Oceanography*, **15**, 451–464.

Proctor, A., C. Bradley, E. Gamroth, and J. Kennedy, 2007: The ocean technology test bed - an underwater laboratory. *OCEANS 2007*, IEEE, 1–10.

Rippeth, T. P., J. C. Gascoigne, J. A. M. Green, M. E. Inall, M. R. Palmer, J. H. Simpson, and P. J. Wiles, 2007: Turbulent dissipation of coastal seas. *Science*.

Romaine, S. J., D. L. Mackas, and M. C. Macaulay, 2002: Comparison of euphausiid population size estimates obtained using replicated acoustic surveys of coastal inlets and block average vs. geostatistical spatial interpolation methods. *Fisheries Oceanography*, **11**, 102–115.

Ross, R. and L. Quetin, 2000: *Reproduction in Euphausiacea*. Blackwell Science, Oxford, 150–181 pp.

Rothschild, B. J. and T. R. Osborn, 1988: Small-scale turbulence and plankton contact rates. *Journal of Plankton Research*, **10**, 465–474.

Rousseau, S., E. Kunze, R. Dewey, K. Bartlett, and J. Dower, 2010: On turbulence production by swimming marine organisms in the open ocean and coastal waters. *Journal of Physical Oceanography*, **40**, 2107–2121.

Sabine, C. L., et al., 2004: The oceanic sink for anthropogenic CO_2. *Science*, **305**, 367–371.

Sameoto, D., L. Guglielmo, and M. K. Lewis, 1987: Day/night vertical distribution of euphausiids in the eastern tropical Pacific. *Marine Biology*, **96**, 235–245.

Sato, M., J. Dower, E. Kunze, and R. Dewey, 2013: Second-order seasonal variability in diel vertical migration timing of euphausiids in a coastal inlet. *Marine Ecology Progress Series*, **480**, 39–56.

Sato, M. and P. Jumars, 2008: Seasonal and vertical variations in emergence behaviors of *Neomysis americana*. *Limnology and Oceanography*, **53**, 1665–1677.

Shaw, C. T., W. T. Peterson, and L. R. Feinberg, 2010: Growth of *Euphausia pacifica* in the upwelling zone off the Oregon coast. *Deep-Sea Research II*, **57**, 584–593.

Simard, Y., G. Lacroix, and L. Legendre, 1985: In situ twilight grazing rhythm during diel vertical migrations of a scattering layer of *Calanus finmarchicus*. *Limnology and Oceanography*, **30**, 598–606.

Simpson, J. H. and T. P. Rippeth, 1993: The Clyde Sea: a model of the seasonal cycle of stratification and mixing. *Estuarine, Coastal and Shelf Science*, **37**, 129–144.

Sourisseau, M., Y. Simard, and F. J. Saucier, 2008: Krill diel vertical migration fine dynamics, nocturnal overturns, and their roles for aggregation in stratified flows. *Canadian Journal of Fisheries and Aquatic Sciences*, **65**, 574–587.

St. Laurent, L. and R. Schmitt, 1999: The contribution of salt fingers to vertical mixing in the North Atlantic tracer release experiment. *Journal of Physical Oceanography*, **29**, 1404–1424.

Stanton, T. K., D. Chu, and P. H. Wiebe, 1996: Acoustic scattering characteristics of several zooplankton groups. *ICES Journal of Marine Science*, **53**, 289–295.

Stanton, T. K., P. H. Wiebe, D. Chu, M. C. Benfield, L. Scanlon, L. Martin, and R. L. Eastwood, 1994: On acoustic estimates of zooplankton biomass. *ICES Journal of Marine Science*, **51**, 505–512.

Steinberg, D. K., C. A. Carlson, N. R. Bates, S. A. Goldthwait, L. P. Madin, and A. F. Michaels, 2000: Zooplankton vertical migration and the active transport of dissolved organic and inorganic carbon in the Sargasso Sea. *Deep-Sea Research I*, **47**, 137–158.

Stigebrandt, A., 1976: Vertical diffusion driven by internal waves in a sill fjord. *Journal of Physical Oceanography*, **6**, 486–485.

Stigebrandt, A. and J. Aure, 1989: Vertical mixing in basin waters of fjords. *Journal of Physical Oceanography*, **19**, 917–926.

Takahashi, M., J. Marwell-Clarke, F. Whitney, and P. Koeller, 1978: Winter condition of marine plankton populations in Saanich Inlet, B.C., Canada. I. Phytoplankton and its surrounding environment. *Journal of Experimental Marine Biology and Ecology*, **31**, 283–301.

Takahashi, M., D. L. Seibert, and W. H. Thomas, 1977: Occasional blooms of phytoplankton during summer in Saanich Inlet, B.C., Canada. *Deep-Sea Research*, **24**, 775–780.

Tanasichuk, R. W., 1998: Interannual variations in the population biology and productivity of *Euphausia pacifica* in Barkley Sound, Canada, with special reference to the 1992 and 1993 warm ocean years. *Marine Ecology Progress Series*, **173**, 163–180.

Tarling, G. A., 2003: Sex-dependent diel vertical migration in northern krill *Meganyctiphanes norvegica* and its consequences for population dynamics. *Marine Ecology Progress Series*, **260**, 173–188.

Tarling, G. A., J. B. L. Matthews, P. David, O. Guerin, and F. Buchholz, 2001: The swarm dynamics of northern krill (*Meganyctiphanes norvegica*) and pteropods (*Cavolinia inflexa*) during vertical migration in the Ligurian Sea observed by an acoustic Doppler current profiler. *Deep-Sea Research I*, **48**, 1671–1686.

Taylor, J. C. and P. S. Rand, 2003: Spatial overlap and distribution of anchovies (*Anchoa* spp.) and copepods in a shallow stratified estuary. *Aquatic Living Resources*, **16**, 191–196.

Tennekes, H. and J. L. Lumley, 1972: *A first course in turbulence*. The MIT Press, Cambridge, MA.

Thomas, W. H. and C. H. Gibson, 1990: Quantified small-scale turbulence inhibits a red tide dinoflagellate, *Gonyaulax polyedra* stein. *Deep-Sea Research*, **37**, 1583–1593.

Thomas, W. H. and C. H. Gibson, 1992: Effects of quantified small-scale turbulence on the dinoflagellate, *Gymnodium sanguineum (splendens)*: contrasts with *Gonyaulax (Lingulodinium) polyedra*, and the fishery implication. *Deep-Sea Research*, **39**, 1429–1437.

Thomson, R. E., 1981: *Oceanography of the British Columbia coast*. Department of Fisheries and Oceans, Ottawa.

Thorpe, S. A., 2005: *The turbulent ocean*. Cambridge University Press, Cambridge.

Timothy, D. A. and M. Y. S. Soon, 2001: Primary production and deep-water oxygen content of two British Columbian fjords. *Marine Chemistry*, **73**, 37–51.

Tinis, S. W., 1995: The circulation and energetics of the Sechelt Inlet system, British Columbia. Ph.D. thesis, University of British Columbia.

Trevorrow, M. V., D. L. Mackas, and M. C. Benfield, 2005: Comparison of multifrequency acoustic and *in situ* measurements of zooplankton abundances in Knight Inlet, British Columbia. *Journal of the Acoustical Society of America*, **117**, 3574–3588.

Tunnicliffe, V., R. Dewey, and D. Smith, 2003: Research plans for a mid-depth cabled seafloor observatory in Western Canada. *Oceanography*, **16**, 53–59.

Turner, J. T., 2002: Zooplankton fecal pellets, marine snow and sinking phytoplankton blooms. *Aquatic Microbial Ecology*, **27**, 57–102.

Tyler, J. E., 1975: The in situ quantum efficiency of natural phytoplankton populations. *Limnology and Oceanography*, **20**, 976–980.

Urick, R., 1983: *Principles of underwater sound*. 3d ed., McGraw-Hill New York.

Vagle, S., K. G. Foote, M. V. Trevorrow, and D. F. Farmer, 1996: A technique for calibration of monostatic echosounder systems. *IEEE Journal of Oceanic Engineering*, **21**, 298–305.

Van Gool, E. and J. Ringelberg, 1995: Swimming of *Daphnia galeata* × *hyalina* in response to changing light intensities: Influence of food availability and predator kairomone. *Marine and Freshwater Behaviour and Physiology*, **26**, 259–265.

Van Gool, E. and J. Ringelberg, 2003: What goes down must come up: symmetry in light-induced migration behaviour of *Daphnia*. *Hydrobiologia*, **491**, 301–307.

Virtue, P., P. Nichols, S. Nicol, and G. Hosie, 1996: Reproductive trade-off in male Antarctic krill, *Euphausia superba*. *Marine Biology*, **126**, 521–527.

Visser, A. W., 2007: Biomixing of the oceans? *Science*, **316**, 838–839.

Waite, A., P. K. Bienfang, and P. J. Harrison, 1992: Spring bloom sedimentation in a subarctic ecosystem ii. Succession and sedimentation. *Marine Biology*, **114**, 131–138.

Walsh, J. J., 1988: *On the nature of continental shelves*. Academic Press, New York.

Watanabe, L. N., 1978: Factors controlling the winter dominance of nanoflagellates in Saanich Inlet, British Columbia. M.S. thesis, University of British Columbia.

Whitney, F. A., H. J. Freeland, and M. Robert, 2007: Persistently declining oxygen levels in the interior waters of the eastern subarctic Pacific. *Progress in Oceanography*, **75**, 179–199.

Widder, E. A. and T. M. Frank, 2001: The speed of an isolume: a shrimp's eye view. *Marine Biology*, **138**, 669–677.

Wiese, K. and Y. Ebina, 1995: The propulsion jet of *Euphausia superba* (Antarctic krill) as a potential communication signal among conspecifics. *Journal of the Marine Biological Association of the United Kingdom*, **75**, 43–54.

Wroblewski, J., 1982: Interaction of currents and vertical migration in maintaining *Calanus marshallae* in the Oregon upwelling zone - a simulation. *Deep-Sea Research*, **29**, 665–686.

Yen, J., 2000: Life in transition: balancing inertial and viscous forces by planktonic copepods. *Biological Bulletin*, **198**, 213–224.

Yen, J., J. Brown, and D. R. Webster, 2003: Analysis of the flow field of the krill, *Euphausia pacifica*. *Mar. Fresh. Behav. Physiol.*, **36**, 307–319.

Zaret, T. M. and J. S. Suffern, 1976: Vertical migraiton in zooplankton as a predator avoidance mechanism. *Limnology and Oceanography*, **21**, 804–813.

Appendix A

Calibration of echosounders

All echosounders (AWCP 1006 − 1009) deployed at the VENUS cabled observatory were calibrated using the target strength (TS) of a 38.1-mm-diameter tungsten carbide reference sphere as prescribed by Vagle et al. (1996). Although the echosounder data presented in this thesis were collected by AWCP 1007 and 1009, calibration values for all echosounders are presented here for users accessing the VENUS echosounder data in Saanich Inlet and the Strait of Georgia in the future.

A.1 Calibration setup

Calibrations were conducted at the buoy of the Ocean Technology Test Bed, an underwater engineering laboratory operated by the University of Victoria in Saanich Inlet (Fig. A.1; Proctor et al., 2007), on 8 November 2011 for AWCP 1006, 9 February 2010 for AWCP 1007, and 31 January 2011 for AWCP 1008 and 1009. Due to technical difficulties in calibrating bottom-mounted echosounders at the operating depth of 100 m, calibrations were conducted near the surface. The calibration system consists of a simple assembly, with a fixed vertical post attached to the buoy onto which the transducer was mounted at $\sim$ 0.7-m depth facing downward (Fig. A.2). A calibration sphere was enmeshed in fine seine woven of monofilament nylon and suspended below the transducer at 18 − 41 m range using monofilament fishing lines. The position of the sphere was controlled vertically and horizontally in order to find the acoustic axis, and the calibration sphere was deepened every 2 − 6 m for calibration measurements at different depths.

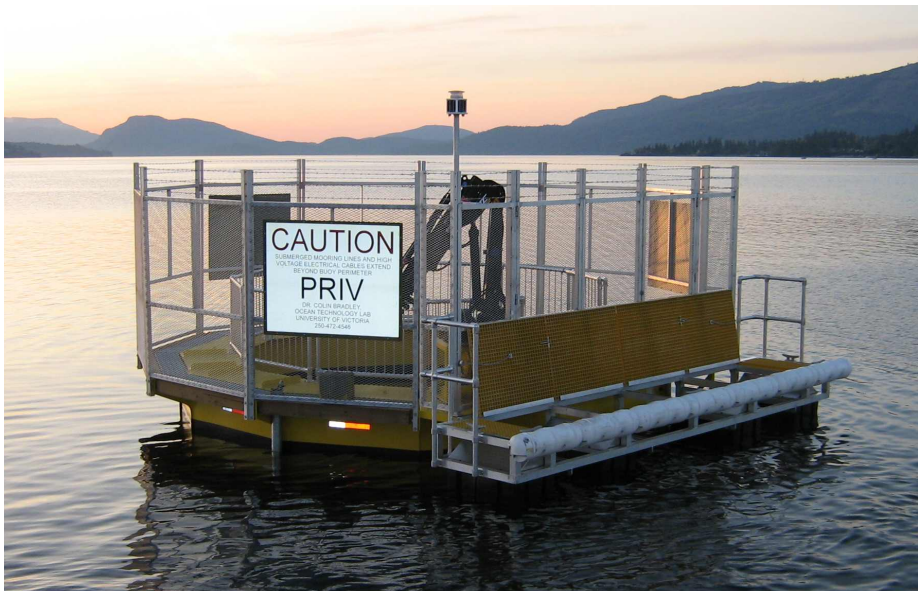

Figure A.1: Picture of the Ocean Technology Test Bed in Saanich Inlet. [*Photo courtesy of Alison Proctor*]

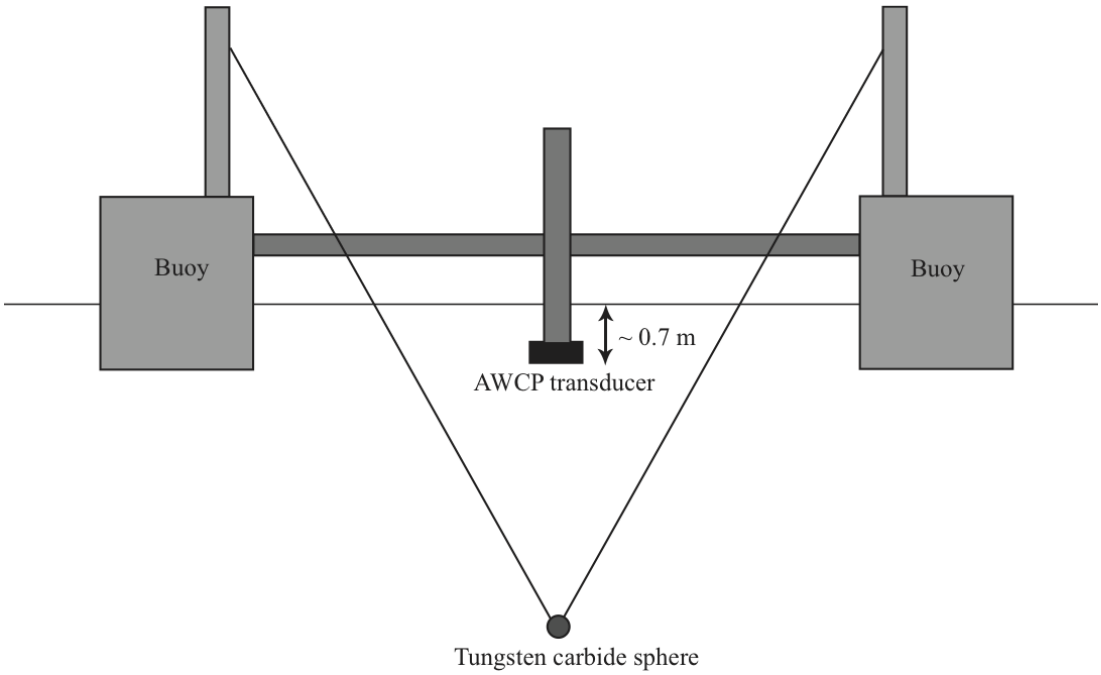

Figure A.2: Schematic of the calibration system at the Ocean Technology Test Bed; the side view.

A.2 Calibration measurements

The equation used in the AWCP systems for estimating TS measured *in situ* was

$$TS = 20log_{10}N_r + 40log_{10}r + 2\alpha r - SL - OCV - G. \quad \text{(A.1)}$$

System calibrations for TS measurements involve guiding the sphere through the beam, measuring its TS, and quantifying adjustment needed in G to compensate for the difference between the TS measured *in situ* and theoretical TS of the sphere as ΔG. The theoretical TS values of the reference sphere were computed based on physical constants of the calibration sphere in seawater (Table A.1) for the center frequency and bandwidth of each echosounder (Table A.2; Faran, 1951; Hickling, 1962; Foote, 1982). The theoretical TS characteristics for a tungsten carbide sphere shows less variability at the AWCP frequency of $\sim$ 200 kHz (Fig. A.3), suggesting that this calibration sphere is appropriate for calibrating the AWCPs.

Table A.1: Physical constants used for calculating the theoretical TS values of a tungsten carbide sphere (Wc) in seawater. Longitudinal and transverse sound speed of the sphere were computed based on the measured density of the tungsten carbide sphere (MacLennan and Dunn, 1984).

Physical properties	Value			
Wc radius (m)	0.01904			
Wc density (kg m^{-3})	14983			
Wc longitudinal sound speed (m s^{-1})	6862			
Wc transverse sound speed (m s^{-1})	4186			
Serial numbers of AWCPs	1006	1007	1008	1009
Mean seawater density (kg m^{-3})	1022.5	1022.5	1022.3	1022.3
Mean seawater sound speed (m s^{-1})	1483.5	1475.9	1473.4	1473.5
TS (dB re 1 m^2)	-39.45	-39.51	-39.51	-39.52

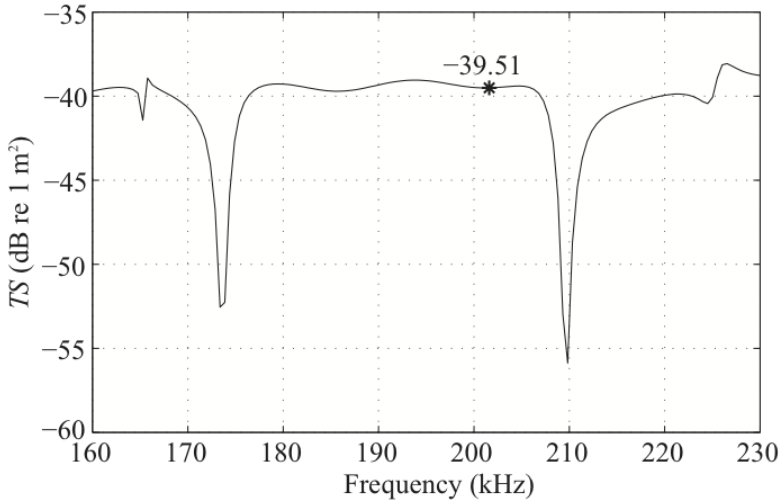

Figure A.3: Changes in theoretical TS values of a 38.1-mm-diameter tungsten carbide reference sphere with frequencies, calculated for AWCP 1007 based on m-file written by Dezhang Chu at Woods Hole Oceanographic Institution.

CTD vertical profiles were collected during the calibrations, from which the sound speed (c) was estimated (Fig. A.4; Mackenzie, 1981). The mean c was computed between the depths of the transducer (0.7 m) and sphere ($18 - 41$ m), and was used to compute theoretical TS values (Table A.1), as well as r and α (Francois and Garrison, 1982). The AWCP 1006 calibration included 2039 TS measurements in 5 different depths averaging 408 TS measurements at each depth; the AWCP 1007 calibration included 846 TS measurements in 4 different depths averaging 212 TS measurements at each depth; the AWCP 1008 calibration included 1713 TS measurements in 7 different depths averaging 245 TS measurements at each depth; and the AWCP 1009 calibration included 1592 TS measurements in 6 different depths averaging 265 TS measurements at each depth.

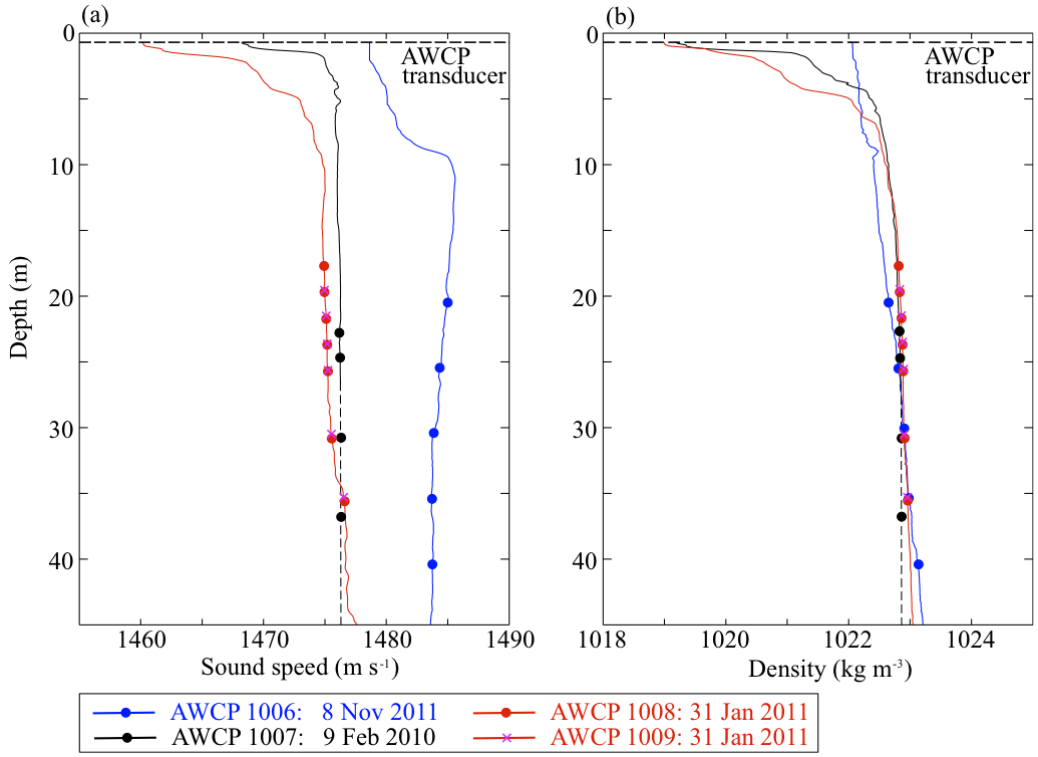

Figure A.4: Profiles of (a) sound speed and (b) density. Dotted lines at 7-m depth indicate the depth of the AWCP transducers, and circles indicate the various depths of the calibration sphere. The CTD profile on 9 February 2010 was not deep enough to cover all the calibration depths. In order to compute the average sound speed and density, the values deeper than the depth of the CTD cast were assumed to be the same as the one observed at the deepest depth ($\sim$ 27 m).

Although weather during calibration was relatively calm and tides are weak in Saanich Inlet (Gargett et al., 2003), positioning of the sphere on the acoustic axis was difficult due to the single-beam echosounder. Since the TS value should become maximum when the sphere is located on the acoustic axis, the maximum TS obtained during calibration runs at each depth was taken to be an on-axis measurement and used for calculating ΔG. On average, the mean adjustment needed in G (ΔG) was -0.89 dB for AWCP 1006, -0.34 dB for AWCP 1007, -1.20 dB for AWCP 1008, and -0.38 dB for AWCP 1009 (Table A.2). Since the measured TS values were within 0.4 dB of the theoretical TS in AWCP 1007 and 1009, and depth dependency of transducer sensitivity could affect the calibration results (Ona, 1999), no correction was applied to G in the echosounder data presented in this study.

Table A.2: Specifications and calibration values for AWCPs.

Serial number of AWCP	1006	1007	1008	1009
Calibration date	8 November 2011	9 February 2010	31 January 2011	31 January 2011
Center frequency (kHz)	201	202	200	200
Bandwidth (kHz)	$197.4 - 204.4$	$198.0 - 205.2$	$196.9 - 202.3$	$197.1 - 204.3$
SL (dB re 1 μPa at 1 m)	213.3	212.6	213.2	212.9
OCV (dB re 1 V per 1 μPa)	-191.2	-191.2	-191.5	-191.2
r (m)	20.61 25.58 30.54 35.61 40.58	22.66 24.69 30.76 36.83	17.69 19.71 21.61 23.64 25.66 30.71 35.53	19.46 21.48 23.49 25.53 30.46 35.28
ΔG (dB)	-0.49 -1.14 -0.75 -1.05 -1.01	-0.22 0.08 -0.11 -1.10	-0.12 -0.90 -1.20 -1.88 -1.77 -1.05 -1.49	-0.78 -0.75 -0.82 0.30 -0.21 0.03
Mean $\pm$ std of ΔG (dB)	-0.89 ± 0.26	-0.34 ± 0.52	-1.20 ± 0.60	-0.38 ± 0.47